Catarina Isabel Gouveia Lopes

Licenciada em Ciências e Engenharia do Ambiente

Mapping the Pasture Steppe in Bayankhongor, Mongolia: comparison of classification methods, using Landsat-8 and geophysical data

Dissertação para obtenção do Grau de Mestre em
Engenharia do Ambiente, Perfil de Engenharia de Sistemas Ambientais

Orientador: Prof. Doutora Maria Júlia Seixas, Professora Auxiliar, FCT/UNL

Co-orientador: Doutor Nuno Santos Grosso, DEIMOS Engenharia SA

Presidente: Prof. Doutora Maria Teresa Calvão Rodrigues
Arguente: Doutor Nuno Miguel Matias Carvalhais
Vogal: Prof. Doutora Maria Júlia Fonseca de Seixas

FACULDADE DE CIÊNCIAS E TECNOLOGIA
UNIVERSIDADE NOVA DE LISBOA

Novembro de 2015

Mapping the Pasture Steppe in Bayankhongor, Mongolia: comparison of classification methods, using Landsat-8 and geophysical data

Acknowledgments

I would like to thank everyone who took part on the elaboration of this thesis, but also to everyone who participated in my academic journey in FCT/UNL.
First, I would like to thank my supervisors, Júlia Seixas and Nuno Grosso. To professor Júlia Seixas, by raising my interest for remote sensing, through her interesting lessons, and for providing the support necessary to finish this thesis; and to Nuno Grosso for having the patience for always guiding, advising and readily clarify any emergent questions throughout the whole development process of this thesis.

To DEIMOS Engenharia SA team who received me on the best possible way and provided me a place to work on my thesis. A special acknowledgement to Carla Patinha, who was always available for helping me whenever I needed to clarify any questions.

A huge thanks to my family, specially to my parents for all the dedication and effort that they have put on my education over the years. To my brother, for helping me on the reviewing process, but also for his support. To Eduardo who has been present for the major part of my academic years and always gave me the motivation and support to get through the most difficult times and helped me solve emerging problems of this thesis, by providing convenient suggestions.

I would also like to thank all of my university colleagues who accompanied me throughout this course. A special acknowledgment to the ones who were always present and to whom I owe all these great academic years: Carolina, Bruno and Diana.

Abstract

Grasslands in semi-arid regions, like Mongolian steppes, are facing desertification and degradation processes, due to climate change. Mongolia's main economic activity consists on an extensive livestock production and, therefore, it is a concerning matter for the decision makers. Remote sensing and Geographic Information Systems provide the tools for advanced ecosystem management and have been widely used for monitoring and management of pasture resources. This study investigates which is the higher thematic detail that is possible to achieve through remote sensing, to map the steppe vegetation, using medium resolution earth observation imagery in three districts (*soums*) of Mongolia: Dzag, Buutsagaan and Khureemaral. After considering different thematic levels of detail for classifying the steppe vegetation, the existent pasture types within the steppe were chosen to be mapped. In order to investigate which combination of data sets yields the best results and which classification algorithm is more suitable for incorporating these data sets, a comparison between different classification methods were tested for the study area. Sixteen classifications were performed using different combinations of estimators, Landsat-8 (spectral bands and Landsat-8 NDVI-derived) and geophysical data (elevation, mean annual precipitation and mean annual temperature) using two classification algorithms, maximum likelihood and decision tree. Results showed that the best performing model was the one that incorporated Landsat-8 bands with mean annual precipitation and mean annual temperature (Model 13), using the decision tree. For maximum likelihood, the model that incorporated Landsat-8 bands with mean annual precipitation (Model 5) and the one that incorporated Landsat-8 bands with mean annual precipitation and mean annual temperature (Model 13), achieved the higher accuracies for this algorithm. The decision tree models consistently outperformed the maximum likelihood ones.

Keywords: Remote sensing; Geographic Information Systems; Landsat-8; geophysical data; maximum likelihood; decision tree

Resumo

As pastagens em regiões semi-áridas, como as estepes da Mongólia, estão actualmente a sofrer processos de desertificação e degradação devido às alterações climáticas. A maior actividade económica da Mongólia consiste na produção extensiva de gado, representando assim uma matéria de grande importância nos processos de tomada de decisão. A detecção remota e os Sistemas de Informação Geográfica providenciam ferramentas para a gestão avançada de ecossistemas e têm vindo a ser utilizados para monitorizar e gerir os recursos associados às pastagens. Este estudo investiga qual o nível mais elevado de detalhe temático que é possível alcançar para mapear a vegetação da estepe, através de detecção remota e do uso de imagens de observação da Terra de média resolução, em três distritos da Mongólia: Dzag, Buutsagaan e Khureemaral. Após terem sido considerados diferentes níveis de detalhe temático para classificar a vegetação da estepe, foi escolhido mapear os diferentes tipos de pastagens da estepe. De forma a investigar qual a combinação de dados que produz melhores resultados e qual o algoritmo de classificação mais apropriado para incorporar esses dados na classificação, foram testados e comparados diferentes métodos de classificação para a área de estudo. Para tal, foram realizadas dezasseis classificações utilizando diferentes combinações de estimadores, Landsat-8 (bandas espectrais e NDVI-derivado de Landsat-8) e dados geofísicos (altitude, precipitação média anual e temperatura média anual) com dois algoritmos de classificação, máxima verosimilhança e árvores de decisão. Os resultados revelam que o melhor modelo gerado para a árvore de decisão foi aquele que incorporava as bandas de Landsat-8 com a precipitação média anual e temperatura média anual (Modelo 13). Para a máxima verosimilhança, tanto o modelo que incorporava as bandas de Landsat-8 com a precipitação média anual (Modelo 5), como o que incorporava as bandas de Landsat-8 com a precipitação média anual e temperatura média anual (Modelo 13), obtiveram as acurácias mais elevadas para este algoritmo. Os modelos relativos à árvore de decisão obtiveram consistentemente melhores resultados do que aqueles que foram gerados pela máxima verosimilhança.

Palavras-chave: Detecção remota; Sistemas de Informação Geográfica; Landsat-8; dados geofísicos; máxima verosimilhança; árvore de decisão

Table of Contents

Acknowledgments v
Abstract vii
Resumo ix
Table of Contents xi
List of Figures xiii
List of Tables xvii
Acronyms xix
1. Introduction 21
1.1 Problem definition and previous approaches review 21
1.2 Scope and objectives 22
1.3 Thesis structure overview 23
2. Literature review 23
2.1 Mapping species composition and other grassland properties through remote sensing data: the importance of spatial resolution and field measurements 24
2.2 Mapping pasture types: satellite data, vegetation indices and geophysical factors 26
2.3 Classification algorithms 27
3. Study area and data 29
3.1 General characterization of the study area 29
3.2 Remotely sensed data 31
3.3 Geophysical data 33
3.3.1 Elevation data 33
3.3.2 Precipitation and temperature data 34
3.4 Data pre-processing 35
4. Methods 37
4.1 Selection of a suitable classification method 37
4.1.1 Main classes – Bare soil, water and vegetation 38
4.1.2 Steppe vegetation classification 41
4.2 Classification accuracy assessment 45
4.3 Overview on the applied methods 46
5. Results and Discussion 47
5.1 Classification of the main classes: bare soil, water and vegetation 47
5.2 Classification of the Pasture Steppe vegetation 52
5.2.1 Comparative analysis of different estimators 52
5.2.2 Comparative analysis of accuracy assessment 61
6. Conclusions 73
7. References 75
A. Annexes 81

List of Figures

Figure 2.1 - Composition of a decision tree. Retrieved from Friedl and Brodley, 1997 28

Figure 3.1 - Average summer temperature trend (1940-2005). Retrieved from Dagvadorj et al., 2009 30

Figure 3.2 - Average winter temperature trend (1940-2005). Retrieved from Dagvadorj et al., 2009..... 30

Figure 3.3 - Warm season precipitation trend (1940-2005). Retrieved from Dagvadorj et al., 2009 30

Figure 3.4 - Study area: Dzag, Khureemaral and Buutsagaan soums located in Bayankhongor aimag, Mongolia 31

Figure 3.5 - Landsat-8 OLI false-color image using OLI-5, OLI-6 and OLI-2 mapped to RGB for Dzag, Khureemaral and Buutsagaan 32

Figure 3.6 – Landsat-8 NDVI-derived with 30 m resolution for the study area 33

Figure 3.7 - Elevation data from SRTM with 30 m resolution for the study area 34

Figure 3.8 - Mean annual precipitation data from 1950 to 2000 with 1 km resolution for the study area 35

Figure 3.9 - Mean annual temperature data from 1950 to 2000 with 1 km resolution for the study area 35

Figure 4.1 – TWI derived from SRTM data set for the study area 39

Figure 4.2 – Selected TWI to fit “water and riparian vegetation” 40

Figure 4.3 –Vector mask covering “water and riparian vegetation” classes 40

Figure 4.4 - Flow chart representing the output models for the main classes (M1, M2, M3 and M4), created using Landsat-8 bands from OLI-1 to OLI-7 (M1) and the same bands with NDVI (M2); and using OLI-5, OLI-6 and OLI-7 (M3) and the same bands with NDVI (M4) 40

Figure 4.5 - Training points provided by the local users 42

Figure 4.6 - Testing points provided by the local users 42

Figure 4.7 - Flow chart for output models created with different combinations of datasets used for classifying the Pasture Steppe classes: bands OLI-2 to OLI-7 with NDVI, SRTM, mean annual (MA) precipitation and mean annual (MA) temperature. The arrows represent the addition of a new estimator or a new model. Each model represents a classification output by using one estimator (base model – M1) or by the addition of one or more estimators to the base model 44

Figure 4.8 - Overview on the methods used to classify the main classes and the steppe vegetation (*ML-maximum likelihood classifier; DT- decision tree classifier) 47

Figure 5.1 - Spectral signatures for the main classes using Landsat-8 bands: OLI-1, OLI-2, OLI-3, OLI-4, OLI-5, OLI-6 and OLI-7 – Model 1 49

Figure 5.2 - Spectral signatures for the main classes using Landsat-8 bands: OLI-1, OLI-2, OLI-3, OLI-4, OLI-5, OLI-6 and OLI-7 and NDVI [band 8] – Model 2 49

Figure 5.3 - Spectral signatures for the main classes using Landsat-8 bands: OLI-5, OLI-6 and OLI-7 – Model 3 50

Figure 5.4 - Spectral signatures for the main classes using Landsat-8 bands: OLI-5, OLI-6 and OLI-7 and NDVI [band 8] – Model 4 50

Figure 5.5 - Main classes using maximum likelihood - Model 4: Landsat-8 bands and NDVI 52

Figure 5.6 - Spectral signatures for the steppe vegetation classes using Landsat-8 bands: OLI-2, OLI-3, OLI-4, OLI-5, OLI-6 and OLI-7 – Model 1 58

Figure 5.7 - Spectral signatures for the steppe vegetation classes using Landsat-8 bands: OLI-2, OLI-3, OLI-4, OLI-5, OLI-6 and OLI-7 and NDVI [band 8] – Model 2 58

Figure 5.8 - Spectral signatures for the steppe vegetation classes using Landsat-8 bands: OLI-2, OLI-3, OLI-4, OLI-5, OLI-6 and OLI-7 and SRTM [band 8] – Model 3 59

Figure 5.9 - Spectral signatures for the steppe vegetation classes using Landsat-8 bands: OLI-2, OLI-3, OLI-4, OLI-5, OLI-6 and OLI-7 and mean annual precipitation (MA precip.) [band 8] – Model 5 59

Figure 5.10 - Spectral signatures for the steppe vegetation classes using Landsat-8 bands: OLI-2, OLI-3, OLI-4, OLI-5, OLI-6 and OLI-7 and mean annual temperature (MA temp.) [band 8] – Model 9 60

Figure 5.11 - “Desert steppe pasture” F1-scores for all tested models using decision tree and maximum likelihood 62

Figure 5.12 - “Steppe pasture” F1-scores for all tested models using decision tree and maximum likelihood 62

Figure 5.13 - “Medium high and low mountain steppe pasture” F1-scores for all tested models using decision tree and maximum likelihood 64

Figure 5.14 - “Mountain steppe pasture” F1-scores for all tested models using decision tree and maximum likelihood 65

Figure 5.15 - Steppe classification using maximum likelihood - Model 5: Landsat-8 bands, MA precipitation 69

Figure 5.16 - Steppe classification using decision tree - Model 5: Landsat-8 bands, MA precipitation 69

Figure 5.17 - Steppe classification using maximum likelihood - Model 13: Landsat-8 bands, MA precipitation and MA temperature 70

Figure 5.18 - Steppe classification using decision tree - Model 13: Landsat-8 bands, MA precipitation and MA temperature 70

Figure 5.19 - F1-scores weighted average for all tested models using decision tree and maximum likelihood 71

Figure A.1 - Main classes using maximum likelihood - Model 1: Landsat-8 bands 82

Figure A.2 - Main classes using maximum likelihood - Model 2: Landsat-8 bands and NDVI 82

Figure A.3 - Main classes using maximum likelihood - Model 4: Landsat-8 bands 5-6-7 and NDVI 83

Figure A.4 - Spectral signatures for the steppe vegetation classes using Landsat-8 bands: OLI-2, OLI-3, OLI-4, OLI-5, OLI-6 and OLI-7, NDVI [band 8] and SRTM [band 9] – Model 4 84

Figure A.5 - Spectral signatures for the steppe vegetation classes using Landsat-8 bands: OLI-2, OLI-3, OLI-4, OLI-5, OLI-6 and OLI-7, NDVI [band 8] and mean annual precipitation (MA precip.) [band 9] – Model 6 84

Figure A.6 - Spectral signatures for the steppe vegetation classes using Landsat-8 bands: OLI-2, OLI-3, OLI-4, OLI-5, OLI-6 and OLI-7, SRTM [band 8] and mean annual precipitation (MA precip.) [band 9] – Model 7 85

Figure A.7 - Spectral signatures for the steppe vegetation classes using Landsat-8 bands: OLI-2, OLI-3, OLI-4, OLI-5, OLI-6 and OLI-7, NDVI [band 8], SRTM [band 9] and mean annual precipitation (MA precip.) [band 10] – Model 8 85

Figure A.8 - Spectral signatures for the steppe vegetation classes using Landsat-8 bands: OLI-2, OLI-3, OLI-4, OLI-5, OLI-6 and OLI-7, NDVI [band 8] and mean annual temperature (MA temp.) [band 9] – Model 10 86

Figure A.9 - Spectral signatures for the steppe vegetation classes using Landsat-8 bands: OLI-2, OLI-3, OLI-4, OLI-5, OLI-6 and OLI-7, SRTM [band 8] and mean annual temperature (MA temp.) [band 9] – Model 11 86

Figure A.10 - Spectral signatures for the steppe vegetation classes using Landsat-8 bands: OLI-2, OLI-3, OLI-4, OLI-5, OLI-6 and OLI-7, NDVI [band 8], SRTM [band 9] and mean annual temperature (MA temp.) [band 10] – Model 12 87

Figure A.11 - Spectral signatures for the steppe vegetation classes using Landsat-8 bands: OLI-2, OLI-3, OLI-4, OLI-5, OLI-6 and OLI-7, mean annual precipitation (MA precip.) [band 8] and mean annual temperature (MA temp.) [band 9] – Model 13 87

Figure A.12 - Spectral signatures for the steppe vegetation classes using Landsat-8 bands: OLI-2, OLI-3, OLI-4, OLI-5, OLI-6 and OLI-7, NDVI [band 8], mean annual precipitation (MA precip.) [band 9] and mean annual temperature (MA temp.) [band 10] – Model 14 88

Figure A.13 - Spectral signatures for the steppe vegetation classes using Landsat-8 bands: OLI-2, OLI-3, OLI-4, OLI-5, OLI-6 and OLI-7, SRTM [band 8], mean annual precipitation (MA precip.) [band 9] and mean annual temperature (MA temp.) [band 10] – Model 15 88

Figure A.14 - Spectral signatures for the steppe vegetation classes using Landsat-8 bands: OLI-2, OLI-3, OLI-4, OLI-5, OLI-6 and OLI-7, NDVI [band 8] SRTM [band 9], mean annual precipitation (MA precip.) [band 10] and mean annual temperature (MA temp.) [band 11] – Model 16 89

Figure A.15 - Steppe classification using maximum likelihood - Model 1: Landsat-8 bands 90

Figure A.16 - Steppe classification using decision tree - Model 1: Landsat-8 bands 90
Figure A.17 - Steppe classification using maximum likelihood - Model 2: Landsat-8 bands and NDVI..... 91
Figure A.18 - Steppe classification using decision tree - Model 2: Landsat-8 bands and NDVI..... 91
Figure A.19 - Steppe classification using maximum likelihood - Model 3: Landsat-8 bands and SRTM 92
Figure A.20 - Steppe classification using decision tree - Model 3: Landsat-8 bands and SRTM 92
Figure A.21 - Steppe classification using maximum likelihood - Model 4: Landsat-8 bands, NDVI and SRTM 93
Figure A.22 - Steppe classification using decision tree - Model 4: Landsat-8 bands, NDVI and SRTM..... 93
Figure A.23 - Steppe classification using maximum likelihood - Model 6: Landsat-8 bands, MA precipitation and NDVI 94
Figure A.24 - Steppe classification using decision tree - Model 6: Landsat-8 bands, MA precipitation and NDVI 94
Figure A.25 - Steppe classification using maximum likelihood - Model 7 Landsat-8 bands, MA precipitation and SRTM..... 95
Figure A.26 - Steppe classification using decision tree - Model 7 Landsat-8 bands, MA precipitation and SRTM..... 95
Figure A.27 - Steppe classification using maximum likelihood - Model 8: Landsat-8 bands, MA precipitation, NDVI and SRTM 96
Figure A.28 - Steppe classification using decision tree - Model 8: Landsat-8 bands, MA precipitation, NDVI and SRTM..... 96
Figure A.29 - Steppe classification using maximum likelihood - Model 9: Landsat-8 bands, MA temperature 97
Figure A.30 - Steppe classification using decision tree - Model 9: Landsat-8 bands, MA temperature..... 97
Figure A.31 - Steppe classification using maximum likelihood - Model 10: Landsat-8 bands, MA temperature and NDVI 98
Figure A.32 - Steppe classification using decision tree - Model 10: Landsat-8 bands, MA temperature and NDVI 98
Figure A.33 - Steppe classification using maximum likelihood - Model 11: Landsat-8 bands, MA temperature and SRTM..... 99
Figure A.34 - Steppe classification using decision tree - Model 11: Landsat-8 bands, MA temperature and SRTM..... 99
Figure A.35 - Steppe classification using maximum likelihood - Model 12: Landsat-8 bands, MA temperature, NDVI and SRTM 100
Figure A.36 - Steppe classification using decision tree - Model 12: Landsat-8 bands, MA temperature, NDVI and SRTM..... 100
Figure A.37 - Steppe classification using maximum likelihood - Model 14: Landsat-8 bands, MA precipitation, MA temperature, NDVI..... 101
Figure A.38 - Steppe classification using decision tree - Model 14: Landsat-8 bands, MA precipitation, MA temperature, NDVI 101
Figure A.39 - Steppe classification using maximum likelihood - Model 15: Landsat-8 bands, MA precipitation, MA temperature, SRTM 102
Figure A.40 - Steppe classification using decision tree - Model 15: Landsat-8 bands, MA precipitation, MA temperature, SRTM 102
Figure A.41 - Steppe classification using maximum likelihood - Model 16: Landsat-8 bands, MA precipitation, MA temperature, NDVI, SRTM..... 103
Figure A.42 - Steppe classification using decision tree - Model 16: Landsat-8 bands, MA precipitation, MA temperature, NDVI, SRTM..... 103

List of Tables

Table 3.1 - Landsat-8 OLI available bands for this work: description, wavelength and resolution. Adapted from Roy et al., 2014.....31

Table 4.1 - Weighting for each pasture class based on the real area extent per class used for calculate F1-scores weighted averages 46

Table 5.1 - Accuracy report for the main classes classification using maximum likelihood for Model 1, Model 2, Model 3 and Model 4 51

Table 5.2 - Increasing (+) and decreasing (-) classification accuracies generated by the addition of Landsat-8 NDVI-derived: comparison of pairs of models with and without NDVI.....54

Table 5.3 - Increasing (+) and decreasing (-) classification accuracies generated by the addition of SRTM data set: comparison of pairs of models with and without SRTM.....55

Table 5.4 - Increasing (+) and decreasing (-) classification accuracies generated by the addition of mean annual precipitation data set: comparison of pairs of models with and without mean annual precipitation…….. 56

Table 5.5 - Increasing (+) and decreasing (-) classification accuracies generated by the addiction of mean annual temperature data set: comparison of pairs of models with and without mean annual temperature 57

Table 5.6 - Accuracy report for the classification of the Pasture Steppe vegetation for the best F1-scores weighted average: Model 5 and Model 13 for maximum likelihood and Model 13 for decision tree (highlighted in blue) 63

Table 5.7 – Mapped areas per class and classified area in proportion to real area extent for the best performing models (highlighted in blue): Model 5 and Model 13 using maximum likelihood and decision tree 68

Table A.1 - Accuracy report of the Pasture Steppe using maximum likelihood and decision tree classifiers for Model 1, Model 2 and Model 3.....104

Table A.2 - Accuracy report of the Pasture Steppe using maximum likelihood and decision tree classifiers for Model 4, Model 6 and Model 7.....105

Table A.3 - Accuracy report of the Pasture Steppe using maximum likelihood and decision tree classifiers for Model 8, Model 9 and Model 10.....106

Table A.4 - Accuracy report of the Pasture Steppe using maximum likelihood and decision tree classifiers for Model 11, Model 12 and Model 14.....107

Table A.5 - Accuracy report of the Pasture Steppe using maximum likelihood and decision tree classifiers for Model 15 and Model 16 108

Acronyms

ASTER - Advanced Spaceborn Thermal Emission and Reflection Radiometer

ADB - Asian Development Bank

AGB - Above Ground Biomass

AVHRR - Advanced Very High Resolution Radiometer

AVIS-2 - Visible/Infrared Imaging Spectrometer

DEM – Digital Elevation Model

DM - Drought Monitoring

EO - Earth Observation

EOTAP - Earth Observation for a Changing Asia Pacific

EVI - Enhanced Vegetation Index

GIS – Geographic Information System

GPS - Global Positioning System

HRV - High Resolution Visible

JFPR - Japan Fund for Poverty Reduction

LAI – Leaf Area Index

Landsat MSS – Landsat Multispectral Scanner

Landsat TM – Landsat Thematic Mapper

Landsat-7 ETM+ - Landsat-7 Enhanced Thematic Mapper Plus

Landsat-8 OLI – Landsat-8 Operational Land Imager

LULC – Land Use/ Land Cover

MODIS - Moderate-Resolution Imaging Spectroradiometer

NDVI – Normalized Difference Vegetation Index

NIR – Near-infrared

Qgis - Quantum GIS

RGB - Red-Green-Blue

RS – Remote sensing

ROI – Region of Interest

SPOT - Satellite for Earth Observation. From French: *Satellite Pour l'Observation de la Terre*

SRTM - Shuttle Radar Topographic Mission

TWI - Topographic Wetness Index

1. Introduction

1.1 Problem definition and previous approaches review

The vast grasslands of Mongolia are part of the steppe that is located between forest and desert belts of Inner Asia and Central Asia (Sutie *et al*., 2005). Steppe vegetation is determined by climatic and edaphic factors which promote grasses and associated herbaceous plants growth and prevent dominance of woody plants, such as trees and shrubs (Wallis de Vries *et al*., 1996). Mongolian steppes occur at a semi-arid climate and are among the largest contiguous expanses of grassland in the world, encompassing a region of considerable ecological importance (Badarch *et al*., 2009).

Grasslands in Mongolia cover 1 210 000 km^2 (around 80 percent of the land area of the country) (Sutie *et al*., 2005) and support around 30 million head of domestic livestock, including camels, cattle, yaks, horses, sheep and goats and also populations of wild ungulates (Fernandez-Gimenez and Allen-Diaz, 2001). Mongolia has an extensive livestock production which constitutes the main economic activity in the country (Sutie *et al*., 2005).

Grasslands in arid and semi-arid regions are facing desertification or degradation processes caused by climate change and human activities (He *et al*., 2005), leading to negative impacts on herder livelihoods, carbon sequestration and biodiversity conservation (Jun Wang *et al*., 2014). Since 1940 average temperature in Mongolia has increased by more than 2 ºC and total precipitation dropped by 7% (16 mm), causing that Mongolia's fragile steppe ecosystem to degrade at a rapid rate (Badarch *et al*., 2009). As a consequence of climate change, there has been an increased frequency of droughts occurrence in Mongolia, causing decreases in phytomass and changes in phenology (Shinoda *et al*., 2010). The occurrence of droughts during the early growth may cause vegetation to die before reaching maturity, shortening the growth period and decrease net primary production (Shinoda *et al*., 2007). Additionally, in the last 70 years, population density increased by more than threefold and total livestock numbers by more than 2,3-fold interfering with ecological balance and causing problems like overgrazing, which accelerated vegetation degradation (Karnieli *et al*., 2013).

The occurrence of land degradation in large areas is problematic because the resources (money, personnel and technology) available are limited (He *et al*., 2005). Monitoring and managing these processes within grasslands using field surveys for mapping vegetation might be difficult to accomplish, since these are expensive, manpower-demanding, time consuming (Karnieli *et al*., 2013) and may be incompatible with the increasing demand for precisely located spatial data of natural sites (Král and Pavlis, 2006). For this reason, satellite remote sensing has been widely used for a large number of vegetation applications (Karnieli *et al*., 2013).

Remote Sensing (RS) and Geographic Information System (GIS) provide the tools for advanced ecosystem management (Koirala, 2010). RS methods have been widely used for monitoring and management of pasture resources and GIS has become the most powerful tool

for providing information about grassland resource inventories and integration of data and mechanisms for analysis, modeling and forecasting. In order to offer the decision-makers the best tools and data to support their decision making process, it is important to define and classify accurately the land cover (Rodriguez, 2014). Satellite remote sensing data can provide data sources for large areas in land cover classification (Kawamura and Akiyama, 2010) . For mapping pasture resources, thematic information may be generated by applying image classification using parametric, non-parametric algorithms or a combination of both (Amarsaikhan and Sato, 2003).

However, there are many factors that can affect the success of a classification procedure, such as the complexity of the landscape in a study area, selected remotely sensed data, image pre-processing and classification approaches. For this reason, classifying remotely sensed data into a thematic map still remains a challenge. Although much research concerned with image classification has been done previously, the continuous emergence of new classification algorithms and techniques demand continuous reviews for guiding and selecting suitable classification procedures for specific studies (Lu and Weng, 2007).

The major problem tackled in this study, concerns the thematic level of detail for mapping vegetation, which is dependent on the imagery spatial resolution of the remotely sensed data. In order to provide information for livestock management resources, mapping vegetation species composition can provide the most detailed information for this purpose. However, since species composition varies within the different pasture types, influenced by geophysical factors, mapping these features can also provide important information. Additionally, mapping grassland properties could indicate which areas are more or less productive for livestock, helping on the definition of emergency grazing reserves (grazing areas in a good state for livestock production that can be used when droughts occur or when overgrazed areas are prominent).

1.2 Scope and objectives

This thesis was motivated and developed under the project “Climate-resilient rural livelihoods in Mongolia” that supports EOTAP (Earth Observation for a Changing Asia Pacific) and conducted at DEIMOS Engenharia SA company. The project aims to help the Mongolian Governmental Agencies to develop a sustainable, climate proof livestock sector, able to overcome the productivity and income loss problems, related to overgrazing and climate change, though Earth Observation (EO) services, that include a Land Use/ Land Cover (LULC) service and a Drought Monitoring (DM) service.

The current study is linked to the LULC mapping service that complements a previous Asian Development Bank (ADB) project funded by the Japan Fund for Poverty Reduction (JFPR), where some non-EO pasture type condition maps for Bayankhongor were already developed to help the local users to implement pasture management measures. The goal of this thesis is to map the steppe vegetation into relevant thematic classes, capable of providing information for the definition of areas to set aside as emergency grazing reserves by the local users, in three districts

(*soums*) - Dzag, Khureemaral and Buutsagaan – within Bayankhongor province (*aimag)*, Mongolia.

The main objectives of this study are:

1. To find out the higher thematic detail to map the steppe vegetation through remote sensing data, to serve the purpose of defining emergency grazing reserves for the livestock.
2. To compare different combinations of Landsat-8 (spectral bands and Landsat-8 NDVI-derived) and geophysical data (including elevation, mean annual precipitation and mean annual temperature data), using two classification algorithms, in order to investigate which combination of data sets yields the best results and which classification algorithm is more suitable for incorporating these data sets when performing the classification.

1.3 Thesis structure overview

This thesis is divided into six chapters. Chapter 1 is an introductory chapter that presents the problem definition and previous approaches review, scope and objectives and the current thesis structure overview. Chapter 2 contains a literature review divided into three sections. The first provides information about the importance of imagery spatial resolution and field measurements, for mapping species composition and other pasture vegetation properties, that could be of importance for the definition of livestock emergency grazing areas. The second section focus on different procedures for mapping pasture types and the third section presents a review about classification algorithms.

Chapter 3 is also divided into three sections. The first gives a general overview about the study area. The second and third sections describe the collected data for performing the LULC classification. Chapter 4 presents the adopted methodology and the procedures to achieve the goal and objectives of this thesis. Chapter 5 describes the results and discussion obtained for the LULC classification, through a comparison analysis between the selected data sets and classification algorithms. Chapter 6 presents the main conclusions, summarizing the developed work, main results and limitations. At the end, recommendations for future research developments are given.

2. Literature review

2.1 Mapping species composition and other grassland properties through remote sensing data: the importance of spatial resolution and field measurements

Spatial dimension of key land elements may range from less than one meter to more than one kilometer, depending on the potential of the optical satellite imagery used in the classification. A key land element is defined as a physical component of the land that characterizes one or more land cover classes. Therefore, the capacity to detect all of the key land elements is strongly correlated with the spatial resolution of the RS data. If the pixel spatial resolution is larger than the dimension of the land elements, it is not possible to detect the single land elements (Martinez and Mollicone, 2012) .

For instance, using a coarse resolution sensor (250-1000 m), such as NOAA-AVHRR (National Oceanic and Atmospheric Administration- Advanced Very High Resolution Radiometer), SPOT (satellite for EO. From French: *Satellite Pour l'Observation de la Terre*,) or Terra-MODIS (Moderate-Resolution Imaging Spectroradiometer), the potentially identifiable key land elements are only broad land cover patterns. Whereas if medium resolution sensor (30-60 m) is used, such as Landsat MSS (MultiSpectral Scanner), Landsat TM (Thematic Mapper), Landsat ETM+ (Enhanced Thematic Mapper Plus) or Landsat OLI (Operational Land Imager), separating extensive masses of evergreen and deciduous forest becomes possible. And by using high resolution sensors (10-30 m), such as Terra-ASTER (Advanced Spaceborn Thermal Emission and Reflection Radiometer) or SPOT-4 HRV (High Resolution Visible), or very high (<10 m) resolution sensors, such as SPOT-5, IKONOS or QuickBird, recognizing large individual trees becomes possible (Martinez and Mollicone, 2012).

Concerning the land use category grassland, the land elements are grasses and shrubs (Martinez and Mollicone, 2012). In fact, even for very high resolution it is difficult to achieve good results in discriminating species composition. For instance, Schmidtlein and Sassin (2004), used Airborne Visible/Infrared Imaging Spectrometer (AVIS-2) with a pixel size of 2 by 2 m, but the models obtained for the cover of single species proved to be weak. Reflectance of vegetation is very complex, because it depends on variables, like plant health, physical and chemical vegetation structure. For this reason, it is only partially correlated with plant species composition, making it the most difficult vegetation attribute to detect with remote sensing techniques (Lewis, 1998).

Apart from species composition, it is important to consider other grassland properties, because they can be used to define areas of major interest within the grasslands and may be important indicators for the classification procedure. Different grassland properties have been quantified from remotely sensed data, including grass cover and its temporal change, grassland biomass, yield and grassland degradation. Quantification of other grassland features, like productivity and carrying capacity, rely on environmental variables that cannot be acquired directly from remotely sensed data. These features require data that is difficult to obtain without field observations and ground sampling (e.g. soil fertility and moisture content) (Gao, 2006).

Zha *et al*. (2003) attempted to apply a reflectance-based method to quantify percent grass cover from Landsat TM data for a semi-arid grassland. Field measurements for the spectral reflectance of grass were made at 68 random sites and each location was determined with a portable Global Positioning System (GPS). Results showed that percent grass cover sampled on the ground does not verify a statistically significant relationship with the value of its corresponding pixel value on TM-derived Normalized Difference Vegetation Index (NDVI) image. The authors concluded that it was impossible to quantify percent grass cover using this sample point method directly. The main explanation for this, is that *in situ* grass cover measurement was made in a sampling plot of 1 m^2, while NDVI pixel value is based on a ground area of 30 by 30 m^2, making very unlikely that the site at which ground cover was sampled is representative at the entire pixel area. Also, NDVI values derived from satellite image range from 0,4067 to 0,5805, much narrower than from *in situ* measurements, ranging within 0,2898 to 0,6283. However, satisfactory results were obtained when the spectral reflectance data measured with the field spectrometer was used to calibrate satellite data (R^2 = 0,74).

Liu *et al*. (2005) used a similar methodology to study grassland cover density in an alpine meadow soil. Similar results were obtained showing that *in situ* sampled grass cover and their corresponding pixel values on the NDVI image were weakly correlated. After calibrating satellite data with the spectral reflectance data, a strong linear regression relationship (R^2 = 0,745) was established. These results reveal the need for combining remotely sensed data with *in situ* sampling and locating ground samples on geometrically rectified satellite images.

Karnieli *et al*. (2013) studied the reliability of remote sensing vegetation indices to provide information about the effect of grazing on vegetation degradation. This research was taken along the Mongolian pastures in six study sites, three of them located within the mountain steppe zone and the other three at the steppe zone. Each site consisted in pairs of study polygons comprising an ungrazed (fenced-off) area and a heavily grazed area (outside the fences). The selected vegetation index was the Enhanced Vegetation Index (EVI), in order to reduce the soil background and atmospheric effects throughout the entire study area and also because it is more sensitive to variations in leaf cellular structure, expressed in the near infrared (NIR) portion of the spectrum. Four Landsat-7 ETM+ images were used to create a continuous scene and EVI was computed from reflectance values. Ground truth data was collected to provide information about biophysical variables (plant density, species composition, above ground biomass (AGB), and percentage cover) and plant spectral reflectance. Field observations showed that plant density, AGB and percentage cover values were significantly higher in the ungrazed areas than in the grazed ones, as expected. However, the grazed areas showed significantly higher EVI values than the ungrazed areas, consistently in each of the study sites. This result was found to be linked with the presence of unpalatable species that invaded into the grazed areas, which promoted the shifting of dominant species composition from “climax” species, like perennial grasses and forbs, to unpalatable forbs and weedy annuals, which have a denser leaf structure and therefore inducing higher spectral responses in near-infrared (NIR) region.

Imagery spatial resolution also plays an important role in obtaining a reliable quantification of grassland properties. For instance, spatial resolutions suitable for estimating Leaf Area Index (LAI) lie between 2 and 18 m (being the most accurate at 2 and 5 m). Also, the ratio of NIR and visible reflectance is considered a poor predictor of LAI or biomass (Sellers, 1985). (Phinn *et al*., 1996) used high spatial resolution Airborne Digital Video Imagery to map AGB for five major semi-arid plant communities in New Mexico. Results show that beyond 2 to 4 m pixel size, shrub forms became unrecognizable. Variations in NDVI values due to spatial differences in vegetation cover, biomass and/or vigor conditions were evident at larger pixel sizes, however NDVI patterns become undistinguishable for detecting biomass from 4,6 m pixel size in the more continuously covered grassland. Up to 8 m pixel sizes features larger than individual shrubs were evident, including bare and vegetated areas and soil.

2.2 Mapping pasture types: satellite data, vegetation indices and geophysical factors

The use of high resolution remotely sensed data presents some disadvantages associated with infrequent coverage, high costs and high data volume. Consequently, coarse and medium resolution satellites have been used by researchers for producing regional scale land cover classifications (Wang and Tenhunen, 2004). Monitoring land cover requires spectral coverage and resolution that is well suited for vegetation characterization. For this tasks, spectral coverage in the visible, near infrared and shortwave infrared are required (Wulder *et al*., 2008). Landsat data provides medium resolution data with no costs for the users. Throughout more than 40 years, Landsat mission has demonstrated capabilities for mapping and monitoring land cover and its value is well established (Roy et al., 2014).

A vegetation index consists on a simple and effective measurement used to access earth's surface vegetation in remote sensing. There are several indices for highlighting vegetation features (Gandhi *et al*., 2015). The Normalized Difference Vegetation Index (NDVI) is one of the most commonly used remote sensing derived measurement (Yu *et al*., 2003). It is calculated as a ratio difference between red and near-infrared (NIR) bands, either from the digital number or reflectance values (Liu *et al*., 2003). NDVI data can be combined with satellite data for improving classification's accuracy, for instance, Gandhi et al. (2015) used Landsat TM data along with satellite NDVI-derived and elevation data, to perform a land cover classification of Vellore District. Sivanpillai *et al*., 2009 verified that the predictive ability for the estimation of sagebrush cover categories using vegetation indices, including NDVI, was 1% higher than the predictive ability of Landsat TM spectral bands over a semi-arid ecosystem in Western US.

Pasture types distribution are strongly influenced by geographic features and their impacts on climate (Yu *et al*., 2003) being mainly affected by elevation, temperature and precipitation (Wen *et al*., 2010). Several studies show improvements when remotely sensed data is combined with geophysical data. For instance, Liu *et al*., 2003 stacked three geophysical data sets (elevation, mean annual precipitation and mean annual temperature) together with Advanced

Very High Resolution Radiometer (AVHRR) and AVHRR NDVI-derived data after dividing China into nine bio-climatic regions. The nine land-cover maps for individual regions of China were then assembled. Results showed that the combination of remotely sensed data with geophysical data sets can improve the classification of spatial patterns of vegetation distribution and contribute for the reduction of confusion in the land cover classification.

Liu *et al*. (1998) verified an improvement on land cover classification of Northeast China, when geophysical data (precipitation, temperature and elevation) was added to an AVHRR image, compared to a conventional classification method using only AVHRR data. Cibula and Nyquist (1987) verified that an increase on the number of land cover classes that could be differentiated using terrain, temperature and precipitation resulted on an improvement of classification's accuracy. Liu *et al*. (1998) combined a model that described the relationships between land cover, slope and elevation, that resulted on an accuracy improvement for the vegetation classification using Landsat TM spectral data on Helan Mountain in China (Liu *et al*., 2003).

2.3 Classification algorithms

GIS plays an important role in developing knowledge-based classification approaches because of its capability of managing different sources of data and spatial modelling. As different types of ancillary data, such as: Digital Elevation Model (DEM), soil map, precipitation and temperature, become available they can be incorporated into the classification procedure. This leads to the possibility of separating vegetation classes using data on terrain features or using temperature, precipitation and soil data to predict land cover distribution at a large scale. Including these relationships in a classification procedure has proven to be effective in improving classification accuracy. A critical step is to develop approaches to identify the best appropriate variables that are most useful in separating land cover classes. The success of an image classification depends mostly on the availability of high-quality remotely sensed imagery and ancillary data, the design of a proper classification procedure, and the analyst's skills and experiences (Lu and Weng, 2007).

Per-pixel classifiers typically develop a signature through the combination of the spectra of all training-set pixels from a given feature. This signature contains the contributions of all the materials present in training pixels. It does not take into account the impact of mixed pixels. Per pixel classification algorithms can be parametric or non-parametric, such as maximum likelihood, minimum distance, artificial neural network, decision tree and support vector machine (Lu and Weng, 2007).

The maximum likelihood classifier is widely used for mapping land cover features. It is based on the assumption that the members of each class follow a Gaussian frequency distribution, that evaluates the membership probability of an unknown pixel to be assigned to a given class. Each pixel is assigned to a class for which it has the highest membership probability

value. This classifier involves the estimation of class mean vectors and covariance matrices from the training data (Pal and Mather, 2003).

When multisource data is used in a classification procedure, parametric algorithms, such as maximum likelihood, are typically not appropriated. Non-parametric classifiers are especially suitable for the incorporation of non-remote-sensing data into the classification procedure, because no statistical parameters are needed to separate image classes (Lu and Weng, 2007).

One of the most commonly used non-parametric classifiers is the decision tree classifier. The decision tree uses a multi-stage or sequential approach to the problem. Unlike conventional statistical classifiers, the labeling process is based on simple decisions based on the results of sequential tests, rather than a simple complex decision (Pal and Mather, 2003).

The decision tree classification procedure consists on a recursively partition of a data set into smaller homogeneous subdivisions on the basis of tests defined at each node in the tree, applied to one or more feature values. Figure 2.1, defines the composition of a tree, where each box is a node at which tests (T) are applied to recursively split data into successively smaller groups. The labels (A, B, C) at each leaf node refer to the class label assigned to each observation (Friedl and Brodley, 1997).

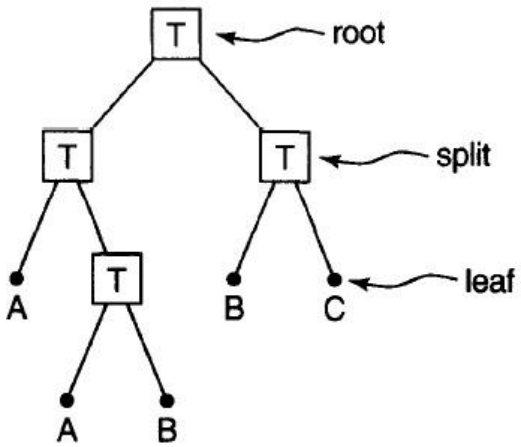

Figure 2.1 - Composition of a decision tree. Retrieved from Friedl and Brodley, 1997

There are univariate and multivariate decision trees. The univariate decision tree is one in which the decision boundaries of each node are defined by the outcome of a test applied to a single feature evaluated at each node. The characteristics of the decision boundaries are estimated empirically from the training data. The test outcome splits the data into two or more subsets. Each test has a discrete number of outcomes. The input data is recursively partitioned until a leaf node is reached and the class label is assigned to the observation. For cases when the locations of decision boundaries in feature space can only be properly defined in terms of combinations of features, the univariate tree is not appropriated (Pal and Mather, 2003).

The multivariate decision tree is a more complex tree, than the univariate which introduces factors that can affect their performance. It allows the extension of the splits to include

linear combinations of features. A set of linear discriminant functions is estimated at each node of the multivariate tree. Also, any number of different algorithms can be used to estimate the splitting rule. When different classification algorithms are used at different nodes it is called a hybrid decision tree (Pal and Mather, 2003).

3. Study area and data

3.1 General characterization of the study area

Mongolia is located in central Asia, being bounded on the north by Russia and on the east, south and west by China. It has a total area of 1 565 000 km^2. The topography of Mongolia consists mainly of a vast plateau with an elevation that ranges from 914 to 1524 m, with mountain ranges in the north and west reaching to heights of 4267 m above sea level (Dagvadorj *et al*., 2009).

There are six vegetation zones in Mongolia based on different elevation, precipitation distribution and soil type: alpine tundra (3,0% of the area), mountain taiga (4,1%), mountain steppe (25,1%), steppe (26,1%), desert steppe (27,2%) and desert (14,5%). Biological yield of Mongolian pastures can range from 1050-1500 kg/ha in high mountain, to 650-1300 kg/ha in steppe and to 290-380 kg/ha in desert steppe. Vegetation growing season is short and very dependent on climate, particularly rainfall. New growth in the northern mountainous areas begins in mid-April, but on other regions it may not begin until mid-May. Some of the pasture species reach their final growth stage in August, but others may continue its vegetative growth until mid-September or remain green until October (Damiran, 2005).

The climate is cold semi-arid and markedly continental (Sutie *et al*., 2005) characterized by short hot summers, in which falls most of the annual precipitation (85-90% in June, July and August) (Dagvadorg *et al*., 2001) and long cold winters. Winter and spring are both typically windy and cold. In early summer and spring frequently occur severe droughts and strong winds (with velocities exceeding 20 m/s) (Sutie *et al*., 2005), that may cause low productivity of vegetation in this area. Increases in spring temperature may stimulate earlier vegetation photosynthesis activity and, at the same time, increase the water stress in arid and semi-arid ecosystems (Dagvadorg *et al*., 2001).

Figures 3.1 and 3.2 show the increase registered on average temperature in summer and winter seasons, respectively. Figure 3.3 presents the 16 mm decrease on average precipitation registered in Mongolia, from 1940 to 2005 (Dagvadorj *et al*., 2009). In Bayankhongor, summer temperatures increased significantly from 1984 to 2003 in mountain steppe, steppe and desert steppe, spring temperatures also increased (Khishigbayar *et al*., 2015).

The study area consists of three *soums*: Dzag (46°56'N, 99°9'E), Khureemaral (46°24'N, 98°17'E) and Buutsagaan (46°10'N, 98°41'E) located in Bayankhongor *aimag*, Mongolia (Figure 3.4). Dzag has a total land area of 432800 ha; Khureemaral, 584000 ha; and Buutsagaan, 256100 ha. A document provided by the local users shows the existing pasture types within the steppe and also the main vegetation species composition.

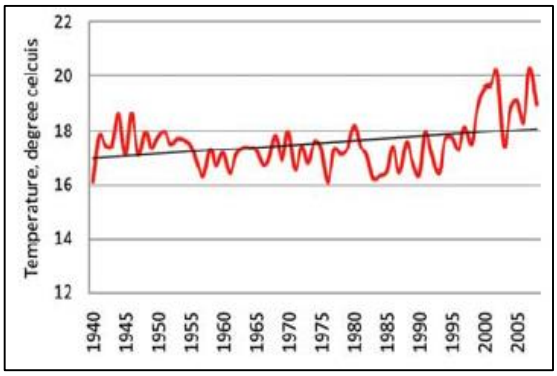

Figure 3.1 - Average summer temperature trend (1940-2005). Retrieved from Dagvadorj *et al*., 2009

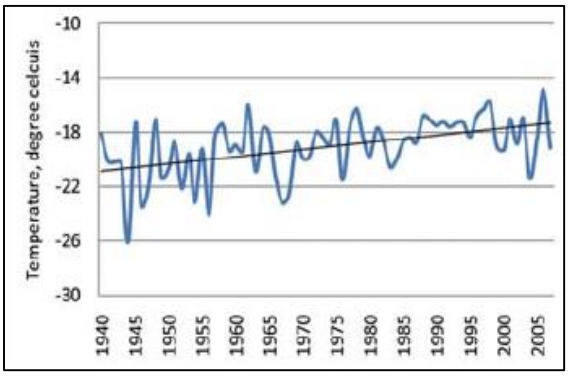

Figure 3.2 - Average winter temperature trend (1940-2005). Retrieved from Dagvadorj *et al*., 2009

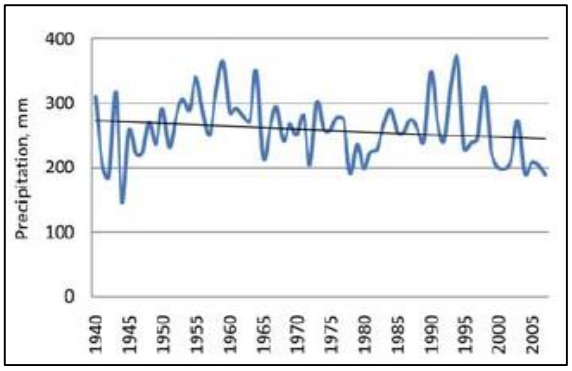

Figure 3.3 - Warm season precipitation trend (1940-2005). Retrieved from Dagvadorj *et al*., 2009

Dzag has 88 km^2 of high mountain pasture, mainly dominated by *Festuca lenensis*. The mountain steppe pasture covers an area of approximately 1426 km^2 , having *Festuca lenensis*, *Stipa krilovii* and *Artemisa frigida* as the dominant species. The steppe pasture covers an area of 779 km^2 and it is mainly composed by *Leymus chinensis*, *Festuca lenensis* and *Stipa orientalis*. Interzonal river valleys and depressions meadow pasture occupies an area of 237 km^2, being mainly composed by *Artemisa frigida*.

Khureemaral has 1571 km^2 of medium high and low mountain steppe pasture with *Festuca lenensis*, *Artemisa frigida* and *Stipa krilovii*. The steppe pasture covers an area of 1990 km^2, being mainly composed by *Stipa krilovii*, *Stipa capilata*, *Artemisa frigida*, *Agropyron cristatum*, *Leymus chinensis* and *Festuca lenensis*. The desert steppe pasture occupies 611 km^2 and it is mainly dominated by *Stipa gobica* and *Artemisa frigida*. It also contains interzonal river valleys and depressions meadow pasture, with *Achnatherum slendens*, *Allium polyrrhizum* and *Kalidium gracile*, covering an area of 159 km^2.

Buutsagaan has 2362 km^2 occupied by medium high and low mountain steppe pasture, mainly composed by *Festuca lenensis*, *Stipa gobica*, *Caragana pygmaea* and *Artemisa frigida*. The steppe pasture covers 1051 km^2 with *Festuca lenensis*, *Stipa krilovii* and *Caragana pygmaea*. The desert steppe pasture covers 1712 km^2, being mainly composed by *Stipa gobica*, *Anabasis brevifolia*, *Allium polyrrhizum*, *Caragana pygmaea*, *Cleistogenes squarrosa*, *Artemisa xerophytica* and *Ajiana fruticosa*. The gobi desert pasture occupies 30 km^2 and it is composed by *Anabasis brevifolia* and *Allium polyrrihizum*. Interzonal river valleys and depressions meadow pasture occupies 166 km^2 within the *soum* and it is mainly composed by *Allium polyrrhizum*, *Kalidium gracile* and *Achnatherum splendens*.

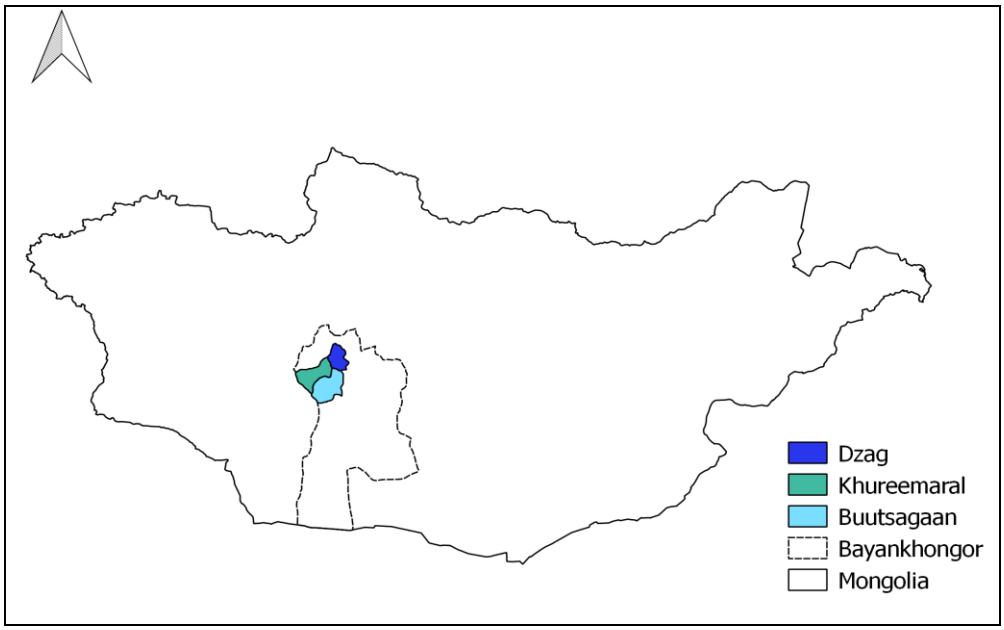

Figure 3.4 - Study area: Dzag, Khureemaral and Buutsagaan soums located in Bayankhongor aimag, Mongolia

3.2 Remotely sensed data

The imagery used for the classification consists of Landsat-8 OLI seven bands with 30 m resolution, retrieved from earthexplorer.usgs.gov. The image is from 30 August 2014, corresponding to the summer season. The Landsat-8 imagery contains the spectral information of seven bands, as listed in Table 3.1.

Table 3.1 - Landsat-8 OLI available bands for this work: description, wavelength and resolution. Adapted from Roy *et al*., 2014*.*

Band description	Wavelength (μm)	Resolution (m)
OLI-1 – blue	0,43 – 0,45	30
OLI-2 - blue	0,45 – 0,51	30

OLI-3 – green	0,53 – 0,59	30
OLI-4 – red	0,64 – 0,67	30
OLI-5 – near infrared	0,85 – 0,88	30
OLI-6 – shortwave infrared	1,57 – 1,65	30
OLI-7 – shortwave infrared	2,11 – 2,29	30

The Landsat-8 false-color image using OLI-5, OLI-6 and OLI-2 mapped to Red-Green-Blue (RGB), is presented in Figure 3.5. In this false-color composite, healthy vegetation appears in shades of orange; green represents sparse grasslands; soils appear in shades of browns and purples; and clear deep water is very dark. Google Earth was used to visually confirm these assumptions.

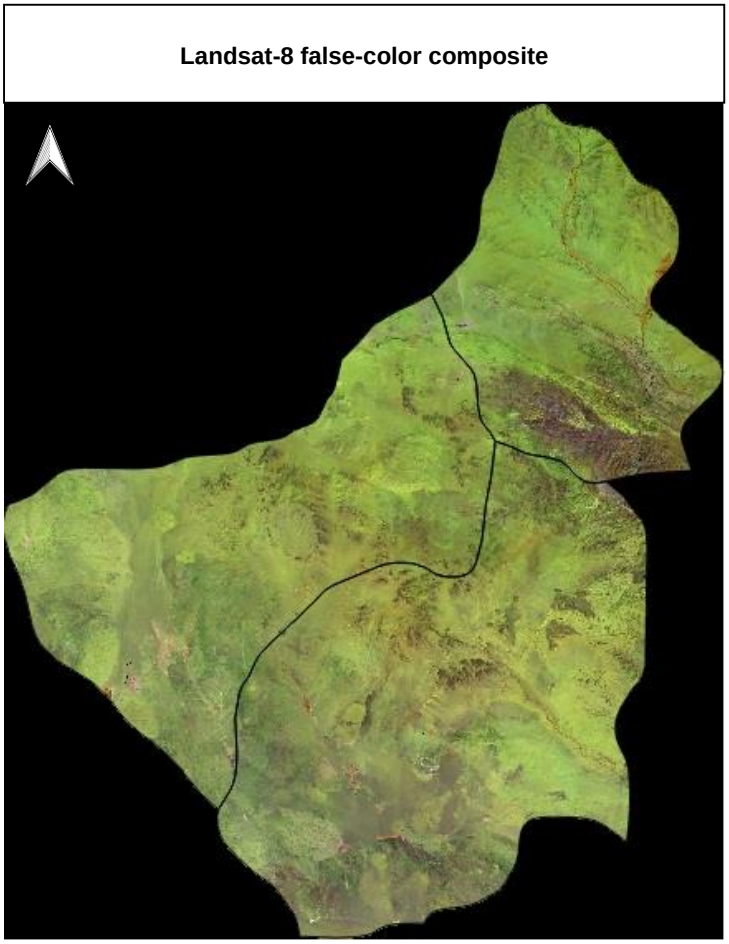

Figure 3.5 - Landsat-8 OLI false-color image using OLI-5, OLI-6 and OLI-2 mapped to RGB for Dzag, Khureemaral and Buutsagaan

NDVI ratio was calculated using red and NIR bands (OLI-4 and OLI-5, respectively), accordingly to Equation 3.1.

$$NDVI = \frac{NIR-RED}{NIR+RED}$$ ***Equation 3.1***

NDVI values range from -1,0 to 1,0 (Weiss *et al*., 2004), variating with the absorption of red light by plant chlorophyll and the reflection of infrared radiation by water-filled leaf cells. In other words, the degree of greenness is equal to vegetation's chlorophyll concentration (Gandhi *et al*., 2015). The positive values (NIR>RED) indicate green vegetated surfaces, and as the NDVI values increase, the vegetation greenness increases with it. Negative values indicate non-vegetated areas, such as water, ice, snow and bare soil (Weiss *et al*., 2004). Landsat-8 NDVI-derived is presented in Figure 3.6.

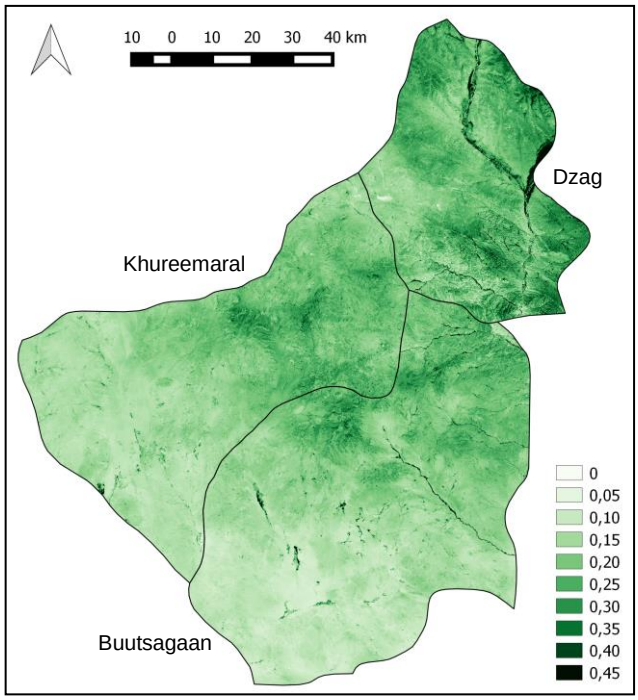

Figure 3.6 – Landsat-8 NDVI-derived with 30 m resolution for the study area

3.3 Geophysical data

3.3.1 Elevation data

The Shuttle Radar Topographic Mission (SRTM) Void Filled data set with 30 m resolution was retrieved from earthexplorer.usgs.gov. It contains elevation data that results from additional processing to address areas of missing data or voids. These voids were filled using interpolation algorithms in conjunction with other sources of elevation data.

Figure 3.7 shows the elevation data from SRTM, used to complement the spectral information from Landsat-8 bands. The elevation at the study area ranges from 1433 m to 3005 m. In Dzag elevation ranges from 1826 m to 3005 m, being the *soum* that reaches the highest elevation. Mountain steppe pasture is expected to be found on the higher elevations of this *soum*, along with steppe pasture, on lower regions. Buutsagaan's elevation ranges from 1432 m to 2919 m, reaching the lower elevation of the three *soums*; Khureemaral's elevation ranges from 1737 m to 2871.The desert steppe pasture is expected to be on the lower elevations of Buutsagaan

and Khureemaral and on the higher elevations of this two *soums*, medium high and low mountain steppe pasture and steppe pasture are expected to be.

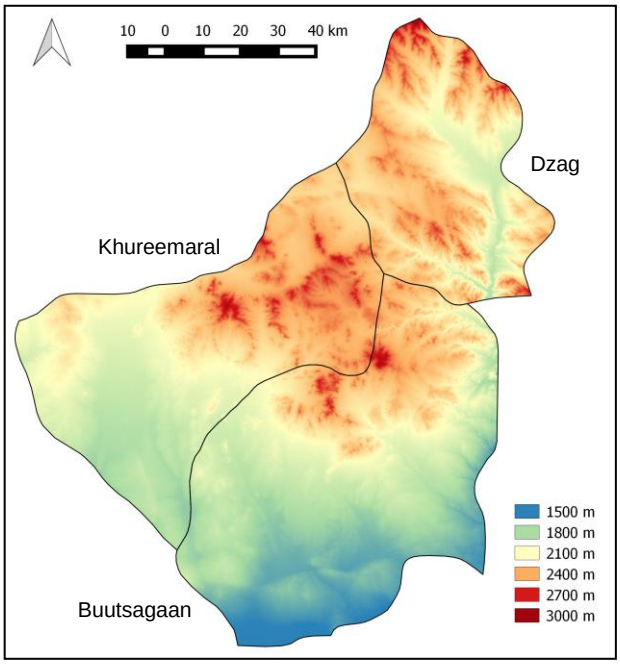

Figure 3.7 - Elevation data from SRTM with 30 m resolution for the study area

3.3.2 Precipitation and temperature data

Mean annual precipitation and mean annual temperature data sets were extracted from worldclim.org, both being for the time period between 1950 to 2000. Despite the time period not including the years between 2000 to 2014, annual climatic means would not change drastically within fourteen years, in order to change the spatial distribution of the Pasture Steppe vegetation.

The resolution of the precipitation and temperature data is 30 seconds (approximately 1 km). Since finding a better resolution for precipitation and temperature data was not possible, these two layers will be taken as a lower resolution than the Landsat-8 and SRTM images.

Mean annual precipitation and mean annual temperature images are represented in figures 3.8 and 3.9, respectively. In Dzag mean annual precipitation ranges from 146 mm to 237 mm and mean annual temperature ranges from -7,5 ºC to -2,3 ºC, reaching the higher mean annual precipitation and the lower temperature values from the three *soums*. Mountain steppe pasture is expected to be found where higher values of mean annual precipitation and lower values of mean annual temperature are present. For lower precipitation values and higher temperature values is where the steppe pasture is expected to be found.

In Buutsagaan, mean annual precipitation ranges from 81 mm to 201 mm and mean annual temperature ranges from -6,5 ºC to 0,8 ºC, reaching the lower mean annual precipitation and the higher mean annual temperature of the study area. In Khureemaral, mean annual precipitation ranges from 93 mm to 184 mm and mean annual temperature ranges from -6,6 ºC to -0,8 ºC. In Khureemaral and Buutsagaan, where the lower mean annual precipitation values and the higher mean annual temperature values are, is where the desert steppe pasture is

expected to be located. Whereas, higher mean annual precipitation and lower mean annual temperature values are correspondent to medium high and low mountain steppe pasture and steppe pasture.

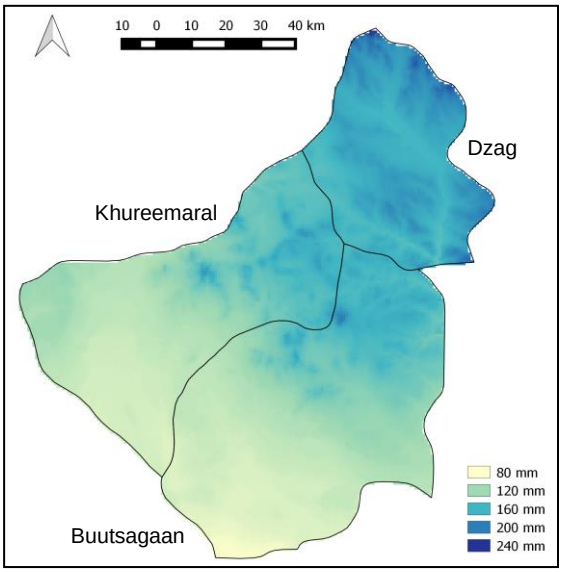

Figure 3.8 - Mean annual precipitation data from 1950 to 2000 with 1 km resolution for the study area

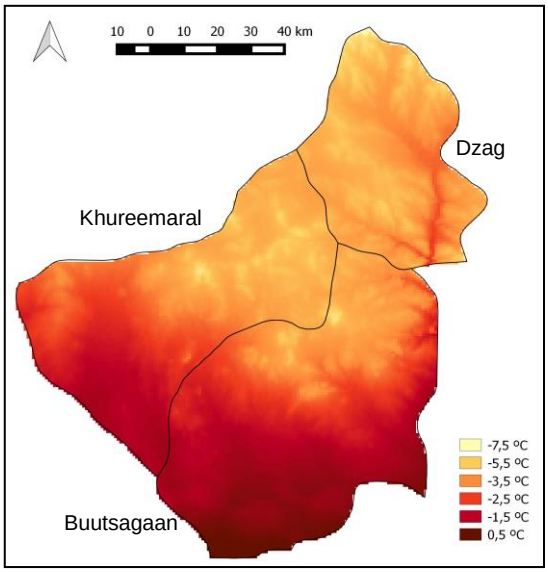

Figure 3.9 - Mean annual temperature data from 1950 to 2000 with 1 km resolution for the study area

3.4 Data pre-processing

Python functions created, in collaboration with DEIMOS team, were applied to perform cloud, water and snow masks to the spectral bands of Landsat-8 and two mosaics comprising the study area were joined on the SRTM data set. Mean annual precipitation and mean annual temperature data sets were subjected to a re-projection from 1 km to 30 m resolution, in order to be used along Landsat-8 and SRTM data. This task was performed on Qgis.

Since multisource estimators (Landsat-8 and geophysical data) were combined on the classification procedure, a standardization of the data was needed. All the estimators (Landsat-8, NDVI, SRTM, mean annual precipitation and mean annual temperature) were converted to z-scores, which is a dimensionless quantity that sets the data values to a zero mean (Helldén and Tottrup, 2008). The z-score is calculated by determining the mean and standard deviation for each estimator and then subtracting the mean from each estimator, finally it divides this value by its standard deviation. It is given by Equation 3.2, where x is a raw score to be standardized, σ is the standard deviation of the population and μ is the mean of the population (Helldén and Tottrup, 2008). The estimators standardization was performed using a Python function created in collaboration with DEIMOS team.

$$z = \frac{x - \mu}{\sigma} \qquad \textbf{\textit{Equation 3.2}}$$

4. Methods

4.1 Selection of a suitable classification method

Since the images available for this study are from Landsat-8 with a spatial resolution of 30 m, discriminating the different species and other vegetation features will not be possible, because the dimension of the land elements (grasses and shrubs) is much smaller than the spatial resolution of the images. Additionally, since collecting field information at the study site was not possible, quantifying grassland properties, like AGB and yield, plant density, productivity, LAI, or percentage cover was considered to be infeasible. It is possible that these properties, relying only on vegetation indices, could provide misleading information, to the local users, for the definition of emergency grazing reserves, because of the possible presence of unpalatable plants that might have invaded the grazed areas. For the stated reasons, discriminating the steppe into its different pasture types was considered to be the best option for achieving the goal of this thesis.

The nomenclature used for the pasture types follows the same of the training points provided by the local users. The training points provided by the local users were collected on field campaigns, by a team of the Ministry of Industry and Agriculture (Project Management Unit – PMU) in collaboration with JFPR. Based on the training points provided, the study area has been classified into: “desert steppe pasture”, “steppe pasture”, “medium high and low mountain steppe pasture” and “mountain steppe pasture”. One point for “gobi desert steppe pasture” and another for “interzonal river valleys and depressions meadow pasture” were also provided, but they were excluded, because it would be necessary more points to map these classes.

On the first attempts to classify the study area into the four aimed classes, the results showed low accuracies, because there was a high confusion among “medium high and low mountain steppe pasture” and “mountain steppe pasture” and also “medium high and low mountain steppe pasture” with “steppe pasture”. The confusion among different land cover classes can be reduced through masking areas that are not to be classified, but have similar spectral properties, providing the capability for achieving a greater control over the classification process (McCloy, 1995). (Xian *et al*., 2015) wanted to map shrubland components across the northwest United States, but a confusion between other land cover classes existed. In order to perform a hierarchical classification approach, a mask of non-shrubland areas, such as forests, urban and agriculture was created.

In this case, classifying and then masking the non-steppe land cover classes, present at the study area, was considered to be the best approach for performing a more accurate classification of the pasture steppe classes. For this reason, the main classes present at the study area were identified, in order to reduce the classification confusion among the Pasture Steppe classes. The next section, 4.1.1, explains in more detail the procedure for the identification and classification of the main classes and section 4.1.2 describes the classification of the steppe vegetation into its different pasture types, after masking the main classes.

4.1.1 Main classes – Bare soil, water and vegetation

Using the Landsat-8 image, with seven spectral bands with false color composition on RGB of OLI-5, OLI-6 and OLI-2 (Figure 3.5) and Google Earth software, five main classes were identified: two classes for bare soil: “desert bare soil” and “mountain bare soil”; one class for rivers and waterbodies “water”; and two classes for vegetation “riparian vegetation” and “steppe vegetation”. Mountain bare soil is mainly seen in Dzag in shades of purples, but also in Khureemaral and Buutsagaan in shades of browns. Desert bare soil appears in shades of gray in Khureemaral and Buutsagaan. Rivers are very dark and waterbodies are black and purple. The riparian vegetation represents the interface between terrestrial and aquatic ecosystems, it appears in shades of orange alongside the rivers and waterbodies of the study area. Because of its proximity to water, the riparian vegetation is much more luxuriant than the sparse vegetation present at the steppe vegetation (shades of greens). NDVI confirms it, because its values are considerably higher alongside rivers and waterbodies (Figure 3.6). Even though this main class consists on vegetation it was chosen to mask it, because the riparian vegetation is not allocated to any of the pasture classes selected for the classification.

Since no training nor testing points, collected in the field, were available, the Regions of Interest (ROI) were defined, based on Landsat-8 image (Figure 3.5) and Google Earth satellite images, in order to perform a supervised classification. These ROIs were created with the semi-automatic classification plugin on Quantum GIS (Qgis). For the collection of the training and testing data preference was given to pixels that were located in homogeneous areas with neighboring pixels belonging to the same class.

The classification was performed using the seven bands: OLI-1, OLI-2, OLI-3, OLI-4, OLI-5, OLI-6 and OLI-7. These bands were also combined with Landsat-8 NDVI-derived to try a better separation of the vegetation classes from soil and water classes. Since non-remotely-sensed data would not be incorporated into this classification procedure, the maximum likelihood classifier was used. When the main classes classification was performed using maximum likelihood, a high confusion among “mountain bare soil” and “water” classes was detected. To reduce this confusion, a classification using only three bands: OLI-5, OLI-6 and OLI-7 was also performed, because in these wavelengths the spectral signatures were better separated, than for the remaining wavelengths. However, since the confusion among “mountain bare soil” and “water” classes still remained, the “water” class was masked, so that the classification of the remaining classes could be performed. To mask the “water” class the Topographic Wetness Index (TWI) derived from the SRTM data set was performed on Qgis.

TWI is a DEM-based index that works as a proxy for soil moisture, functioning as a relative measure of the long-term soil moisture availability of a given site. TWI is defined by Equation 4.1, where As is the specific catchment area (the cumulative upslope area draining through a cell divided by the contour width), and β is the local slope (Kopecký and Cizková, 2010).

$$TWI = ln\ \frac{As}{tag\ \beta} \qquad \textbf{Equation 4.1}$$

Figure 4.1 reveals the obtained TWI for the study area, ranging from 5 to 26. Since TWI is derived from the SRTM data set, it covered not only the areas correspondent to rivers and waterbodies, but also the riparian vegetation that occurs along them. For this reason, these two classes were aggregated in one: “water and riparian vegetation”. The final main classes to be mapped were: “mountain bare soil”, “desert bare soil”, “water and riparian vegetation” and “steppe vegetation”.

In order to adjust the TWI values to fit “water” and “riparian vegetation” occupied areas, a 17≤TWI≤26 was selected to represent those classes. In Figure 4.2, the selected values for TWI can be observed, where 0 stands for 5<TWI<17 and 1 for 17 ≤TWI≤ 26. Nevertheless, there are still many areas where it is known, by looking at the Landsat-8 image, that there is no water or riparian vegetation, but since TWI is derived from elevation data (SRTM), all valley regions existent at the study area are included in this index. For this reason, it was created a vector mask, on top of the selected TWI values, where water and riparian vegetation were more likely to exist, by looking at the Landsat-8 image. At this point, “water and riparian vegetation” were turned into “no data” values, while the rest of the pixel values were 1 (Figure 4.3).

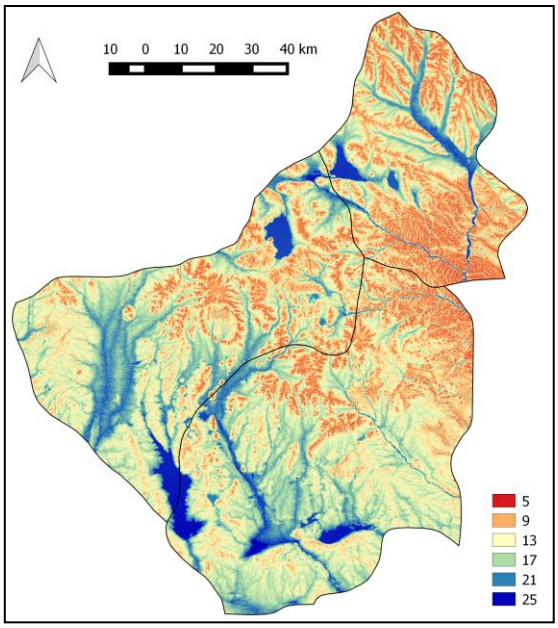

Figure 4.1 – TWI derived from SRTM data set for the study area

The layer containing “no data” values on “water and riparian vegetation”, was added to the Landsat-8 image. When the layer containing “no data” was added to each one of the OLI spectral bands, the maximum likelihood classifier could not perform the classification. But by adding the “no data” values to only one of the bands, the classification could be performed. This layer with “no data” values was included into the OLI-5 band by multiplying the raster that contained the “no data” (Figure 4.2) with the raster with the original OLI-5 band data. Then it was made a layer stack with the desired combination of bands, having the new OLI-5 band containing “no data” values in “water and riparian vegetation” class, instead of the original OLI-5 band.

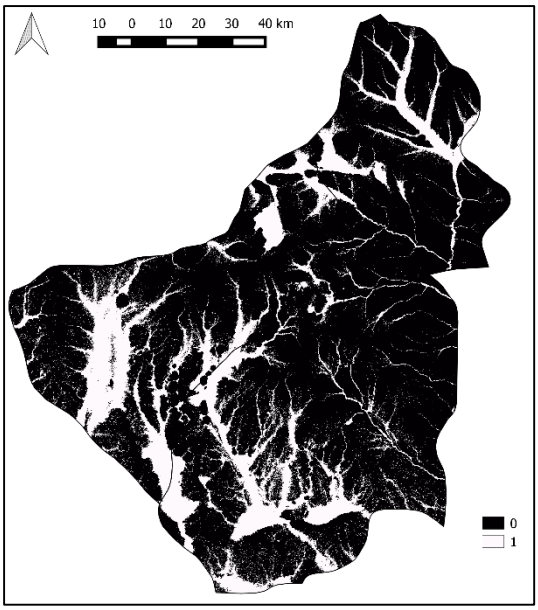

Figure 4.2 – Selected TWI to fit "water and riparian vegetation"

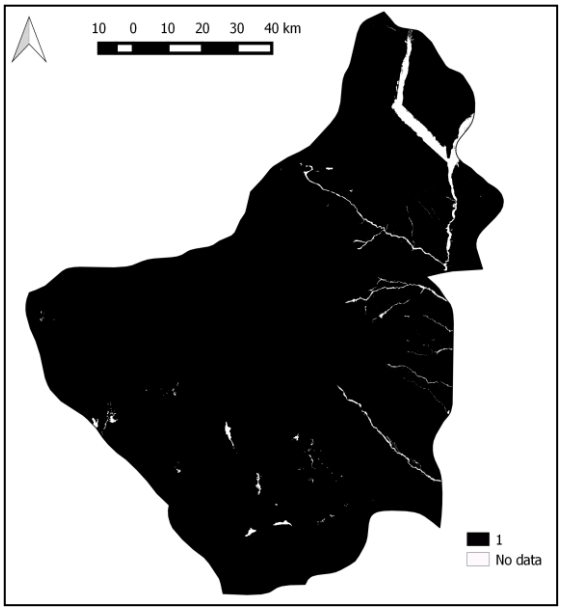

Figure 4.3 –Vector mask covering "water and riparian vegetation" classes

Finally, the image was classified into "mountain bare soil", "desert bare soil" and "steppe vegetation", by different combinations of Landsat-8 bands and Landsat-8 bands with NDVI, using the maximum likelihood classifier, while "water and riparian vegetation" class remained masked (unclassified). The combinations of output models generated in this classification are presented in Figure 4.4. Each arrow represents the addition of a new estimator (Landsat-8 and NDVI) or a new model that results from the classification using an estimator or a combination of estimators. Model 1 (M1) results from the classification using only Landsat-8 bands from OLI-1 to OLI-7. Model 2 (M2) is the output result for the classification using Landsat-8 from OLI-1 to OLI-7 bands and NDVI. Model 3 (M3) represents the output model generated by using OLI-5, OLI-6 and OLI-7 bands. And Model 4 (M4) is the output model that contains OLI-5, OLI-6 and OLI-7 bands and NDVI.

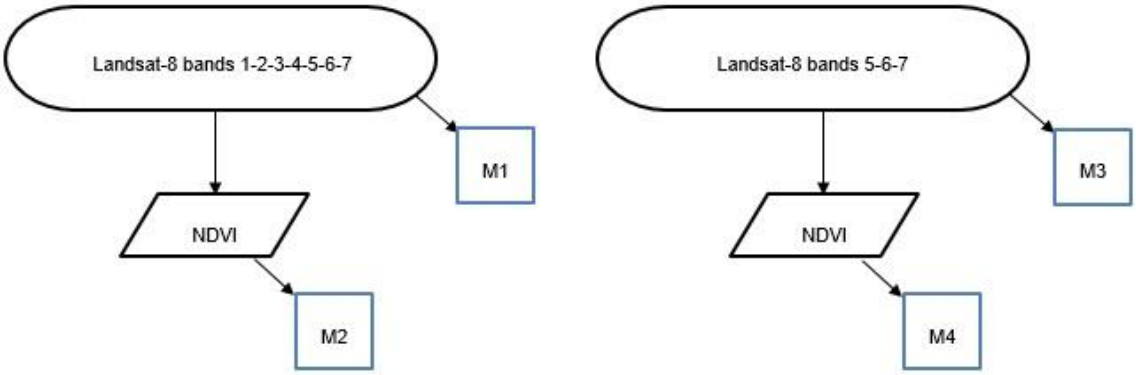

Figure 4.4 - Flow chart representing the output models for the main classes (M1, M2, M3 and M4), created using Landsat-8 bands from OLI-1 to OLI-7 (M1) and the same bands with NDVI (M2); and using OLI-5, OLI-6 and OLI-7 (M3) and the same bands with NDVI (M4)

4.1.2 Steppe vegetation classification

Concerning the steppe vegetation, a supervised classification was applied by defining ROIs for each one of the pasture types: “desert steppe pasture”, “steppe pasture”, “medium high and low mountain steppe pasture” and “mountain steppe pasture” within the three *soums*.

The selected classification algorithms – maximum likelihood and decision tree– were used to classify the pasture types with multiple combinations of remotely sensed data (Landsat-8 spectral bands and Landsat-8 NDVI-derived) and geophysical data (SRTM, mean annual precipitation and mean annual temperature), in order to evaluate the best method for classifying the pasture types at the study site.

4.1.2.1 Maximum likelihood classifier

From the total number of training points provided by the local users, 60% were selected to train the classification (Figure 4.5) and the remaining 40% to validate (test) the classification (Figure 4.6). For each training and testing point, a buffer of 100 m was created for defining the area where each ROI should be confined to. These ROIs were defined on top of the training points provided by the local users using the semi-automatic classification plugin on Qgis.

For the “desert steppe pasture” class 8 training points (3 for Khureemaral and 5 for Buutsagaan) and 6 testing points (3 for Khureemaral and 3 for Buutsagaan) were available. The “steppe pasture” class had a total of 35 training points (14 for Khureemaral, 10 for Buutsagaan and 11 for Dzag) and 23 testing points (9 for Khureemaral, 6 for Buutsagaan and 8 for Dzag). “Medium high and low mountain steppe pasture” had available 14 training points (4 for Khureemaral and 9 for Buutsagaan) and 6 testing points (2 for Khureemaral and 4 for Buutsagaan). Finally, the “mountain steppe pasture” class had available 6 training points (6 for Dzag) and 5 testing points (5 for Dzag).

The spectral signatures generated by the training ROIs were then used to perform the classification into a thematic map. First, a classification using Landsat-8 bands OLI-2, OLI-3, OLI-4, OLI-5, OLI-6 and OLI-7 was performed. The OLI-1 band was excluded, because its output is very similar to OLI-2. OLI-1 is mainly used for atmospheric and coastal purposes, being able to detect fine particles like dust and smoke and also for detecting shallow water (Sternberg *et al*., 2011). In order to test which combination of ancillary data provides the best classification accuracy, the data sets were added one by one to perform several classifications with different combinations of estimators (Landsat-8 data and geophysical data).

Figure 4.7 shows each combination of estimators for all sixteen models. The arrows represent the addiction of a new estimator or a new model. Each model represents a classification output resulting from the use of one estimator (base model – M1) or the addiction of estimators to the base model.

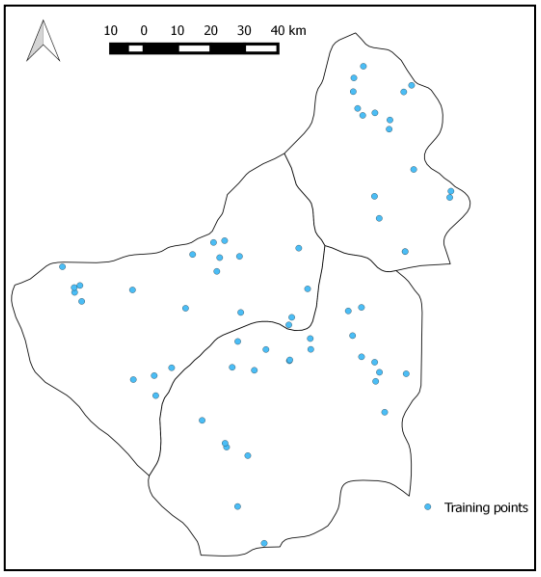

Figure 4.5 - Training points provided by the local users

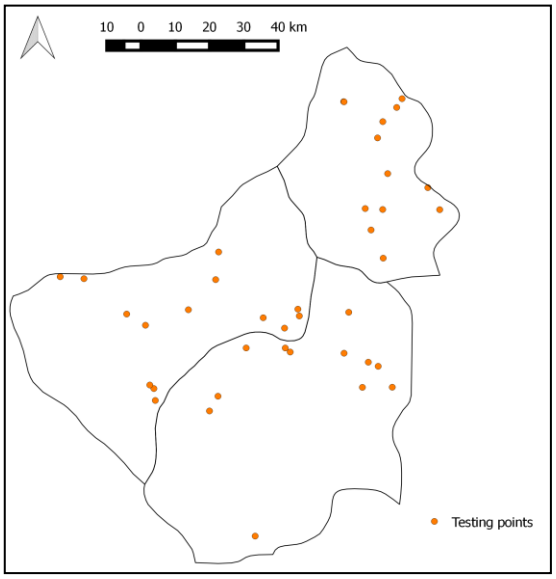

Figure 4.6 - Testing points provided by the local users

4.1.2.2 Decision tree classifier

For performing classifications with the decision tree classifier, Python functions were created in collaboration with DEIMOS team. These functions were based on Scikit Learn Python library functions from scikit-learn.org. For this reason, a slightly different procedure was applied for collecting the spectral signatures from the same ROIs used for maximum likelihood classifier. Two Python functions were used: one for training and testing the classification, based on different estimator combinations (Landsat-8 and geophysical data), and another to apply the algorithms and generate the classification maps. For the training and testing function a csv file was required, as input data, for providing the information about the different pasture classes and estimators, for training and then testing the classification.

In this case, instead of using the entire ROIs, ten random points were created inside each one of the training and testing ROIs, which contained the information of all the estimators (Landsat-8 bands, NDVI, SRTM, mean annual precipitation and mean annual temperature) and also latitude, longitude and the assigned class. The function created a file for each one of the output models generated by each estimator or the combination of several. The estimator combinations used for the decision tree classifier are the same tested for the maximum likelihood classifier, represented in Figure 4.7. To apply the algorithms and generate the classification maps, the previously created models were used to generate the sixteen classified maps for each estimator combinations.

Decision trees can become over complex, causing an overfitting (not generalizing the data well). For avoiding this problem, it was important to set the minimum number of samples required at a leaf node (min samples leaf) and the maximum depth (max depth) of the tree. To make this possible, a Python function was created to report the accuracy results for different combinations of the two parameters (max depth and min samples leaf) for all the sixteen models,

in order to find the best performing tree. After looking at the accuracy report, the selected values for each parameter were: (max depth=6, min samples leaf=1).

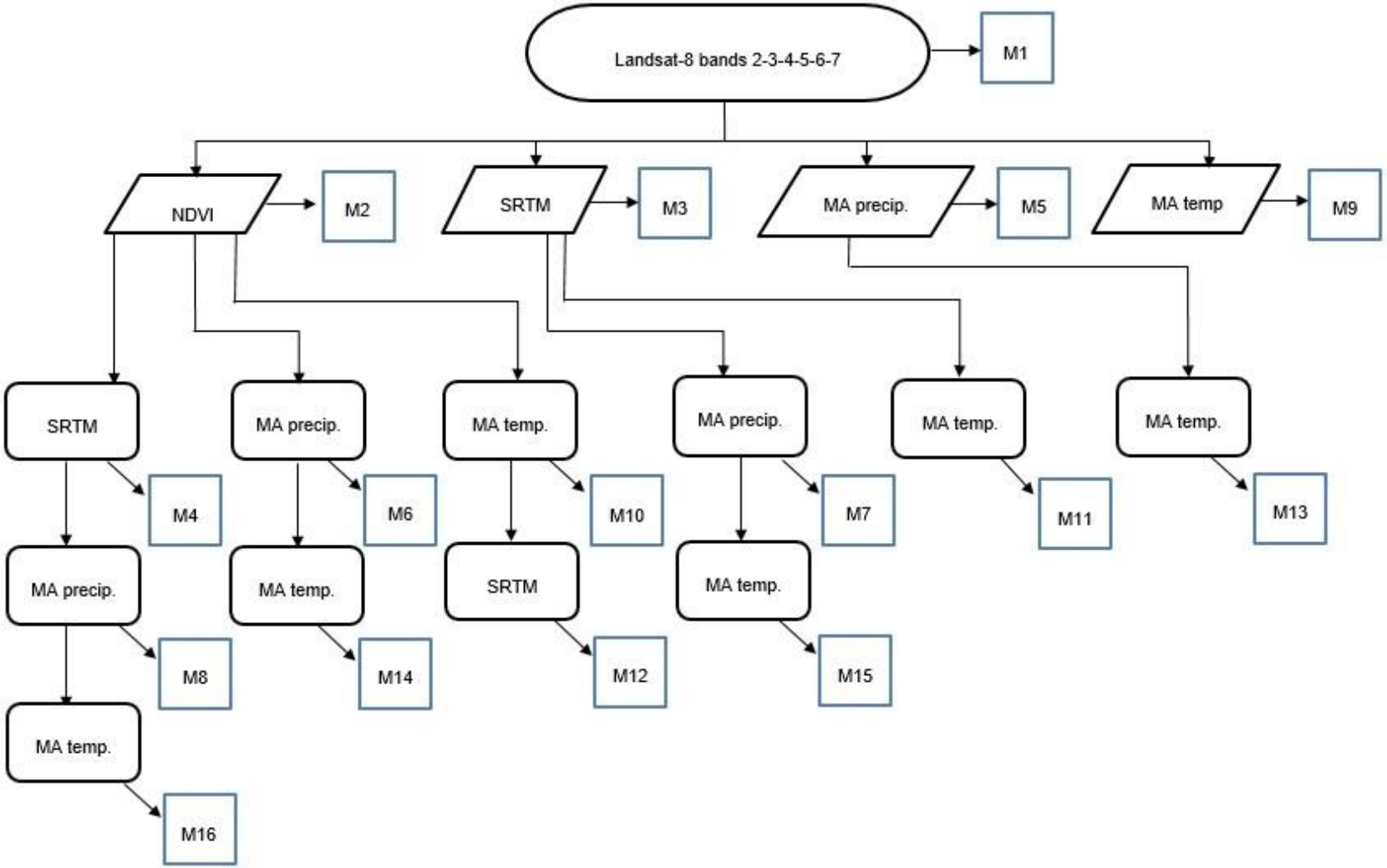

Figure 4.7 - Flow chart for output models created with different combinations of datasets used for classifying the Pasture Steppe classes: bands OLI-2 to OLI-7 with NDVI, SRTM, mean annual (MA) precipitation and mean annual (MA) temperature. The arrows represent the addition of a new estimator or a new model. Each model represents a classification output by using one estimator (base model – M1) or by the addition of one or more estimators to the base model

4.2 Classification accuracy assessment

The accuracy assessment is required for evaluating the quality of the land cover classification results, in order to identify the most suitable method, by comparing different classification results (Moran, 2010). A variety of parameters have been suggested to determine the land cover accuracy, such as overall accuracy, various forms of kappa coefficient of agreement, tau coefficient, user's and producer's accuracy and conditional kappa, but no consensus has been reached on which measures are appropriate for a given objective of accuracy assessment (Liu *et al*., 2007). Being one of the most commonly used tools for this purpose, error matrices were generated to access classification's accuracies, among other elements, such as overall accuracy, precision, recall and F1-score, both for main classes and the Pasture Steppe classification.

For the maximum likelihood classifier, the accuracy assessment was performed using the semi-automatic classification plugin on Qgis, taking as input data each one of the classified maps and the testing ROIs (main classes and Pasture Steppe vegetation). For the decision tree classifier, a Python function generated an accuracy report using ten testing points inside each one of the previously created ROIs (used for maximum likelihood classifier) and the models generated for each one of the combinations of estimators (Pasture Steppe vegetation).

The overall accuracy is given by the correctly classified pixels divided by the total number of pixels. Precision and recall are a measure for the accuracy response for each class. Precision is given by Equation 4.3 and recall by Equation 4.4, where TP stands for true positive, TN for true negative, FP stands for false positive and FN for false negative (Goutte and Gaussier, 2005).

$$precision = \frac{TP}{TP + FP} \qquad \textbf{Equation 4.3}$$

$$recall = \frac{TP}{TP + FN} \qquad \textbf{Equation 4.4}$$

F1-score is a statistical analysis that consists on a harmonic average of precision and recall. This measure effectively reflects the TP to the arithmetic mean of predicted positives and real positives, being a constructed rate normalized to an idealized value, being known as a proportion of specific agreement as it is applied to a specific class (Powers, 2011) . F1-score is given by Equation 4.5 (Goutte and Gaussier, 2005).

$$F1\ score = 2 * \frac{precision * recall}{precision + recall} \qquad \textbf{Equation 4.5}$$

Since the decision of which map has more value to the user, depends both on the map's accuracy and the relevance of the land cover classification scheme to mapping objectives, it is not clear how the overall accuracy or another accuracy parameter can incorporate this component. Additionally, when the assessment objectives require comparing error matrices, the choice of an appropriate accuracy parameter is difficult to determine (Liu *et al*., 2007).

Due to the unbalanced number of training and testing points among the four classes of the Pasture Steppe vegetation, the overall accuracy does not provide a reliable estimation for model accuracies. For interpretation of the Pasture Steppe classification results, individual class accuracies, like precision and recall, constitute a more reliable estimation for comparing model accuracies. Since the F1-score aggregates the information provided by precision and recall, it will be used for analyzing the accuracy results.

For the stated reasons, a comparison among F1-scores weighted averages will be performed for comparing the tested model accuracies (in section 5.2). The weighting for each class was attributed based on the provided information by the local users about the total occupied areas per class (Table 4.1). This procedure was applied because the training points provided were not in proportion to class's occupied areas. For instance, "medium high and low mountain steppe pasture" covers a slightly higher area, than the "steppe pasture", but the latter has a lot more training points than the former.

Since "medium high and low mountain steppe pasture" and "steppe pasture" cover more than half of the study area (67,4%), when these class accuracy results are low, the error introduced into the classification is larger, than when low accuracies are registered for "desert steppe pasture" and "mountain steppe pasture" on a model. Consequently, when an increase (or decrease) on the accuracy results occur for classes that occupy a larger area than others, the increase (or decrease) on model's global accuracy is greater, than when an accuracy increase (or decrease) occur on classes that cover a smaller area within the three *soums*.

Table 4.1 - Weighting for each pasture class based on the real area extent per class used to calculate F1-scores weighted averages

Pasture class	Area (km^2)	Weighting (%)
Desert steppe pasture	2323	20,2
Steppe pasture	3820	33,2
Medium high and low mountain steppe pasture	3933	34,2
Mountain steppe pasture	1426	12,4
Total	**11502**	**100,0**

4.3 Overview on the applied methods

Due to the occurrence of a high level of confusion between the Pasture Steppe classes, the land cover features that were not part of the steppe vegetation and were introducing errors into the classification were masked (main features). Figure 4.8 provides an overview on the applied methods for performing the main classes and the steppe vegetation classifications. For classifying the main classes into "desert bare soil", "mountain bare soil" and "steppe vegetation" the maximum likelihood classifier was used, while "water" and "riparian vegetation" classes were masked. The next step was to perform an accuracy assessment using the testing ROIs. After this step, all the main classes were masked besides the "steppe vegetation" class. The steppe vegetation was then classified into its different pasture types: "desert steppe pasture", "steppe

pasture", "medium high and low mountain steppe pasture" and "mountain steppe pasture", using both maximum likelihood and decision tree classifiers. The final step was to perform an accuracy assessment for the generated thematic maps for each one of the algorithms.

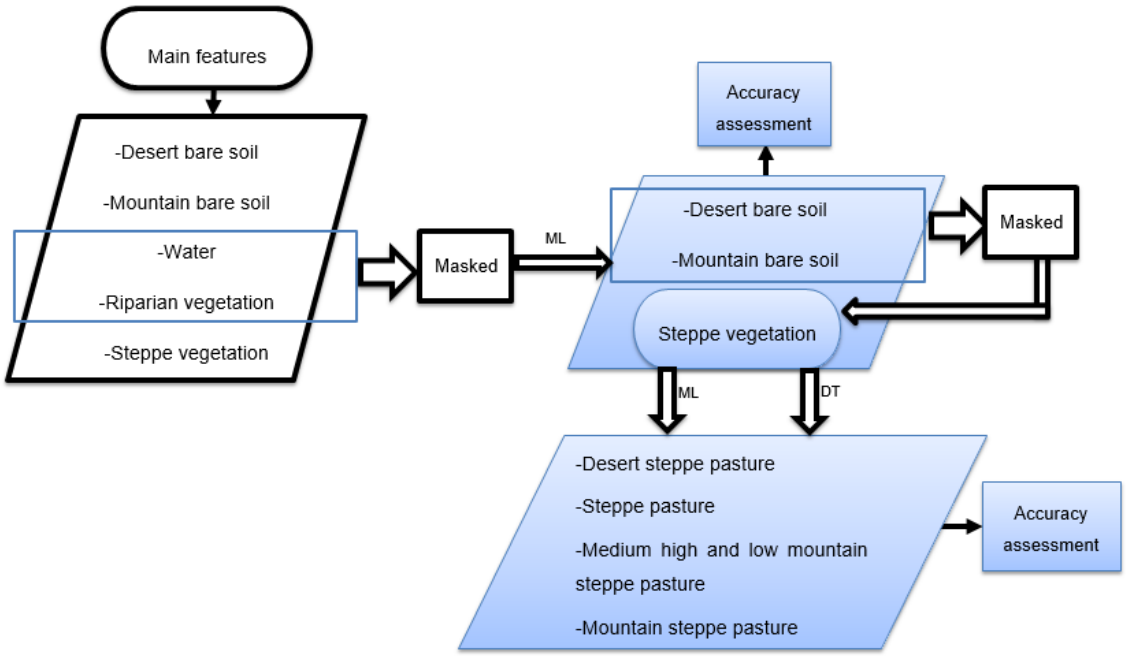

*Figure 4.8 - Overview on the methods used to classify the main classes and the steppe vegetation (*ML- maximum likelihood classifier; DT- decision tree classifier)*

5. Results and Discussion

5.1 Classification of the main classes: bare soil, water and vegetation

The spectral signatures generated by the created ROIs for the main classes using Landsat-8 bands OLI-1, OLI-2, OLI-3, OLI-4, OLI-5, OLI-6 and OLI-7 (Model 1), Landsat-8 bands with NDVI (Model 2), Landsat-8 bands OLI-5, OLI-6 and OLI-7 (Model 3) and Landsat-8 bands OLI-5, OLI-6 and OLI-7 with NDVI (Model 4) are presented in Figures 5.1, 5.2, 5.3 and 5.4, respectively. By looking at the signature plots, Landsat-8 bands OLI-5, OLI-6 and OLI-7 can better separate the three main classes (Figure 5.3). Figures 5.2 and 5.4 shows that NDVI provides a good separation among the main classes, with higher NDVI values for the "steppe vegetation" class and lower values for the "desert bare soil" and "mountain bare soil".

The tested models to classify the main classes turned to be very similar, because no training and testing points collected on the field for "desert bare soil" and "mountain bare soil" were available. The only main class with available training and testing points was the "steppe vegetation" class, for which the points provided by the local users were used to define training and testing ROIs. Whereas for "desert bare soil" and "mountain bare soil", both training and testing

ROIs were created by looking at the Landsat-8 and Google Earth images. For this reason, all the tested models presented very high accuracy results, as it can be seen in Table 5.1. Such high accuracy results should be looked with caution, because a very high level of uncertainty exists for this classifications, which constitutes a limitation to the applied procedure.

In this case, because a very high margin of error for the performed classifications exists, any of the four models could be selected to mask the main classes. Model 4 was selected to mask the main classes, because it achieved the highest overall accuracy from the tested models. Also, both precision and recall achieved 100% accuracy results in Model 4 (the same for Model 1 and Model 2) for the “steppe vegetation” class. This is an important factor, because the “steppe vegetation” was the only main class for which the training and testing ROIs had a high confidence level of being correct, since they were based on the points provided by the local users, collected in field campaigns. This accuracy result for the “steppe vegetation” on Model 4 (the same for Model 1 and Model 2) suggests that this class remained intact after the classification of the main classes, which is a very important factor, because the goal of this procedure was to mask the main classes, leaving the “steppe vegetation” class to be classified into its pasture classes (in section 5.2) and to reduce the classification confusion among those classes.

Figure 5.5 shows the selected model (Model 4) to mask “desert bare soil” and “mountain bare soil”. On the main classes map, “water and riparian vegetation” class can be seen as unclassified, because it has been previously masked, to perform the classification of the remaining main classes. “Mountain bare soil” is mainly located on Dzag, but also on the mountainous region of Khureemaral and Buutsagaan. The “desert bare soil” is mainly seen on Buutsagaan *soum,* but also on Khureemaral, near the area where the “desert steppe pasture” should be. The “steppe vegetation” covers the major part of the study area. Model 1, Model 2 and Model 3 maps are presented on Figures A.1, A.2 and A.3, respectively, in Annex.

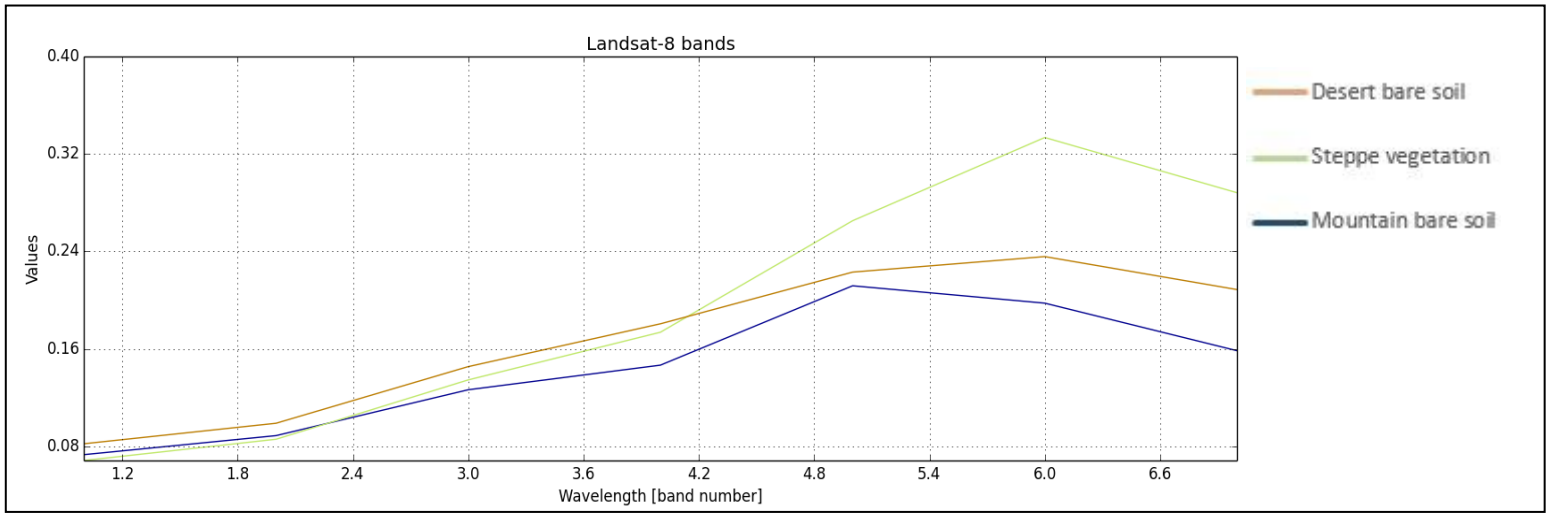

Figure 5.1 - Spectral signatures for the main classes using Landsat-8 bands: OLI-1, OLI-2, OLI-3, OLI-4, OLI-5, OLI-6 and OLI-7 – Model 1

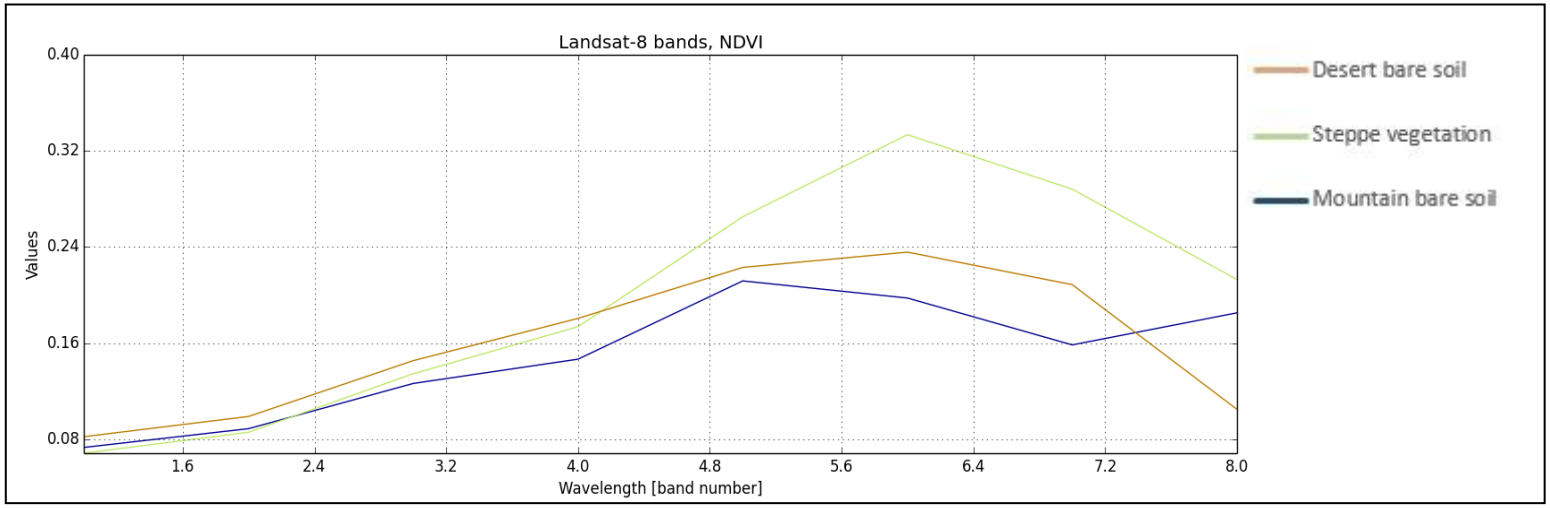

Figure 5.2 - Spectral signatures for the main classes using Landsat-8 bands: OLI-1, OLI-2, OLI-3, OLI-4, OLI-5, OLI-6 and OLI-7 and NDVI [band 8] – Model 2

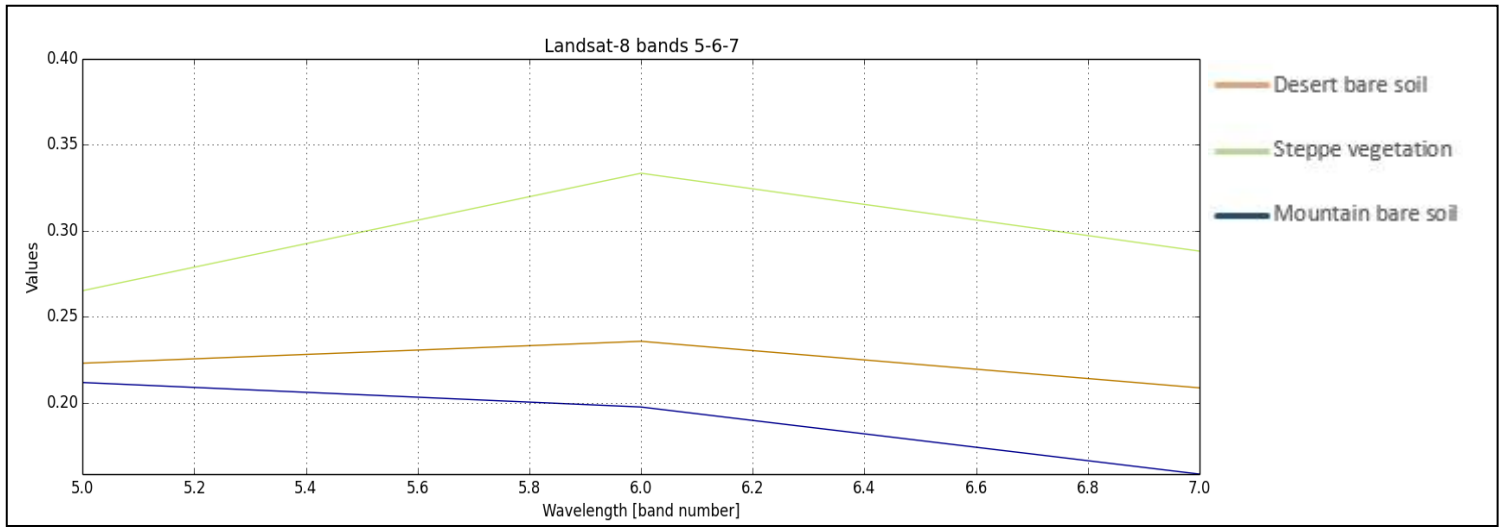

Figure 5.3 - Spectral signatures for the main classes using Landsat-8 bands: OLI-5, OLI-6 and OLI-7 – Model 3

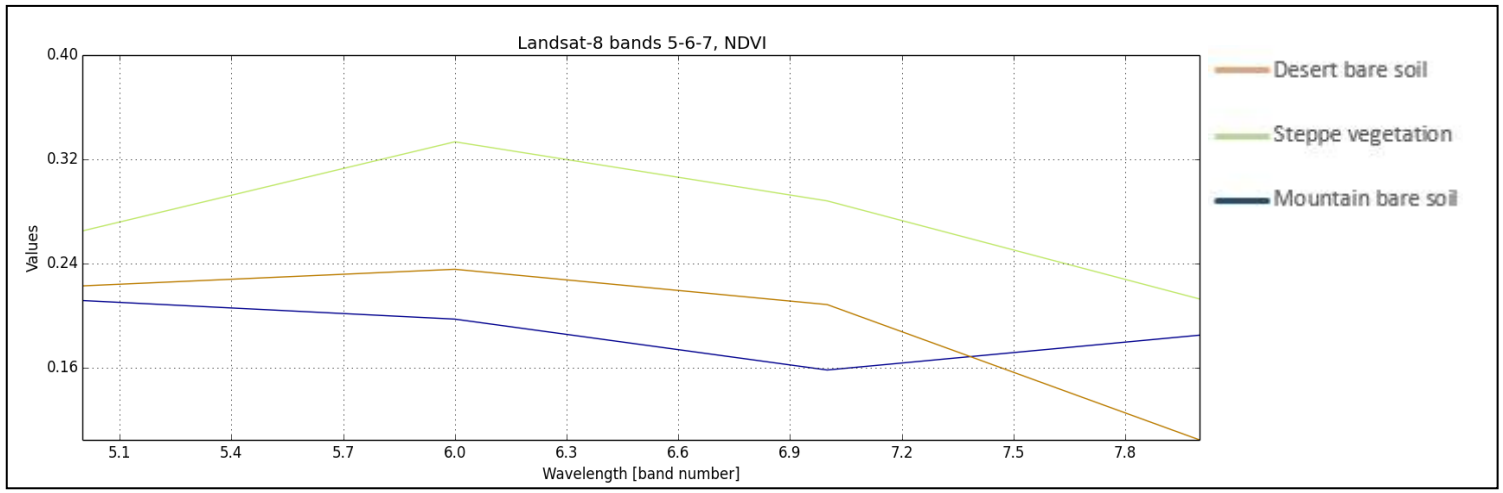

Figure 5.4 - Spectral signatures for the main classes using Landsat-8 bands: OLI-5, OLI-6 and OLI-7 and NDVI [band 8] – Model 4

Table 5.1 - Accuracy report for the main classes classification using maximum likelihood for Model 1, Model 2, Model 3 and Model 4

Model 1: Landsat-8 bands	**Maximum likelihood**			
	Precision [%]	**Recall [%]**	**F1 score [%]**	**Overall accuracy [%]**
Mountain bare soil	90,7	98,39	94,4	**99,7**
Steppe vegetation	100,0	100,0	100,0	
Desert bare soil	99,9	98,9	99,4	
Model 2: Landsat-8 bands, NDVI	**Maximum likelihood**			
	Precision [%]	**Recall [%]**	**F1 score [%]**	**Overall accuracy [%]**
Mountain bare soil	94,0	99,0	96,5	**99,8**
Steppe vegetation	100,0	100,0	100,0	
Desert bare soil	100,0	99,5	99,7	
Model 3: Landsat-8 bands 5-6-7	**Maximum likelihood**			
	Precision [%]	**Recall [%]**	**F1 score [%]**	**Overall accuracy [%]**
Mountain bare soil	97,7	95,5	96,6	**99,6**
Steppe vegetation	100,0	99,6	99,8	
Desert bare soil	99,3	99,9	99,1	
Model 4: Landsat-8 bands 5-6-7, NDVI	**Maximum likelihood**			
	Precision [%]	**Recall [%]**	**F1 score [%]**	**Overall accuracy [%]**
Mountain bare soil	98,0	99,1	99,0	**99,9**
Steppe vegetation	100,0	100,0	100,0	
Desert bare soil	99,6	100,0	99,8	

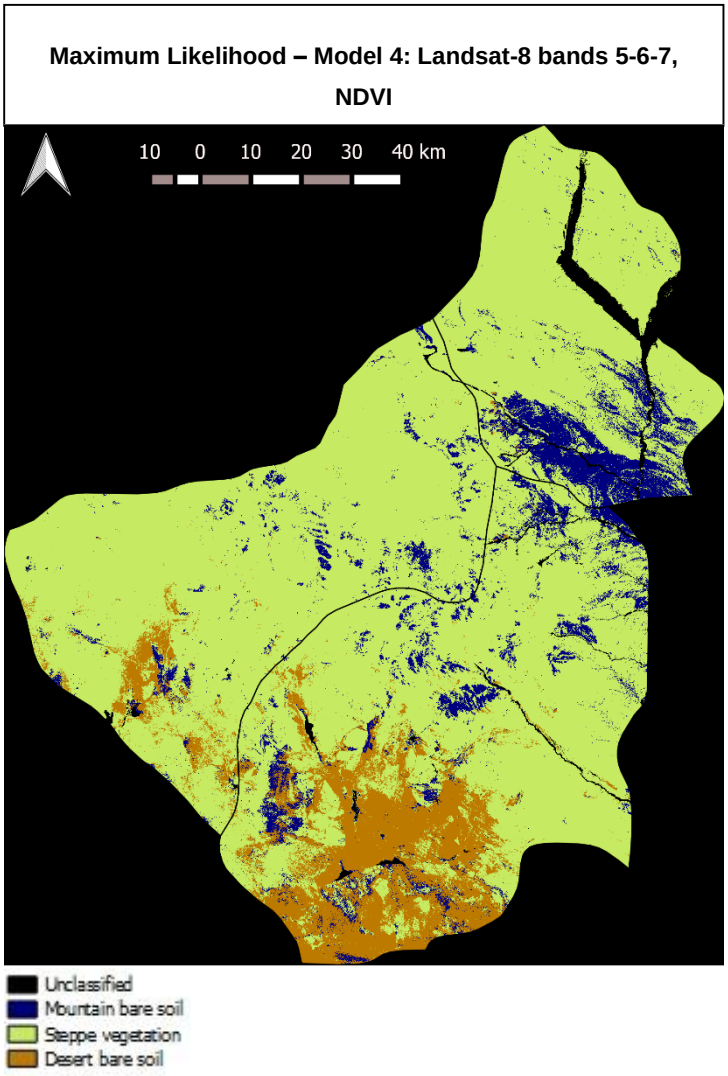

Figure 5.5 - Main classes using maximum likelihood - Model 4: Landsat-8 bands and NDVI

5.2 Classification of the Pasture Steppe vegetation

5.2.1 Comparative analysis of different estimators

The spectral signatures of Landsat-8 bands (from OLI-2 to OLI-7 – Model 1), in Figure 5.6, provide a good separation between “desert steppe pasture” and “mountain steppe pasture”, but “ steppe pasture” and “medium high and low mountain” classes have a very similar behavior. This may be due to the fact that the “steppe pasture” class training points cover the major part of the study area, causing a wide variation on the vegetation present. So, the “steppe pasture” may be incorporating characteristics that most likely of belong to “medium high and low mountain steppe pasture” and “mountain steppe pasture”. Figures 5.7, 5.8, 5.9 and 5.10, show the spectral signatures created by the combination of Landsat-8 bands and each one of the tested data sets: NDVI (Model 2), SRTM, (Model 3), mean annual precipitation (Model 5) and mean annual temperature (Model 9), respectively. On these signature plots, the data sets that were added to

the Landsat-8 bands correspond to band number 8. The remaining signature plots are presented in Annex from Figure A.4 to A.14

On the next sections, Tables 5.2, 5.3, 5.4 and 5.5 present the contribution provided by each one of the tested data sets (NDVI, SRTM, mean annual precipitation and mean annual temperature, respectively) for the tested models. The role of those data sets in order to improve classification accuracies is estimated and given by the difference between F1-scores weighted average (based on the occupied area of each class, presented in Table 4.1) of a model to which a data set was added and a model that does not include that data set.

5.2.1.1 The role of a satellite-derived vegetation index to improve classification accuracies: NDVI

On the signature plot, where NDVI ratio was added to the Landsat-8 bands (Figure 5.7), the higher vegetation greenness is present in “mountain steppe pasture”, followed by “medium high and low mountain steppe pasture”, then “steppe pasture”, whereas the lower vegetation greenness is present in “desert steppe pasture”, as expected.

The contribution of Landsat-8 NDVI-derived to the F1-scores weighed average for the pairs of models to which it was added is presented in Table 5.3. This table synthetizes the increasing (+) and decreasing (-) F1-scores weighted average calculated as the difference between the models with and without NDVI. NDVI did not had influence on the majority of models to which it was added, because such low increases and decreases on the F1-scores weighted average are irrelevant, when some level of uncertainty inherent to the classification procedure exists.

Results for Model 2, compared to Model 1 using the decision tree, and also for Model 10, compared to Model 9 using maximum likelihood, indicate some level of influence caused by the NDVI addition to the models. A decrease of 10% and 11% was registered for these two models, which indicates that adding NDVI to Landsat-8 bands or to mean annual temperature estimators, reduced classification accuracies. These decreases may be caused by the introduction of redundant information on the spectral signatures of the training samples, because NDVI was extracted from single pixel data. Also the possible existence of strong noise from background soil effects and canopy gaps, could have also caused accuracies to decrease (Uno *et al*., 2005).

On a general overview, NDVI did not had influence on the models to which it was added, for both maximum likelihood and decision tree. In the two cases that this vegetation index had influence, it decreased the accuracy results of the models.

Table 5.2 - Increasing (+) and decreasing (-) classification accuracies generated by the addition of Landsat-8 NDVI-derived: comparison of pairs of models with and without NDVI

Pairs of models with and without NDVI data set	Increase (+) or decrease (-) in F1-scores weighted average (%)	
	Maximum likelihood	Decision tree
Model 2 (Landsat-8 bands, NDVI) **vs. Model 1** (Landsat-8 bands)	-5,1	**-10,3**
Model 4 (Landsat-8 bands, NDVI, SRTM) **vs. Model 3** (Landsat-8 bands, SRTM)	+0,5	-0,1
Model 6 (Landsat-8 bands, NDVI, MA precipitation) **vs. Model 5** (Landsat-8 bands, MA precipitation)	-0,8	-4,4
Model 8 (Landsat-8 bands, NDVI, SRTM, MA precipitation) **vs Model 7** (Landsat-8 bands, SRTM, MA precipitation)	-3,7	-1,0
Model 10 (Landsat-8, NDVI, MA temperature) **vs. Model 9** (Landsat-8, MA temperature)	**-10,5**	-3,0
Model 12 (Landsat-8 bands, NDVI, SRTM, MA temperature) **vs. Model 11** (Landsat-8 bands, SRTM, MA temperature)	+0,7	+2,4
Model 16 (Landsat-8 bands, NDVI, SRTM, MA precipitation, MA temperature) **vs. Model 15** (Landsat-8 bands, SRTM, MA precipitation, MA temperature)	+0,3	+2,8
Average contribution caused by NDVI addiction to the models (%)	**-3,7**	**-1,9**

5.2.1.2 The role of elevation data to improve classification accuracies: SRTM

The SRTM data set adds to the spectral signature of Landsat-8 bands (Figure 5.8) the information about classes elevation. The “steppe pasture”, “mountain steppe pasture“ and “medium high and low mountain” classes are present at higher elevations than the “desert steppe pasture” class. However, “mountain steppe pasture”, “steppe pasture” and “medium high and low mountain steppe pasture” have very similar values, and the “steppe pasture” class is above all others, when it should be the “mountain steppe pasture”.

Table 5.3 synthetizes the increasing (+) and decreasing (-) F1-scores weighted averages calculated as the difference between the models with and without SRTM. The only models in which SRTM had some influence were Model 4, compared to Model 2, and Model 13 compared to Model 15. For Model 4, by adding SRTM to Landsat-8 bands and NDVI, some improvement (11%) occurred on the accuracy of the classification. However, for Model 15 a considerable decrease (20%) was caused by the addition of SRTM to Landsat-8 bands, mean annual precipitation and mean annual temperature.

Similarly to NDVI, on a general overview, SRTM had no influence on the tested models to which it was added. Additionally, since the “steppe pasture” class had a lot more training points than the remaining classes and several training points of the “steppe pasture” were located in Dzag (that contains the higher elevation values of the three *soums*), it might have caused a high elevation variability within this class, causing an increase on the elevation values of the “steppe pasture” class and, consequently, some confusion among the “steppe pasture”, “medium high and low mountain steppe pasture” and “mountain steppe pasture”.

Table 5.3 - Increasing (+) and decreasing (-) classification accuracies generated by the addition of SRTM data set: comparison of pairs of models with and without SRTM

Pairs of models with and without SRTM data set	Increase (+) or decrease (-) in F1-scores weighted average	
	Maximum likelihood	Decision tree
Model 3 (Landsat-8 bands, SRTM) **vs. Model 1** (Landsat-8 bands)	-2,2	+0,9
Model 4 (Landsat-8 bands, NDVI, SRTM) **vs. Model 2** (Landsat-8 bands, NDVI)	+3,4	**+11,2**
Model 7 (Landsat-8 bands, SRTM, MA precipitation) **vs. Model 5** (Landsat-8 bands, MA precipitation)	-0,9	-1,9
Model 8 (Landsat-8 bands, NDVI, SRTM, MA precipitation) **vs Model 6** (Landsat-8 bands, NDVI, MA precipitation)	+3,4	+1,5
Model 11 (Landsat-8, SRTM, MA temperature) **vs. Model 9** (Landsat-8, MA temperature)	-3,9	-6,5
Model 12 (Landsat-8 bands, NDVI, SRTM, MA temperature) **vs. Model 10** (Landsat-8 bands, NDVI, MA temperature)	+7,3	-1,1
Model 15 (Landsat-8 bands, SRTM, MA precipitation, MA temperature) **vs. Model 13** (Landsat-8 bands, MA precipitation, MA temperature)	-1,3	**-19,7**
Average contribution caused by SRTM addiction to the models (%)	**+0,8**	**-2,2**

5.2.1.3 The role of climate data to improve classification accuracies: mean annual precipitation

.

The mean annual precipitation data set (Figure 5.9), provides a good separation between “mountain steppe pasture” and “desert steppe pasture” from all classes. The “mountain steppe pasture” class has the highest mean annual precipitation values and the “desert steppe pasture” has the lowest. The “steppe pasture” class has slightly higher mean annual precipitation values than the “medium high and low mountain steppe pasture”. This data set can better separate the spectral signatures of the pasture classes, compared to the previous ones.

Mean annual precipitation data set contribution to the Pasture Steppe classification is presented in Table 5.4. Using both maximum likelihood and decision tree, the addition of mean annual precipitation improved some model accuracies. By adding mean annual precipitation to Landsat-8 bands (Model 5 vs. Model 1), to Landsat-8 bands and SRTM (Model 7 vs. Model 3) and to Landsat-8 bands, NDVI and mean annual temperature (Model 14 vs. Model 10), improvements on F1-score weighted averages occurred, using the maximum likelihood classifier. The same has occurred using the decision tree classifier, when mean annual precipitation was added to Landsat-8 bands, NDVI (Model 6 vs. Model 2), to Landsat-8 and mean annual temperature (Model 13 vs. Model 9) and Landsat-8 bands, NDVI and mean annual temperature (Model 14 vs. Model 10). On an overall analysis, this data set demonstrated a good ability to improve the accuracies of some of the models to which it was added.

Table 5.4 - Increasing (+) and decreasing (-) classification accuracies generated by the addition of mean annual precipitation data set: comparison of pairs of models with and without mean annual precipitation

Pairs of models with and without mean annual precipitation data set	Increase (+) or decrease (-) in F1-scores weighted average	
	Maximum likelihood	Decision tree
Model 5 (Landsat-8 bands, MA precipitation) **vs. Model 1** (Landsat-8 bands)	**+10,2**	+7,1
Model 6 (Landsat-8 bands, NDVI, MA precipitation) **vs. Model 2** (Landsat-8 bands, NDVI)	+7,2	**+13,0**
Model 7 (Landsat-8 bands, SRTM, MA precipitation) **vs. Model 3** (Landsat-8 bands, SRTM)	**+11,5**	+4,2
Model 8 (Landsat-8 bands, NDVI, SRTM, MA precipitation) **vs. Model 4** (Landsat-8 bands, NDVI, SRTM)	+7,3	+3,3
Model 13 (Landsat-8, MA precipitation, MA temperature) **vs. Model 9** (Landsat-8, MA temperature)	+4,3	**+16,3**
Model 14 (Landsat-8 bands, NDVI, MA precipitation, MA temperature) **vs. Model 10** (Landsat-8 bands, NDVI, MA temperature)	**+13,8**	**+17,9**
Model 15 (Landsat-8 bands, SRTM, MA precipitation, MA temperature) **vs. Model 11** (Landsat-8 bands, SRTM, MA temperature)	+7,0	+3,1
Model 16 (Landsat-8 bands, NDVI, SRTM, MA precipitation, MA temperature) **vs. Model 12** (Landsat-8 bands, NDVI, SRTM, MA temperature)	+6,6	+3,5
Average contribution caused by SRTM addiction to the models (%)	**+8,5**	**+8,5**

5.2.1.4 The role of climate data to improve classification accuracies: mean annual temperature

The mean annual temperature spectral signatures (Figure 5.10), can provide a good separation of the spectral signatures. The “desert steppe pasture” has the highest temperature values and “mountain steppe pasture” has the lowest. The “steppe pasture” class has a slightly lower mean annual temperature values than the “medium high and low mountain steppe pasture”, as expected.

The contribution of mean annual temperature data set to the tested models is presented in Table 5.5. The maximum likelihood classified models, were not influenced by the addition of mean annual temperature. However, the addition of mean annual temperature to Landsat-8 and mean annual precipitation (Model 13 vs. Model 5) and to Landsat-8 bands, NDVI and mean annual precipitation (Model 14 vs. Model 6) improved F1-scores weighted averages for those models. On an overall analysis, maximum likelihood classifications were not influenced by the addition of mean annual temperature to the tested models, whereas two decision tree model’s registered some improvements on the accuracy results by the addition of this data set.

Table 5.5 - Increasing (+) and decreasing (-) classification accuracies generated by the addiction of mean annual temperature data set: comparison of pairs of models with and without mean annual temperature

Pairs of models with and without mean annual temperature data set	Increase (+) or decrease (-) in F1-scores weighted average	
	Maximum likelihood	Decision tree
Model 9 (Landsat-8 bands, MA temperature) **vs. Model 1** (Landsat-8 bands)	+5,7	+1,5
Model 10 (Landsat-8 bands, NDVI, MA temperature) **vs. Model 2** (Landsat-8 bands, NDVI)	+0,3	+8,8
Model 11 (Landsat-8 bands, SRTM, MA temperature) **vs. Model 3** (Landsat-8 bands, SRTM)	+4,0	-6,0
Model 12 (Landsat-8 bands, NDVI, SRTM, MA temperature) **vs. Model 4** (Landsat-8 bands, NDVI, SRTM)	+4,2	-3,5
Model 13 (Landsat-8, MA precipitation, MA temperature) **vs. Model 5** (Landsat-8, MA precipitation)	-0,2	+10,7
Model 14 (Landsat-8 bands, NDVI, MA precipitation, MA temperature) **vs. Model 6** (Landsat-8 bands, NDVI, MA precipitation)	+6,8	+13,7
Model 15 (Landsat-8 bands, SRTM, MA precipitation, MA temperature) **vs. Model 7** (Landsat-8 bands, SRTM, MA precipitation)	-0,6	-7,1
Model 16 (Landsat-8 bands, NDVI, SRTM, MA precipitation, MA temperature) **vs. Model 8** (Landsat-8 bands, NDVI, SRTM, MA precipitation)	+3,5	-6,1
Average contribution caused by SRTM addiction to the models (%)	**+2,9**	**+1,5**

5.2.1.5 Overview on the role of a satellite-derived vegetation index, elevation and climatic data to improve classification accuracies

The addition of mean annual precipitation caused increases on model accuracies whereas, NDVI and SRTM did not show any influence. Mean annual temperature, improved some of the models when combined to mean annual precipitation, but alone did not had influence on accuracy results. This may be explained by the fact that the Pasture Steppe vegetation is a lot more influenced by the spatial distribution of precipitation, than temperature (Damiran, 2005).

Wang *et al*. (2001) observed that the general spatial distribution of NDVI (as a productivity proxy for vegetation) under different climate regimes, corresponds directly with spatial pattern of mean annual precipitation, while temperature showed a weaker correlation. Helldén and Tottrup (2008) also verified a high correlation between NDVI and precipitation. And that the vegetation response to precipitation is more pronounced in Mongolia than for other regions of the globe. The correlation analysis confirmed that dryland vegetation behavior is the first and foremost a reflection of precipitation behavior. Vandandorj *et al*. (2015) reported that the spatial variability in vegetation cover (NDVI or biomass) of Mongolia was highly dependent on the amount, distribution and coefficient of variation of precipitation.

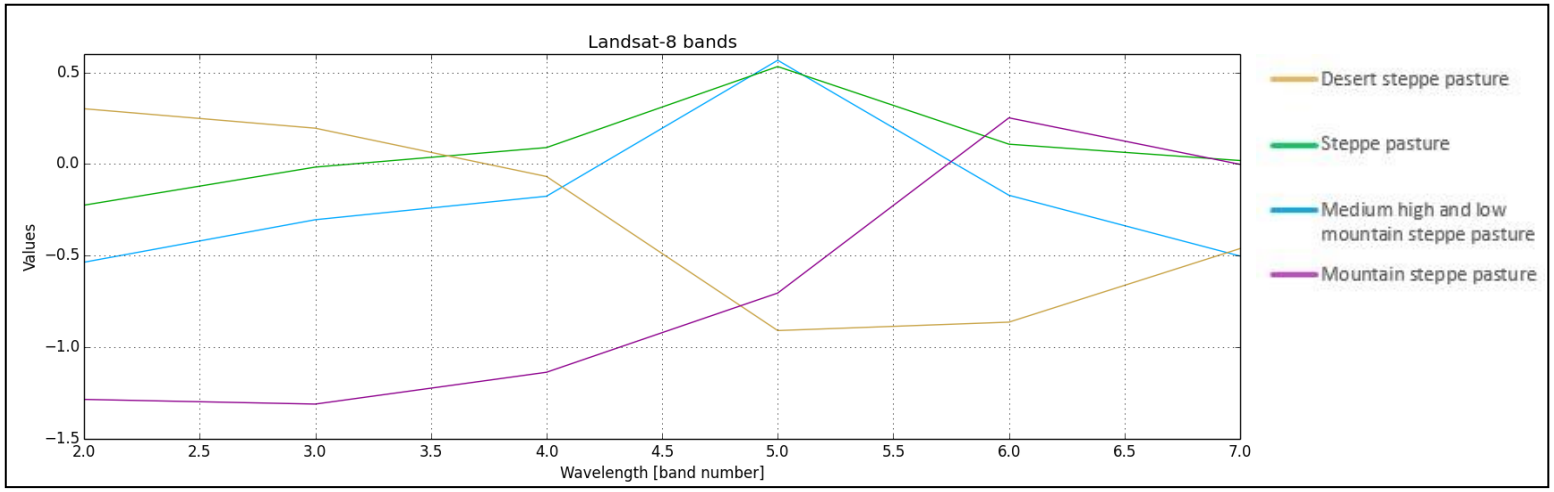

Figure 5.6 - Spectral signatures for the steppe vegetation classes using Landsat-8 bands: OLI-2, OLI-3, OLI-4, OLI-5, OLI-6 and OLI-7 – Model 1

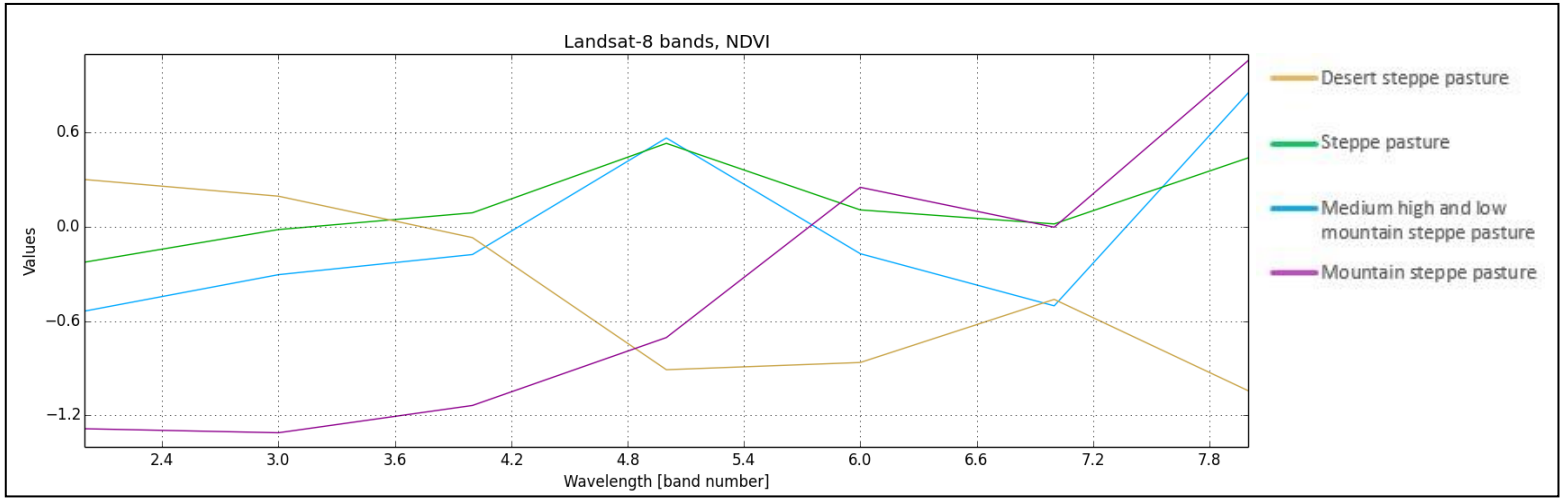

Figure 5.7 - Spectral signatures for the steppe vegetation classes using Landsat-8 bands: OLI-2, OLI-3, OLI-4, OLI-5, OLI-6 and OLI-7 and NDVI [band 8] – Model 2

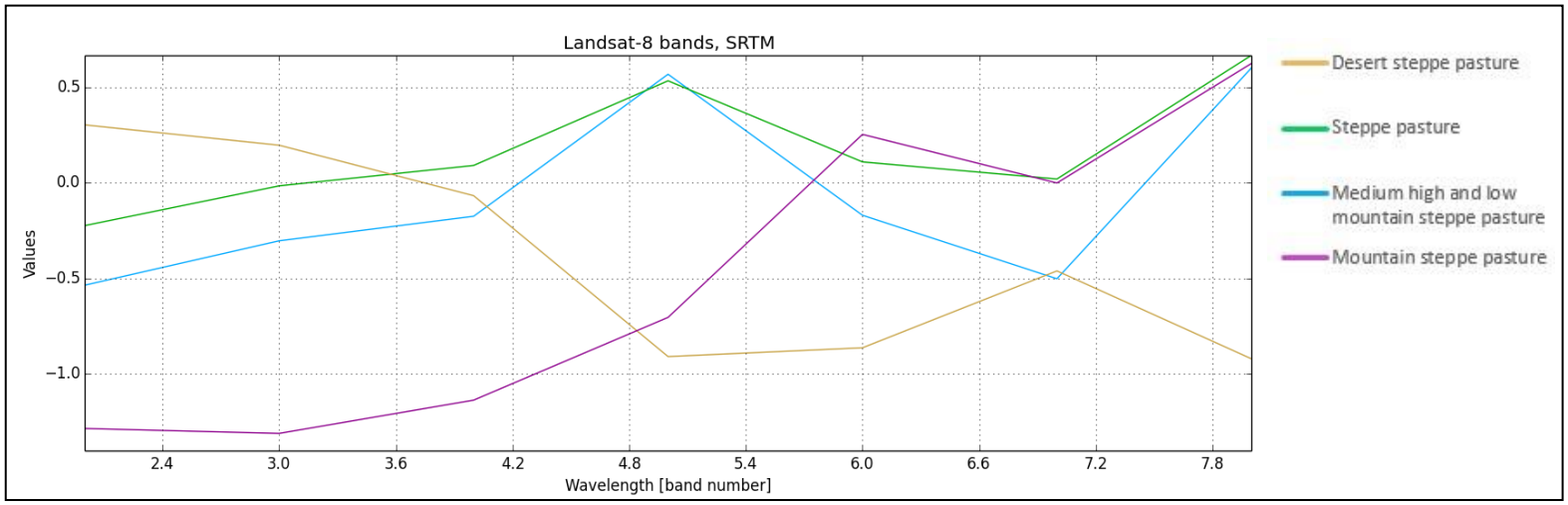

Figure 5.8 - Spectral signatures for the steppe vegetation classes using Landsat-8 bands: OLI-2, OLI-3, OLI-4, OLI-5, OLI-6 and OLI-7 and SRTM [band 8] – Model 3

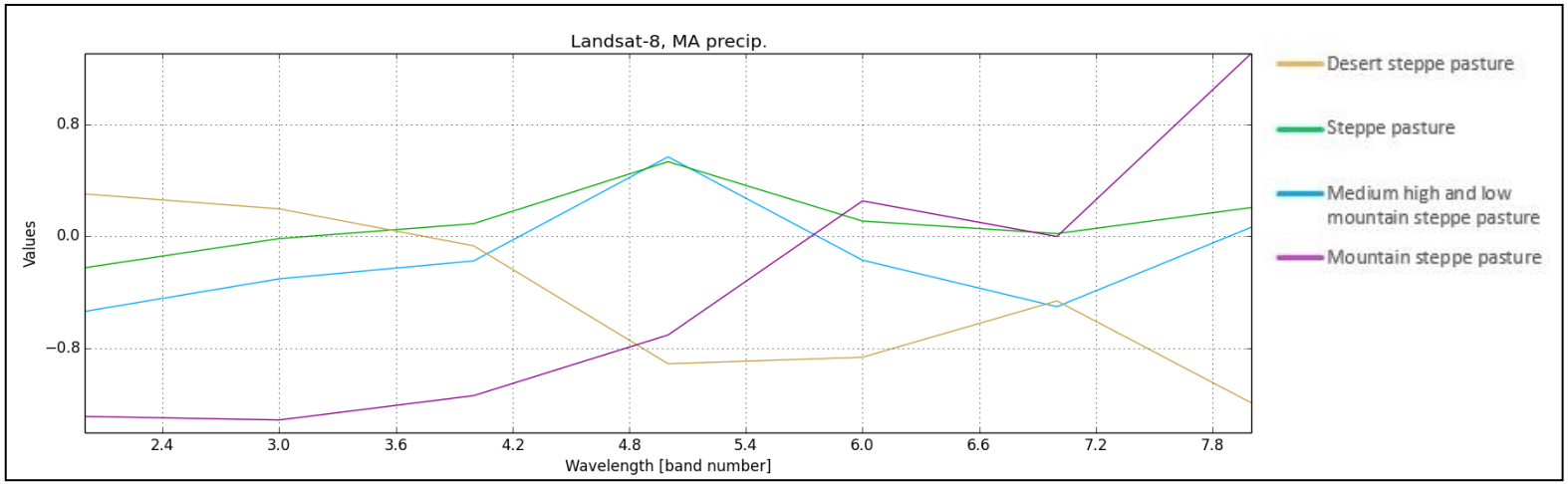

Figure 5.9 - Spectral signatures for the steppe vegetation classes using Landsat-8 bands: OLI-2, OLI-3, OLI-4, OLI-5, OLI-6 and OLI-7 and mean annual precipitation (MA precip.) [band 8] – Model 5

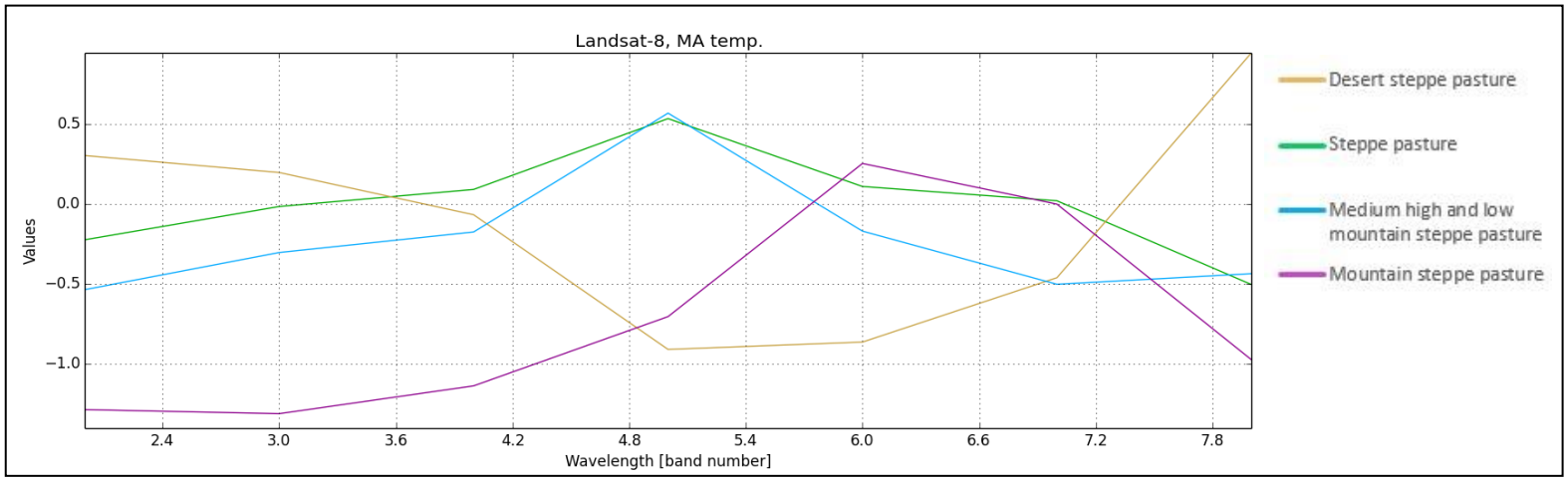

Figure 5.10 - Spectral signatures for the steppe vegetation classes using Landsat-8 bands: OLI-2, OLI-3, OLI-4, OLI-5, OLI-6 and OLI-7 and mean annual temperature (MA temp.) [band 8] – Model 9

5.2.2 Comparative analysis of accuracy assessment

In this section, a discussion about the best performing models (Models 5 and 13 for maximum likelihood and Model 13 for the decision tree) and classification algorithms performance will be done, through a comparative analysis of the obtained F1-scores for individual classes and F1-scores weighted averages. As addressed in section 4.2, the overall accuracies do not provide a reliable estimation for model accuracies, because of the unbalanced number of training and testing points among the pasture classes.

This can be easily seen by comparing model's overall accuracies with F1-scores (or precision and recall) for each class. For instance, the higher overall accuracies for the maximum likelihood classifier were obtained for Model 7 (Table A.2 in Annex) and for Model 15 (Table A.5 in Annex) (79,1%), but looking at the F1-scores of "medium high and low mountain steppe pasture" the algorithm performed very poorly for both models. This overestimated overall accuracy is due to the high accuracy achieved for the "steppe pasture" class, that has a lot more training points, than the remaining classes, resulting on biased accuracy results for the two models.

5.2.2.1 Accuracy assessment for the best models and individual classes performance

Table 5.6 shows the best performing models for both maximum likelihood and decision tree. The higher F1-score weighted average was obtained for Model 13 using the decision tree classifier (74%). The maximum likelihood classifier achieved the higher F1-scores weighted averages on Model 5 and Model 13 (57%).

Figure 5.11 shows the "desert steppe pasture" F1-scores for all tested models, using maximum likelihood and decision tree (for more detailed results see Table 5.6 and Tables A.1 to A.5 in Annex). Decision tree's Model 13, shows a much higher F1-score in this class compared to maximum likelihood's Models 5 and 13. In fact, for this class, the decision tree outperformed maximum likelihood F1-scores in all models. The models that include mean annual precipitation (Models 5 to 8) and the ones that combine mean annual precipitation with mean annual temperature (Models 13 to 16), achieved the higher F1-scores, for both classification algorithms.

Figure 5.12 presents the "steppe pasture" F1-scores for all tested models, using maximum likelihood and decision tree (for more detailed results see Table 5.6 and Tables A.1 to A.5 in Annex). Maximum likelihood best performing models (Model 5 and Model 13) registered slightly higher F1-scores on this class. However, because some uncertainty level is associated with the classification, the differences among the F1-scores of the three best performing models are not significant. An overview on the maximum likelihood and decision tree F1-scores, shows that some of the maximum likelihood models registered significant improvements compared to the decision tree ones (Models 6, 7, 8, 11, 12 and 15). On the other hand, Model 2 and Model 4 showed better results using the decision tree classifier.

Models containing mean annual precipitation (Model 5, 7 and 8), mean annual temperature (Model 9) and the ones that combine both (Model 13, 14,15 and 16), were the models for which maximum likelihood verified the higher accuracy results on the “steppe pasture” class (F1-score>85%). Whereas decision tree registered the highest accuracy result (F1-score>85%) for the best performing model (Model 13).

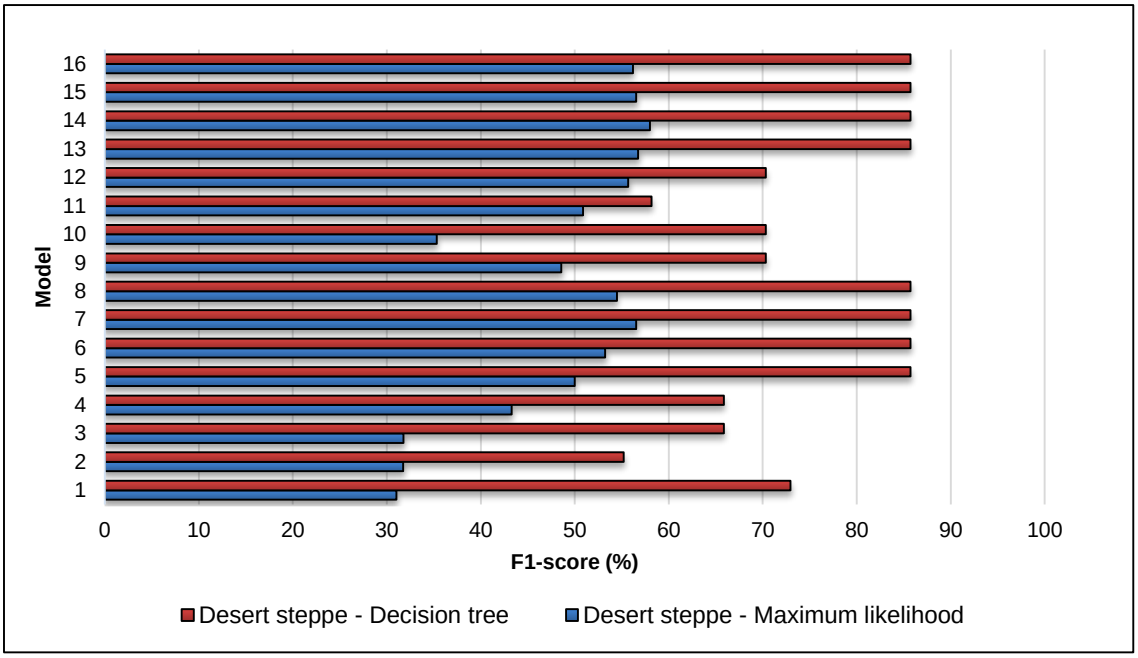

Figure 5.11 - “Desert steppe pasture” F1-scores for all tested models using decision tree and maximum likelihood

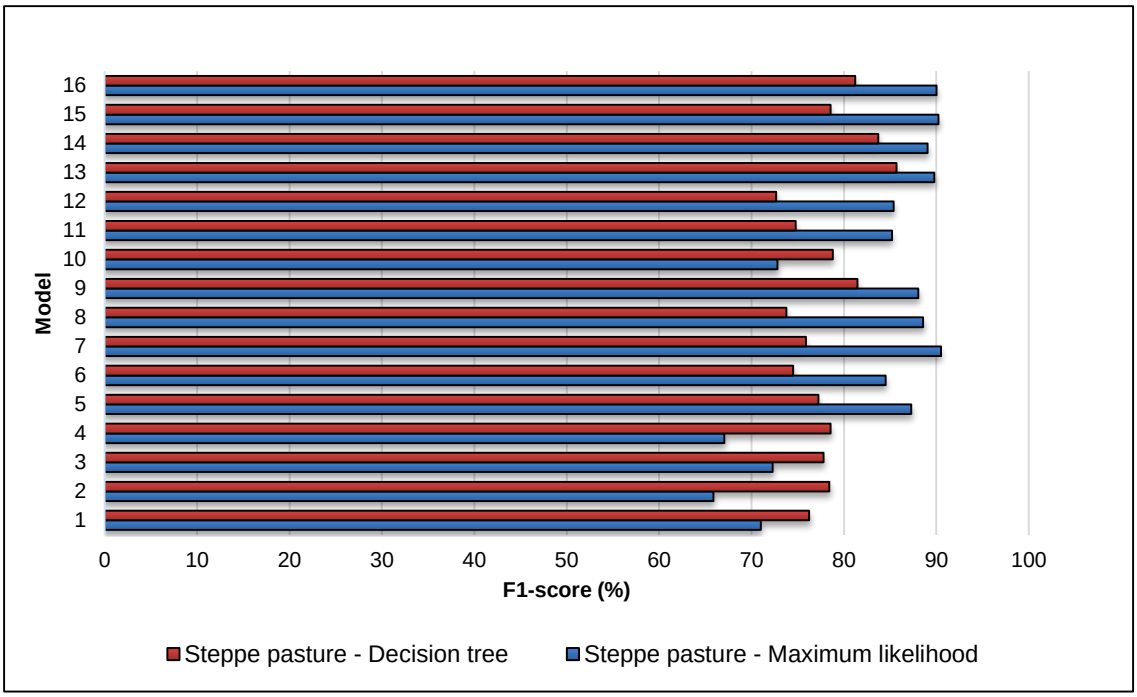

Figure 5.12 - “Steppe pasture” F1-scores for all tested models using decision tree and maximum likelihood

Table 5.6 - Accuracy report for the classification of the Pasture Steppe vegetation for the best F1-scores weighted average: Model 5 and Model 13 for maximum likelihood and Model 13 for decision tree (highlighted in blue)

Model 5: Landsat-8 bands, MA precipitation	**Maximum likelihood**					**Decision tree**				
	F1-score [%]	**F1-score weighted average [%]**	**Precision [%]**	**Recall [%]**	**Overall accuracy [%]**	**F1-score [%]**	**F1-score weighted average [%]**	**Precision [%]**	**Recall [%]**	**Overall accuracy [%]**
Desert steppe pasture	50	**57**	73	38	79	86	**63**	100	75	70
Steppe pasture	87		83	92		77		82	73	
Medium high and low mountain steppe pasture	28		26	31		31		25	40	
Mountain steppe pasture	68		64	74		76		70	82	
Model 13: Landsat-8 bands, MA precipitation, MA temperature	**Maximum likelihood**					**Decision tree**				
	F1-score [%]	**F1-score weighted average [%]**	**Precision [%]**	**Recall [%]**	**Overall accuracy [%]**	**F1-score [%]**	**F1-score weighted average [%]**	**Precision [%]**	**Recall [%]**	**Overall accuracy [%]**
Desert steppe pasture	57	**57**	99	40	79	86	**74**	100	75	80
Steppe pasture	90		89	90		86		81	91	
Medium high and low mountain steppe pasture	22		14	49		58		75	47	
Mountain steppe pasture	66		59	75		65		64	66	

"Medium high and low mountain steppe pasture" F1-scores for all tested models, using maximum likelihood and decision tree, are presented in Figure 5.13 (for more detailed results see Table 5.6 and Tables A.1 to A.5 in Annex). For this class, decision tree's best performing model (Model 13) outperformed the maximum likelihood ones (Models 5 and 13) by a great margin on F1-scores. Significant differences among the two classification algorithms were seen. On an overall basis, decision tree outperformed maximum likelihood's classification performance for this class. Being the most problematic class, the higher F1-score was obtained on two models that combine mean annual precipitation with mean annual temperature (Model 13 and Model 14) using the decision tree classifier, achieving a F1-score of 58%. Using the maximum likelihood classifier, only two models registered F1-scores above 25%, the base model (Model 1) with Landsat-8 bands (F1-score=27%) and Model 5 that achieved the highest F1-score on this class (F1-score=31%), by adding to Landsat-8 spectral bands the mean annual precipitation.

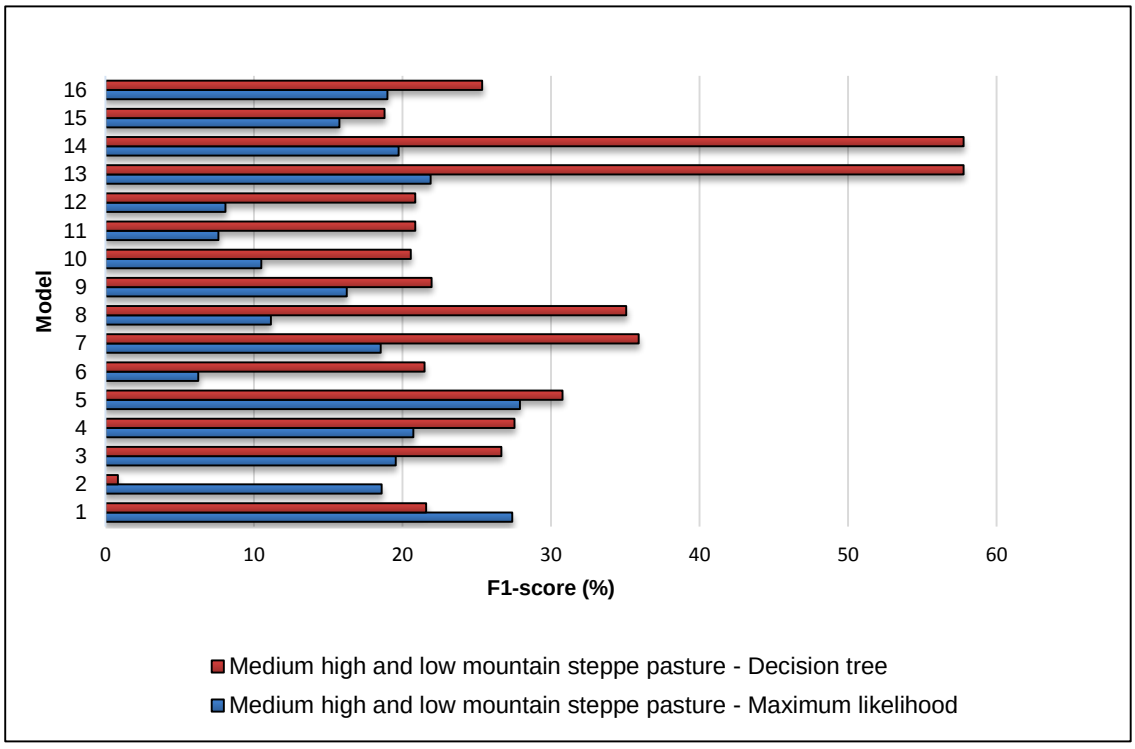

Figure 5.13 - "Medium high and low mountain steppe pasture" F1-scores for all tested models using decision tree and maximum likelihood

Figure 5.14 presents "mountain steppe pasture" F1-scores for all tested models, using maximum likelihood and decision tree (for more detailed results see Table 5.6 and Tables A.1 to A.5 in Annex). No significant differences were registered comparing the best performing decision tree model (Model 13) with maximum likelihood ones (Model 5 and Model 13) on this class. The decision tree obtained the highest F1-score (F1-score>75%) on a model containing mean annual precipitation (Model 5), whereas maximum likelihood obtained the highest F1-score (F1-score>70%) on a model that combined mean annual precipitation with mean annual temperature (Model 15).

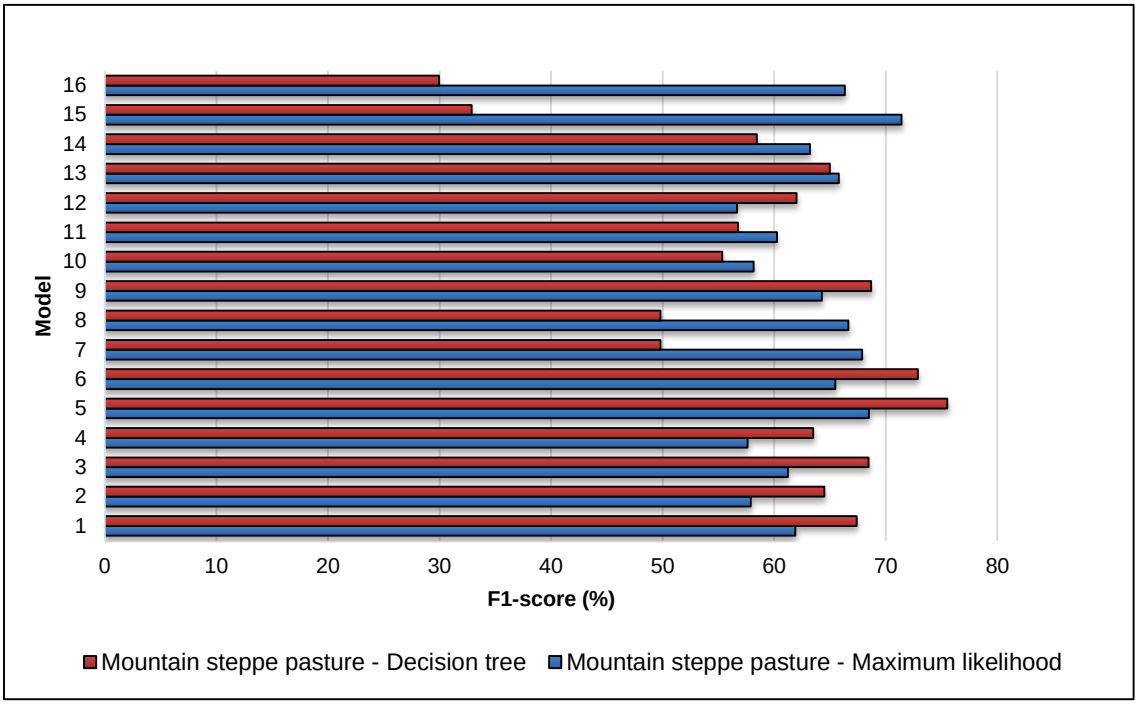

Figure 5.14 - "Mountain steppe pasture" F1-scores for all tested models using decision tree and maximum likelihood

Individual classes accuracy analysis reinforces the role of each data set on the performed classifications. On Figures 5.11, 5.12, 5.13 and 5.14, NDVI, SRTM and mean annual temperature data sets did not influence F1-scores accuracy results for individual classes. However, when mean annual precipitation and mean annual temperature are both present, improvements can be seen on some classes.

In fact, using the decision tree, major improvements were seen on "medium high and low mountain steppe pasture" class, by adding mean annual temperature to the model that only contained mean annual precipitation (Model 13), which is very important because this was the most problematic class and it covers a great part of the study area. For the "steppe pasture" class, improvements were also registered by combining these two data sets. However, on "mountain steppe pasture" a decrease on the F1-score occurred by the addition of mean annual temperature to mean annual precipitation (Model 13) and "desert steppe pasture" registered the same F1-scores for both cases.

Despite having achieved better F1-scores than maximum likelihood, the decision tree never exceeded 58% on "medium high and low mountain steppe pasture" (Model 13). On "desert steppe pasture" the model containing mean annual precipitation (Model 5) and the one containing both mean annual precipitation and mean annual temperature (Model 13) achieved the highest F1-scores of 86% using the decision tree. For both "steppe pasture" and "mountain steppe pasture" no significant differences on the accuracies were registered when comparing maximum likelihood best performing models (Model 5 and Model 13), with the decision tree best performing model (Model 13). F1-scores between 86% and 90% were achieved on the "steppe pasture" and between 65% and 69% on "mountain steppe pasture".

The existence of similar spectral reflectance characteristics, caused by the similar phonologies of the pasture classes may have promoted a high confusion between some of the classes (Liu *et al*., 2003). For maximum likelihood's best performing models (Models 5 and 13), a high confusion was verified among "medium high and low mountain steppe pasture", "desert steppe pasture" and "steppe pasture" classes. Whereas for decision tree's best performing model (Model 13) a high confusion among "medium high and low mountain steppe pasture" and the steppe pasture class" was registered, but not with "desert steppe pasture", which indicates that by adding climatic data sets, the decision tree was capable of achieving higher accuracy results compared to models that do not contain these data sets and, also, of achieving much better results than maximum likelihood on this class.

5.2.2.2 Spatial distribution variations caused by different combinations of estimators and classification algorithms

Accordingly to the training points provided by the local users, the "desert steppe pasture" class should be confined to Khureemaral and Buutsagaan and the same is applied to "medium high and low mountain steppe pasture". The "steppe pasture" class should be distributed along the three *soums* and "mountain steppe pasture" should be confined to Dzag.

The maps classified by the maximum likelihood and the ones classified by the decision tree (Figures 5.15 to 5.18 and Figures A.15 to A.42 in Annex), show that the classes distribution for each algorithm are very different. The maximum likelihood maps typically present "desert steppe pasture" located on the south region of Khureemaral and Buutsagaan, having a smaller area compared to decision tree "desert steppe pasture" areas. "Medium high and low mountain steppe pasture" is located right above "desert steppe pasture", also in Khureemaral and Buutsagaan. "Mountain steppe pasture" is mainly located in Dzag, but also in the north region of Buutsagaan for the majority of the models.

For the decision tree models that include Landsat-8 bands (Model 1 – Figure A.16 in Annex) and NDVI (Model 2 - Figure A.18 in Annex), the "desert steppe pasture" presents really small areas, mainly located in Khureemaral and Buutsagaan. On these models Buutsagaan's "desert steppe pasture" is almost inexistent, when it should be the *soum* containing the major area extent of this class. The models containing SRTM (Models 3 and 4 – Figures A.20 and A.22 in Annex), registered a great increase on "medium high and low mountain steppe pasture" for the whole study area, including Dzag, that should only contain "mountain steppe pasture". "Mountain steppe pasture" is almost inexistent. Comparatively to the last two models, this data set increased the "desert steppe pasture" area in Buutsagaan, but decreased in Khureemaral, having also "mountain steppe pasture" on the south region of this *soum*.

Mean annual temperature (Models 9, 10, 11 and 12 - Figures A.30, A.32, A.34 and A.36 in Annex) brings "medium high and low mountain steppe pasture" to an area right above the "desert steppe pasture", similarly to the majority of models generated by maximum likelihood. The "desert steppe pasture" area increases in Buutsagaan with this data set. "Medium high and low

mountain steppe pasture" is present in Dzag, however it should be confined to Khureemaral and Buutsagaan.

For models to which mean annual precipitation was added (Models 5, 6, 7 and 8 – Figure 5.16 and Figures A.24, A.26 and A.28 in Annex) and for the ones that combine both mean annual precipitation and mean annual temperature (Models 13, 14, 15 and 16 - Figure 5.18 and Figures A.38, A.40 and A.42 in Annex), "medium high and low mountain steppe pasture" switches its spatial distribution to the central area of Khureemaral and Buutsagaan. The "desert steppe pasture" is broken by some "medium high and low mountain steppe pasture" small areas. There are also some smaller areas of "mountain steppe pasture" near the "desert steppe pasture" class. Mean annual precipitation and mean annual temperature data sets reduced the variability among classes, caused by the lower resolution of these data sets (1 km), which can be seen by comparing the models that include climatic data sets with Model 1, Model 2, Model 3 and Model 4 (Figures A.16, A.18, A.20 and A.22 in Annex). In fact, the possibility that this variability reduction might have caused an increase on the accuracy of the models, should not be discarded.

The mapped areas per class for the best performing models, using maximum likelihood and decision tree (Model 5 and Model 13), are presented in Table 5.7 (the corresponding maps can be seen in Figures 5.15, 5.17 and 5.18). These values are only informative about the differences among the real area extent and the thematic-derived areas for each class and, therefore, should not be taken as a proxy for selecting the best performing model, because by achieving similar areas for each class, between the mapped areas and real ones, it does not imply a more accurate spatial distribution of a class (Foody, 2002).

Looking at the classified areas in proportion to real area extent for each class (real areas extent per class are presented in Table 4.1), "desert steppe pasture", "medium high and low mountain steppe pasture" and "mountain steppe pasture" occupy smaller areas on the maps, compared to real areas extent. However, the "steppe pasture" class always exceeded the real area extent, which was caused by the higher number of training points provided for this class, compared to the remaining three classes.

It is important to notice that, although "mountain steppe pasture" class seemed to have similar F1-scores accuracy results on the best performing models for the two classifiers (Models 5 and 13 using maximum likelihood and Model 13 using decision tree), the decision tree model presented a more approximate mapped area to the real area extent for this class. Additionally, decision tree's Model 5, was the model that obtained both higher F1-score on this class and the more approximate mapped area to the real area extent.

The "desert steppe pasture" obtained considerably higher F1-scores for the best performing models, using the decision tree (Model 13), compared to maximum likelihood (Models 5 and 13), and also a more approximate area to the real extent was mapped. For "medium high and low mountain steppe pasture", the maximum likelihood best performing models (Models 5 and 13) achieved a more approximate area to the real area extent, however the spatial distribution of the decision tree best performing model (Model 13) is by far the most accurate, because a much higher F1-score was achieved for decision tree's best performing model (Model 13),

compared to the maximum likelihood ones (Models 5 and 13). For the “steppe pasture” class the mapped area is similar on the best performing models for both algorithms, also no significant differences were registered on F1-scores.

Table 5.7 – Mapped areas per class and classified area in proportion to real area extent for the best performing models (highlighted in blue): Model 5 and Model 13 using maximum likelihood and decision tree

	Maximum likelihood		Decision tree	
Model 5 - Landsat-8 bands and mean annual precipitation	**Area (m^2)**	**Mapped area in proportion to real area extent (%)**	**Area (m^2)**	**Mapped area in proportion to real area extent (%)**
Desert steppe pasture	1349	58	1755	76
Steppe pasture	5685	149	5046	132
Medium high and low mountain steppe pasture	1985	50	1818	46
Mountain steppe pasture	824	58	1224	86
Model 13 - Landsat-8 bands, mean annual precipitation and mean annual temperature	**Area (m^2)**	**Mapped area in proportion to real area extent (%)**	**Area (m^2)**	**Mapped area in proportion to real area extent (%)**
Desert steppe pasture	1199	52	1678	72
Steppe pasture	5149	135	5553	145
Medium high and low mountain steppe pasture	2745	70	1619	41
Mountain steppe pasture	751	53	993	70

5.2.2.3 Global overview on classification algorithms performance

Figure 5.19 presents F1-scores weighted averages in pairs for all tested models, using maximum likelihood and decision tree. For all models that contain relevant data sets to improve classification accuracies: Model 1 (Landsat-8 bands), Model 5 (Landsat-8 bands and mean annual precipitation) and Model 13 (Landsat-8 bands, mean annual precipitation and mean annual temperature), the decision tree outperformed maximum likelihood models. De Fries *et al*. (1998) has also compared the performance of the decision tree with maximum likelihood, using three types of decision tree classifier (univariate, multivariate and hybrid), for land cover mapping. Classification accuracies also showed that decision tree algorithms consistently outperformed the maximum likelihood.

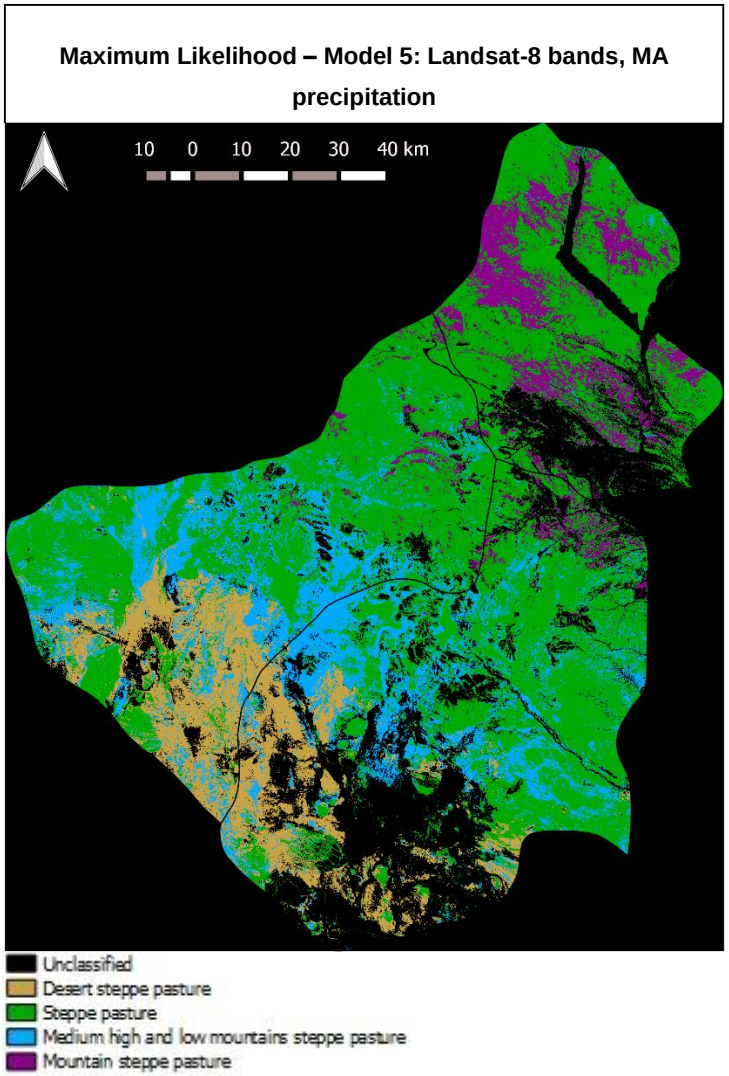

Figure 5.15 - Steppe classification using maximum likelihood - Model 5: Landsat-8 bands, MA precipitation

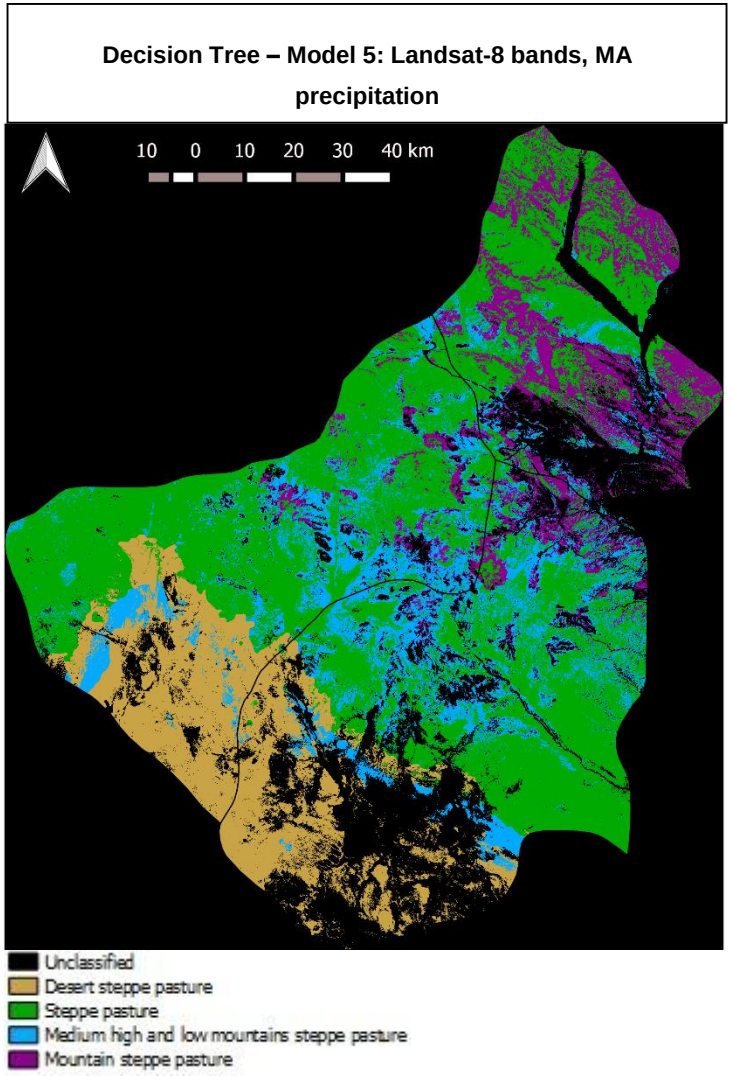

Figure 5.16 - Steppe classification using decision tree - Model 5: Landsat-8 bands, MA precipitation

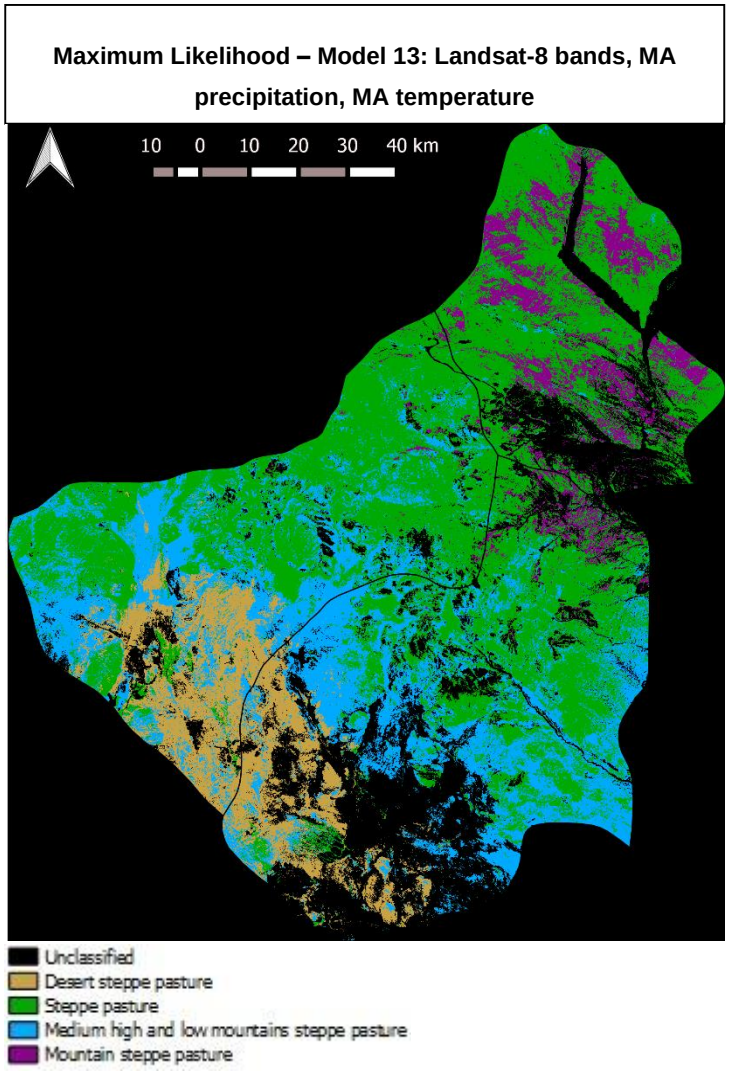

Figure 5.17 - Steppe classification using maximum likelihood - Model 13: Landsat-8 bands, MA precipitation and MA temperature

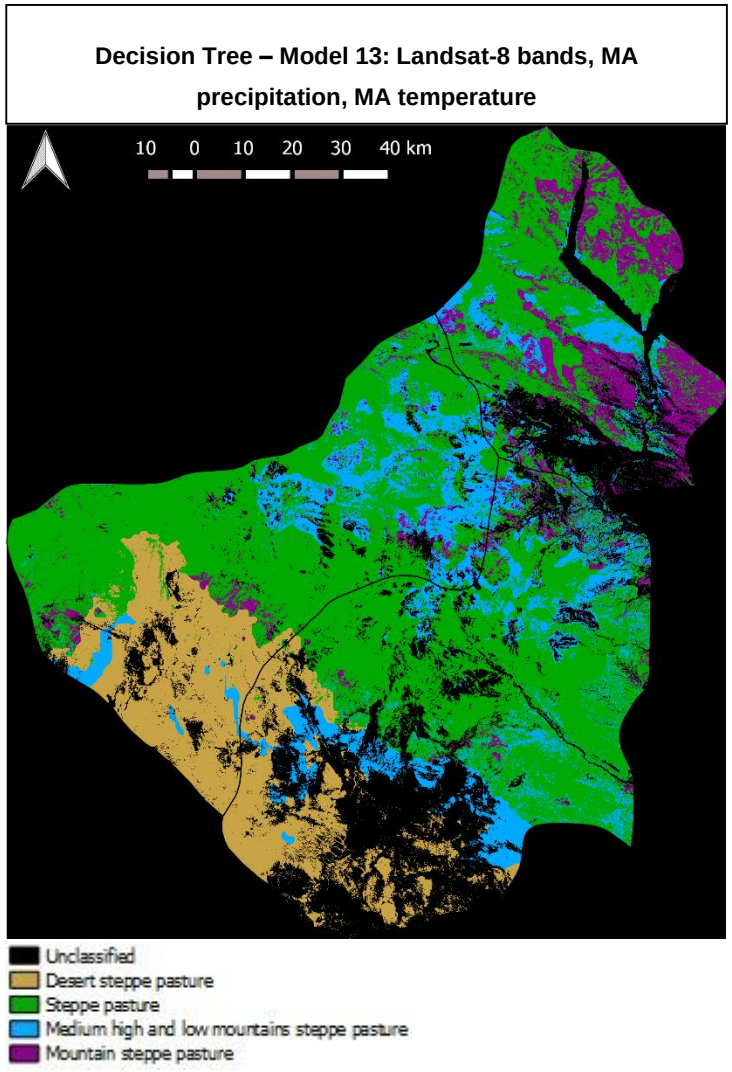

Figure 5.18 - Steppe classification using decision tree - Model 13: Landsat-8 bands, MA precipitation and MA temperature

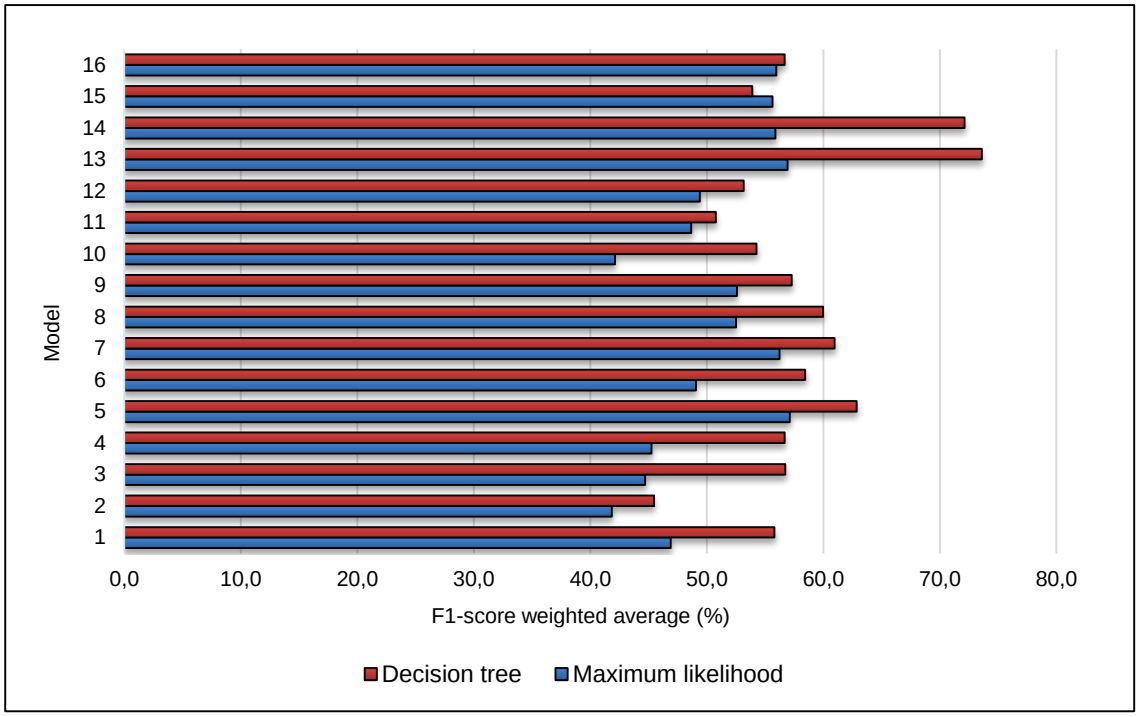

Figure 5.19 - F1-scores weighted average for all tested models using decision tree and maximum likelihood

The decision tree seemed to be more influenced by the addition of different data sets into the classification, compared to the maximum likelihood, because more variations on the spatial distribution of the classes were seen throughout the different models. This is due to the fact that the decision tree, being a non-parametric algorithm, makes no assumptions regarding the distribution of input data, it is flexible and robust with respect to nonlinear and noisy relations among input features and class labels (De Fries *et al*., 1998), also the decision tree allowed the possibility to adjust parameters like maximum depth and minimum number of samples required at a leaf node, in order to find the best performing tree.

Furthermore, since maximum likelihood takes the variability of classes into account by using the covariance matrix, it requires a sufficient number of representative training samples for each class to accurately estimate the mean vector and covariance matrix, required for performing the classification. In fact, maximum likelihood F1-scores were lower for two of the classes that had a smaller number of training points (“desert steppe pasture” and “medium high and low mountain steppe pasture”) compared to the decision tree classifier. The inaccurate estimation of those classes might have been caused by the limited number of training samples (Moran, 2010).

A possible reason for decision tree models to have achieved higher accuracy results on “desert steppe pasture” and “medium high and low mountain steppe pasture” classes, may be related to the fact that the decision tree does not require very large training samples to be effective when performing the classification. Whereas, for maximum likelihood an important requirement is that a representative number of training samples exist for each class, that should be 10 to 30 times the number of features within the study area. In this case, the small training sample size might have implied standard errors of the estimates, causing decision boundaries to be located incorrectly or imprecisely (Pal and Mather, 2003).

However, even decision tree performed poorly for “medium high and low mountain steppe pasture” and “mountain steppe pasture” on the best performing model (Model 13). For achieving better results, a more balanced number of training points were required, since the presence of an unbalanced data set, with some classes more heavily represented than others, can affect decision tree’s performance, with the analysis sometimes dividing heavily represented classes, rather than splitting out lightly those classes (Pal and Mather, 2003).

6. Conclusions

In order to provide information for the definition of areas to set aside as emergency grazing reserves for livestock (grazing areas in a good state for livestock production that can be used when droughts occur or when overgrazed areas are prominent), this study investigated, on a first stage, which was the highest thematic level of detail, that was possible to achieve through remote sensing, to map the steppe vegetation, using medium resolution earth observation imagery in three districts (*soums*) of Mongolia: Dzag, Buutsagaan and Khureemaral.

From the three levels of thematic detail chosen to achieve the goal of this thesis, mapping among species composition would not be feasible, due to Landsat-8 imagery resolution. Additionally, other grassland properties, such as AGB and yield, plant density, productivity, LAI, or percentage cover could mislead the definition of emergency grazing areas, due to the possible presence of unpalatable plants that might have invaded the grazed areas. For the stated reasons, mapping the different pasture types was the selected thematic level of detail.

On a second stage, a comparison of different classification methods, using Landsat-8 (spectral bands and Landsat-8 NDVI-derived) and geophysical data (including elevation, mean annual precipitation and mean annual temperature data), was performed using two classification algorithms, maximum likelihood (parametric) and decision tree (non-parametric), in order to investigate which combination of data sets yields the best results and which classification algorithm is more suitable for incorporating these data sets for mapping the Pasture Steppe.

On the first attempts to perform the classification of the pasture classes using the training and testing points provided by the local users, a high level of confusion among classes was registered. In order to reduce this confusion, masking non-steppe features present at the study area (main classes) was considered to be important. These main classes consisted of “mountain bare soil”, “desert bare soil” and “water and riparian vegetation” and “steppe vegetation”.

Since no training points were available for the main classes “mountain bare soil”, “desert bare soil” and “water and riparian vegetation” classes (with exception for the steppe vegetation class), ROIs were defined based on Landsat-8 and Google Earth images. For this reason, very high accuracies were achieved for all tested models used to map the main classes. This classification procedure constitutes a limitation and such high accuracy results should be looked with caution, because a very high level of uncertainty exists. However, since the definition of these classes was only performed to obtain a mask of non-steppe vegetation and to reduce the confusion among the pasture classes, the procedure consisted on an effective method for the purpose, because the accuracy results for the pasture classes, within the steppe vegetation, improved after masking the main classes.

For the Pasture Steppe classification, sixteen models with different combinations of estimators (Landsat-8 OLI-2, OLI-3, OLI-4, OLI-5, OLI-6 and OLI-7 bands, Landsat-8 NDVI-derived, SRTM, mean annual precipitation and mean annual temperature), using maximum likelihood and decision tree classifiers, were tested. Through a comparison between pairs of

models, the estimators performance was accessed. Results showed that NDVI, SRTM and mean annual temperature, did not had influence on the tested models accuracy. Whereas, mean annual precipitation models and the ones that combined mean annual precipitation with mean annual temperature, improved the accuracy results on both algorithms.

The major limitation concerning the steppe classification into its pasture types, is related with the unbalanced number of training points between the “steppe pasture” class and the remaining classes. The number of training points for each class was not in proportion to the classes occupied areas, which hindered the algorithms performance. In such cases, caution must be taken when choosing the best performing models by looking at the overall accuracy results, because by having some classes more heavily represented than others, the overall accuracy tends to overestimate or underestimate accuracy results, being mostly dependent on the more heavily represented class. However, F1-scores weighted averages provided the means to select, as the best performing models, the ones in which more balanced accuracy results were achieved among classes. F1-scores weighted averages were accessed in function to the real area extents for each class for comparison purposes between models and for accessing estimators and classification algorithms performance.

The best performing model belongs to the decision tree classifier, Model 13, containing Landsat-8 OLI-2, OLI-3, OLI-4, OLI-5, OLI-6 and OLI-7 bands, mean annual precipitation and mean annual temperature. This model achieved the higher F1-score weighted average from all models (74%). Model 5 containing Landsat-8 OLI-2, OLI-3, OLI-4, OLI-5, OLI-6 and OLI-7 bands and mean annual precipitation and Model 13, achieved the higher F1-scores weighted averages for the maximum likelihood classifier (57%). Results showed that the decision tree models consistently outperformed the maximum likelihood ones, which may be explained by the fact that the decision tree does not require very large training samples to be effective when performing the classification. Whereas, for maximum likelihood an important requirement is that a representative number of training samples exists for each class (Pal and Mather, 2003).

Furthermore, the decision tree, being a non-parametric algorithm, was more influenced by the addiction of different data sets into the classification procedure, than maximum likelihood, because more variations were seen throughout the decision tree maps compared to the maximum likelihood ones. However, even the decision tree was not capable of achieving satisfactory results for “medium high and low mountain steppe pasture” and “mountain steppe pasture” classes on the same model, which might have been caused by the unbalanced number of training points, since it can affect decision tree’s performance, with the analysis sometimes dividing heavily represented classes, rather than splitting out lightly represented classes (Pal and Mather, 2003). The negative influence of the unbalanced data set can also be seen by comparing the real area extents of the classes with the mapped areas. The “desert steppe pasture”, “medium high and low mountain steppe pasture” and “mountain steppe pasture” consistently presented inferior areas on the map compared to the real areas extent, while the mapped “steppe pasture” exceeded the real area extent by a great margin.

The results suggest that a correlation must exist when combining precipitation with temperature data (Model 13), of a long period of time (1950-2000), and the spatial distribution of the Pasture Steppe vegetation. Although higher accuracy results were achieved using climatic data sets, the lower resolution of these estimators (1 km) compared to the remaining ones (30 m), has caused a sampling variability reduction. The possibility that this variability reduction might have caused an increase on the accuracy of the models, should not be discarded and should be further investigated.

To overcome the major limitations inherent to this study, a more reliable classification of the non-steppe features (main classes) should be done, using training and testing points collected in the field. Also, more training and testing points for “medium high and low mountain steppe pasture” and “mountain steppe pasture” should be available and in proportion to pasture classes occupied areas, to perform a more accurate classification of the Pasture Steppe classes. Furthermore, although a single date image approach offers some advantages for detecting differences among vegetation types within grasslands, the selection of a single date may be difficult, since vegetation types spectral signatures may be more or less separated depending on the growing period and season (Peterson *et al*., 2002).

The Landsat-8 image used in this study was from 30 August, which may have hindered the results, because some pasture species reach their final growth in August, while others may continue its vegetative growth until mid-September or remain green until October (Damiran, 2005). This limitation might be overcome by using multi-temporal satellite data (Peterson *et al*., 2002) or instead of using Landsat-8 NDVI-derived, a NDVI time series covering the growing season period, could be added to the classification, since each pasture class has a different growing period (Damiran, 2005).

7. References

Amarsaikhan, D. and Sato, M. (2003). A conceptual framework for development of a cadastral information system linked to an environmental information system in Mongolia, Full paper published in Proceedings of the Computers for Urban Planning and Urban Management (CUPUM)’03 International Conference, Sendai, Japan, 1-10.

Cibula, W. G. and Nyquist, M. O. (1987). Use of topographic and climatological models in a geographical data base to improve Landsat MSS classification for Olympic National Park. Photogrammetric Engineering and Remote Sensing, 1, 67–75.

Badarch, M., Dorjgotov, B. and Enknbat, A. (Eds.) (2009). Mongolian´s fourth national report on implementation of convention of biological diversity. Agriculture and Environment Standing Committee, State Great Khural; MNET; Sustainable Pasture Management; Bio-Safety National Committee; Institute of Biology; Institute of Botany; Institute of Geo-ecology; NUM;

MUST; UNDP; GTZ; Conservation of the Great Gobi Ecosystem and its Endangered Species; Natural Resource Management and Geo-information Center project; and World Bank. 124 pp. Retrieved April 3, 2015, from https://www.cbd.int/doc/world/mn/mn-nr-04-en.pdf

Dagvadorg, D., Batima, P. and Natsagdorj, L. (2001). Climate change and its impacts on ecosystem of Mongolia. Open Symposium on Change and Sustainability of Pastoral Land Use Systems in Temperate and Central Asia. Ulanbaatar, Mongolia, June 28–July 1, 2001.

Dagvadorj, D., Natsagdorj, L., Dorjpurev, J. and Namkhainyam, B. (2009). Mongolia Assessment Report on Climate Change 2009. *Ministry of Environment, Nature and Tourism, Mongolia*, Ulaanbaatar, Mongolia, Setember 2009. ISBN: 978-99929-934-3-X

Damiran, D. (2005). Palatability of Mongolian Rangeland Plants. *Eastern Oregon Agricultural Research Center, Circular of Information No.3, Eastern Oregon Agricultural Research Center*, Oregon State University

De Fries, R. S., Hansen, M., Townshend, J. R. G. and Sohlberg, R. (1998). Global land cover classifications at 8 km spatial resolution: The use of training data derived from Landsat imagery in decision tree classifiers. *International Journal of Remote Sensing*, *19*(16).

Fernandez-Gimenez, M. and Allen-Diaz, B. (2001). Vegetation change along gradients from water sources in three grazed Mongolian ecosystems. *Plant Ecology*, *157*, 101–118.

Foody, G. M. (2002). Status of land cover classification accuracy assessment. *Remote Sensing of Environment*, 80(1), 185–201.

Friedl, M. A. and Brodley, C. E. (1997). Decision tree classification of land cover from remotely sensed data. *Remote Sensing of Environment*, *61*(3), 399–409.

Gandhi, G. M., Parthiban, S., Thummalu, N. and Christy, A. (2015). Ndvi : Vegetation change detection using using remote sensing and gis – A case study of Vellore District. *Procedia Computer Science*, *57*, 1199–1210.

Gao, J. (2006). Quantification of grassland properties: how it can benefit from geoinformatic technologies? *International Journal of Remote Sensing*, *27*(7), 1351–1365.

Goutte, C. and Gaussier, E. (2005). A Probabilistic Interpretation of Precision, Recall and F-score, with Implication for Evaluation, 345–359.

He, C., Zhang, Q., Li, Y., Li, X. and Shi, P. (2005). Zoning grassland protection area using remote sensing and cellular automata modeling - A case study in Xilingol steppe grassland in northern China. *Journal of Arid Environments*, *63*(4), 814–826.

Helldén, U. and Tottrup, C. (2008). Regional desertification: A global synthesis. *Global and Planetary Change*, *64*(3-4), 169–176.

Karnieli, A., Bayarjargal, Y., Bayasgalan, M., Mandakh, B., Dugarjav, C., Burgheimer, J., Khudulmur, S., Bazha, S. N. and Gunin, P. D. (2013). Do vegetation indices provide a reliable indication of vegetation degradation? A case study in the Mongolian pastures. *International Journal of Remote Sensing*, *34*(17), 6243–6262.

Kawamura, K. and Akiyama, T. (2010). Simultaneous Monitoring of Livestock Distribution and Desertification. *Global Environmental Research*, *14*, 29–36.

Khishigbayar, J., Reid, R. S., Fernandez-Gimenez, M. E., Angerer, Jay, P., Chantsallkham, J., Baasandorj, Y. and Zumberelmaa, D. (2015). Mongolian rangelands at a tipping point? Biomass and cover are stable but composition shifts and richness declines after 20 years of grazing and increasing temperatures. *Journal of Arid Environments*, *115*, 100–112.

Koirala, S. (2010). Land use/land cover change and its impact on soil erosion process in Begnas Tal Rupa Tal watershed using geospatial tools, Kaski district, Nepal. Dissertation submitted in partial fulfilment on the requiremets for the Degree of Master of Science in Geospatial Technologies, *ISEGI Universidade Nova de Lisboa*, Lisboa, pp. 62 Retrieved from http://run.unl.pt/handle/10362/2732

Kopecký, M. and Cizková, S. (2010). Using topographic wetness index in vegetation ecology : does the algorithm matter? *Applied Vegetation Science*, *13*, 450–459.

Král, K. and Pavliš, J. (2006). The first detailed land-cover map of Socotra Island by Landsat/ETM+ data. *International Journal of Remote Sensing*, *27*(15), 3239–3250.

Lewis, M. M. (1998). Numeric classification as an aid to spectral mapping of vegetation communities. *Plant Ecology*, *136*(2), 133–149.

Liu, C., Frazier, P. and Kumar, L. (2007). Comparative assessment of the measures of thematic classification accuracy. *Remote Sensing of Environment*, *107*(4), 606–616.

Liu, J., Zhuang, D. and Ling, Y. (1998) Vegetation integrated classification and mapping using remote sensing and GIS techniques in Northeast China. Journal of Remote Sensing, 4, 285–291.

Liu, W., Gong, J., and Fang, H., 1998, Information extraction from GIS data base and its applications in vegetation classification. Journal of Remote Sensing, 3, 235–239.

Liu, J. Y., Zhuang, D. F., Luo, D. and Xiao, X. (2003). Land-cover classification of China: Integrated analysis of AVHRR imagery and geophysical data. *International Journal of Remote Sensing*, *24*(12), 2485–2500.

Liu, Y-S, Hu, Y- and Peng, L.-Y. (2005). Accurate Quantification of Grassland Cover Density in an Alpine Meadow Soil Based on Remote Sensing and GPS. *Pedosphere*, *15*(6), 778–783.

Lu, D., and Weng, Q. (2007). A survey of image classification methods and techniques for improving classification performance. *International Journal of Remote Sensing*, *28*(5), 823–870.

Martinez, S. and Mollicone, D. (2012). From Land Cover to Land Use: A Methodology to Assess Land Use from Remote Sensing Data. *Remote Sensing*, *4*(4), 1024–1045.

McCloy, K. R. (1995). Resource management information systems: process and practice. *Taylor & Francis Ltd*. 616 pp. ISBN: 07484-0120-2

Moran, E. F. (2010). Land cover classification in a complex urban-rural landscape with Quickbird imagery. *Photogramm Eng Remote Sensing*, *76*(10), 1159–1168.

Pal, M. and Mather, P. M. (2003). An assessment of the effectiveness of decision tree methods for land cover classification. *Remote Sensing of Environment*, *86*(4), 554–565.

Peterson, D. L., Price, K. P. and Martinko, E. (2002). Discriminating between cool season and warm season grassland cover types in northeastern Kansas. *International Journal of Remote Sensing*, *23*(23), 5015–5030.

Phinn, S., Franklin, J., Hope, A., Stow, D. and Huenneke, L. (1996). Biomass distribution mapping using airborne digital video imagery and spatial statistics in a semi-arid environment. *Journal of Environmental Management*, *47*(2), 139–164.

Powers, D. M. W. (2011). Evaluation: From Precision, Recall and F-Measure to ROC., Informedness, Markedness & Correlation. *Journal of Machine Learning Technologies*, *2*(1), 37–63.

Rodriguez, H. C. (2014). Classifiers ensemble in remote sensing : a comparative analysis. Dissertation document, Erasmus Mundus Master Program in Geospatial Technologies, *ISEGI Universidade Nova de Lisboa*, Lisboa, pp. 52.

Roy, D. P., Wulder, M. A., Loveland, T. R., Woodcock, C. E., Allen, R. G., Anderson, M. C., Helder, D., Irons, J. R., Johnson, D. M., Kennedy, R., Scambos, T. A., Schaaf, C. B., Schott, J. R., Sheng, Y., Vermore, E. F., Belward, A. S., Bindschadler, R., Cohen, W. B., Gao, F., Hipple, J. D., Hostert, P., Huntington, J., Justice, C. O., Kilic, A., Kovalskyy, V., Lee, Z. P., Lymburmer, L., Masek, J. G., McCorkerl, J., Shuai, Y., Trezza, R., Vogelmann, J., Wynne, R. H. and Zhu, Z. (2014). Landsat-8 : Science and product vision for terrestrial global change research. *Remote Sensing of Environment*, *145*, 154–172.

Schmidtlein, S. and Sassin, J. (2004). Mapping of continuous floristic gradients in grasslands using hyperspectral imagery. *Remote Sensing of Environment*, *92*(1), 126–138.

Sellers, P. J. (1985). Canopy reflectance, photosynthesis and transpiration. *International Journal of Remote Sensing*, *6*(8), 1335–1372.

Shinoda, M., Ito, S., Nachinshonhor, G. U. and Erdenetsetseg, D. (2007). Phenology of Mongolian Grasslands and Moisture Conditions. *Journal of the Meteorological Society of Japan*, *85*(3), 359–367.

Shinoda, M., Nachinshonhor, G. U. and Nemoto, M. (2010). Impact of drought on vegetation dynamics of the Mongolian steppe: A field experiment. *Journal of Arid Environments*, *74*(1), 63–69.

Sivanpillai, R., Prager, S. D. and Storey, T. O. (2009). Estimating sagebrush cover in semi-arid environments using Landsat Thematic Mapper data. *International Journal of Applied Earth Observation and Geoinformation*, *11*(2), 103–107.

Sternberg, T., Thomas, D. and Middleton, N. (2011). Drought dynamics on the Mongolian steppe, 1970-2006. *International Journal of Climatology*, *31*(12), 1823–1830.

Sutie, J. M., Reynolds, S. G. and Batello, C. (Eds.) (2005). Grasslands of the World*, Plant Production and Protection Series,* FAO, No. 34, Rome, pp.514. ISBN: 92-5-105337-5

Uno, Y., Prasher, S. O., Lacroix, R., Goel, P. K., Karimi, Y., Viau, A. and Patel, R. M. (2005). Artificial neural networks to predict corn yield from Compact Airborne Spectrographic Imager data. *Computers and Electronics in Agriculture*, *47*, 149–161.

Vandandorj, S., Gantsetseg, B. and Boldgiv, B. (2015). Spatial and temporal variability in vegetation cover of Mongolia and its implications. *Journal of Arid Land*.

Wallis de Vries, M. F., Manibazar, N. and Dugerlham, S. (1996). The vegetation of the forest-steppe region of Hustain Nuruu, Mongolia. *Vegetatio*, *122*(2), 111–127.

Wang, J., Brown, D. G. and Bai, Y. (2014). Investigating the spectral and ecological characteristics of grassland communities across an ecological gradient of the Inner Mongolian grasslands with *in situ* hyperspectral data. *International Journal of Remote Sensing*, *35*(20), 7179–7198.

Wang, J., Price, K. P. and Rich, P. M. (2001). Spatial patterns of NDVI in response to precipitation and temperature in the central Great Plains. *International Journal of Remote Sensing*, *22*(18), 3827–3844.

Wang, Q. and Tenhunen, J. D. (2004). Vegetation mapping with multitemporal NDVI in North Eastern China Transect (NECT). *International Journal of Applied Earth Observation and Geoinformation*, *6*(1), 17–31.

Weiss, J. L., Gutzler, D. S., Coonrod, J. E. A. and Dahm, C. N. (2004). Long-term vegetation monitoring with NDVI in a diverse semi-arid setting , central New Mexico, USA. *Journal of Arid Environments*, *58*, 249–272.

Wen, Q., Zhang, Z., Liu, S., Wang, X. and Wang, C. (2010). Classification of grassland types by MODIS time-series images in Tibet, China. *IEEE Journal of Selected Topics in Applied Earth Observations and Remote Sensing*, *3*(3), 404–409.

Wulder, M. A., White, J. C., Goward, S. N., Masek, J. G., Irons, J. R., Herold, M., Cohen, W. B., Loveland, T. R. and Woodcock, C. E. (2008). Landsat continuity: Issues and opportunities for land cover monitoring. *Remote Sensing of Environment*, *112*(3), 955–969.

Xian, G., Homer, C., Rigge, M., Shi, H. and Meyer, D. (2015). Characterization of shrubland ecosystem components as continuous fields in the northwest United States. *Remote Sensing of Environment*, *168*, 286–300.

Yu, F., Price, K. P., Ellis, J. and Shi, P. (2003). Response of seasonal vegetation development to climatic variations in eastern central Asia. *Remote Sensing of Environment*, *87*(1), 42–54.

Zha, Y., Gao, J., Ni, S., Liu, Y., Jiang, J. and Wei, Y. (2003). A spectral reflectance-based approach to quantification of grassland cover from Landsat TM imagery. *Remote Sensing of Environment*, *87*(2-3), 371–375.

A. Annexes

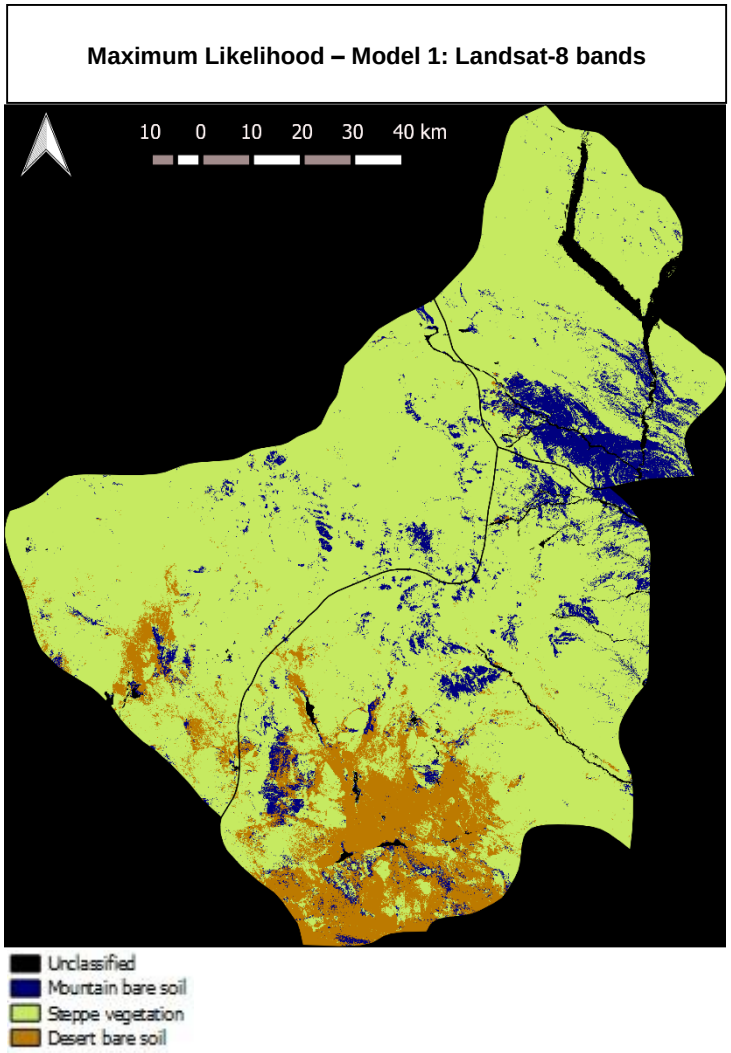

Figure A.1 - Main classes using maximum likelihood - Model 1: Landsat-8 bands

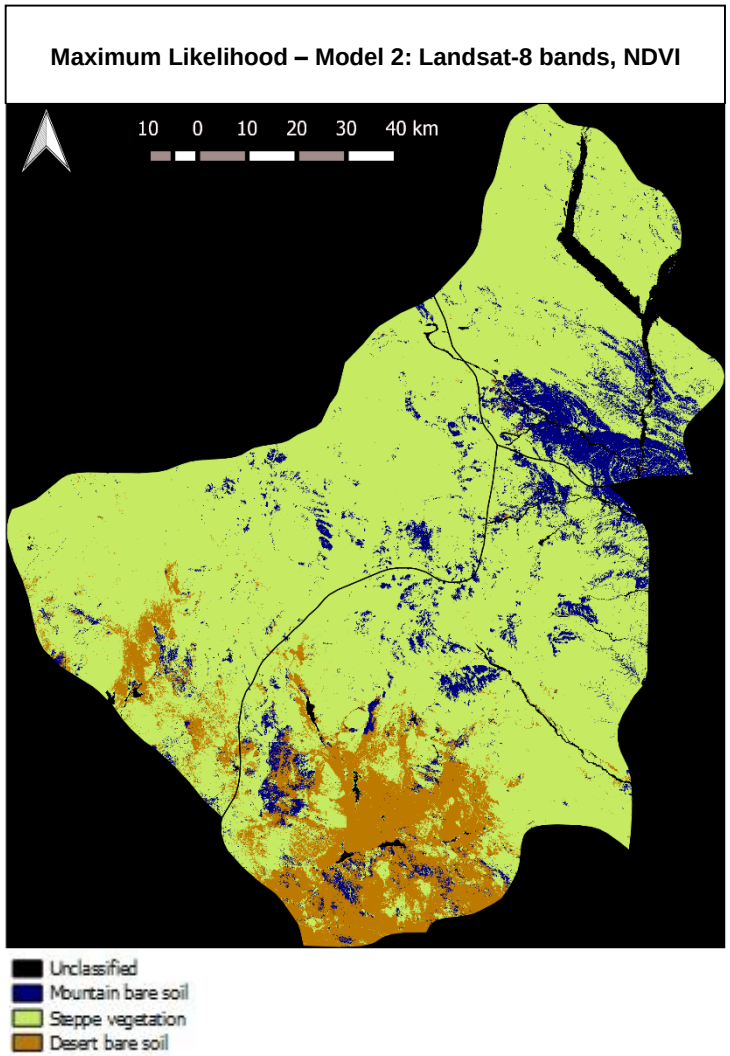

Figure A.2 - Main classes using maximum likelihood - Model 2: Landsat-8 bands and NDVI

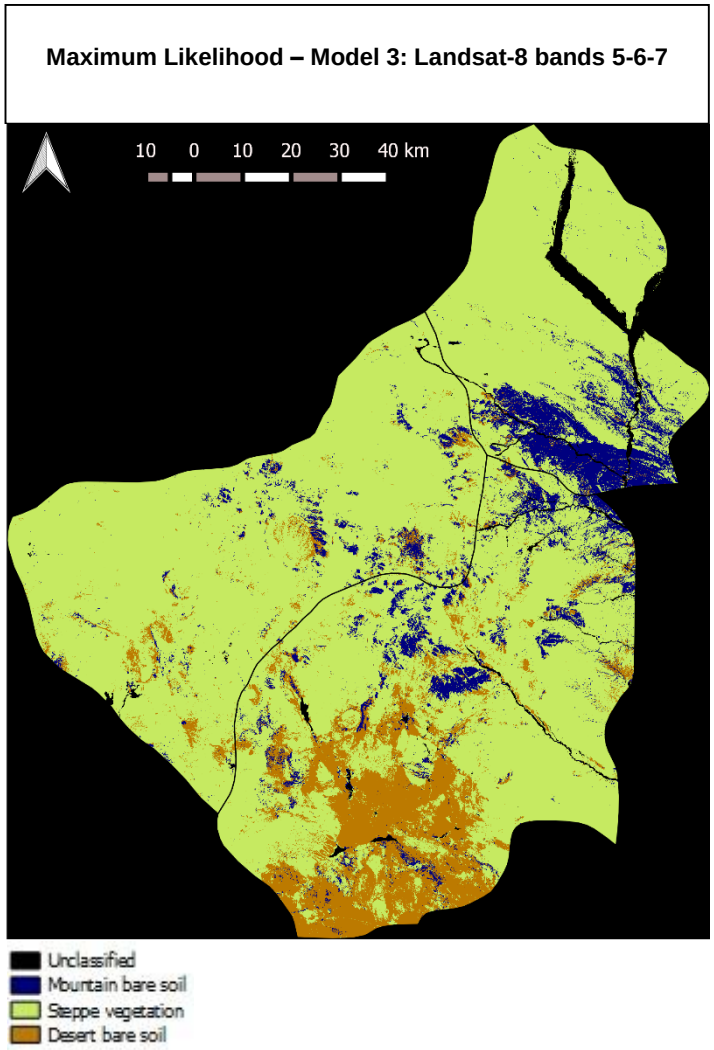

Figure A.3 - Main classes using maximum likelihood - Model 4: Landsat-8 bands 5-6-7 and NDVI

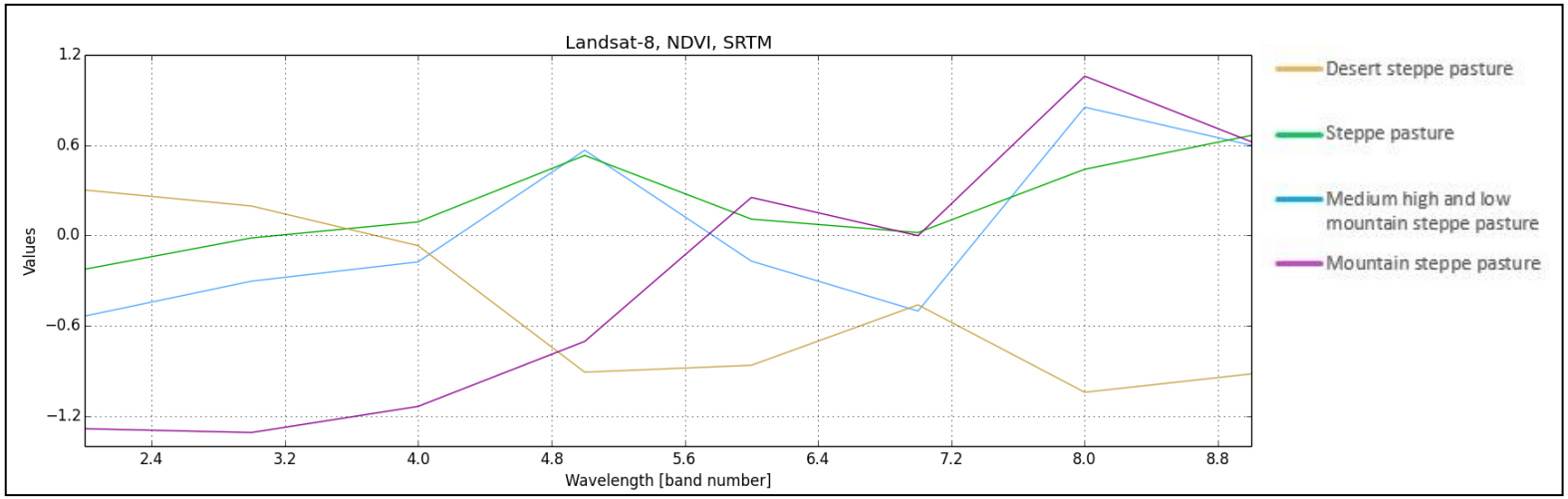

Figure A.4 - Spectral signatures for the steppe vegetation classes using Landsat-8 bands: OLI-2, OLI-3, OLI-4, OLI-5, OLI-6 and OLI-7, NDVI [band 8] and SRTM [band 9] – Model 4

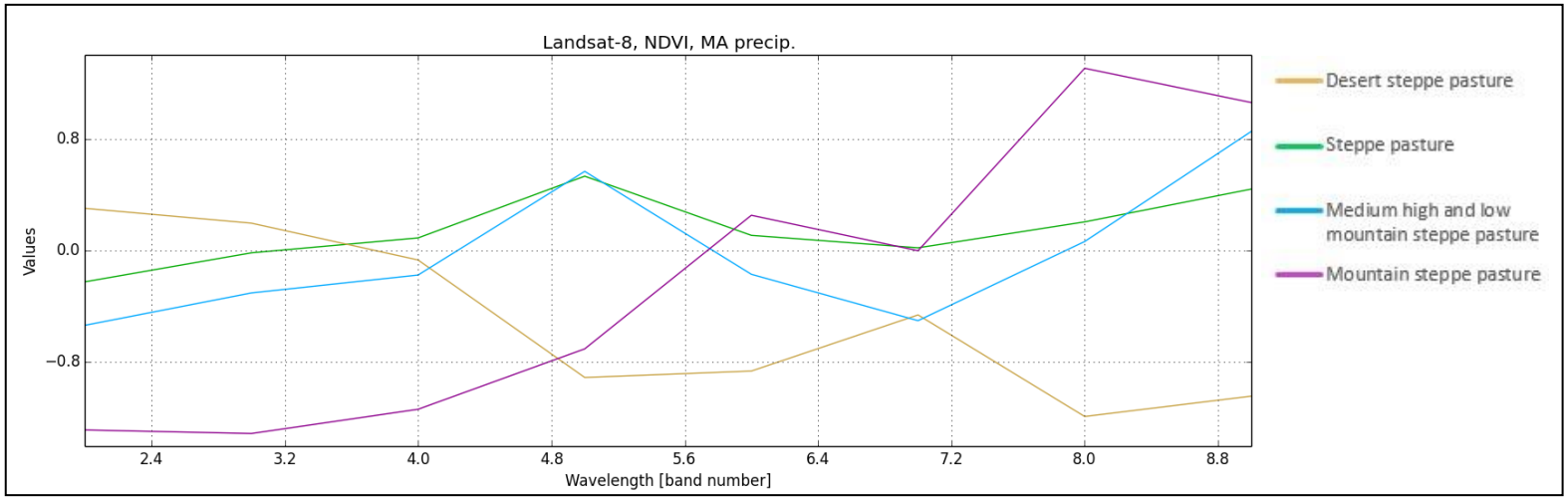

Figure A.5 - Spectral signatures for the steppe vegetation classes using Landsat-8 bands: OLI-2, OLI-3, OLI-4, OLI-5, OLI-6 and OLI-7, NDVI [band 8] and mean annual precipitation (MA precip.) [band 9] – Model 6

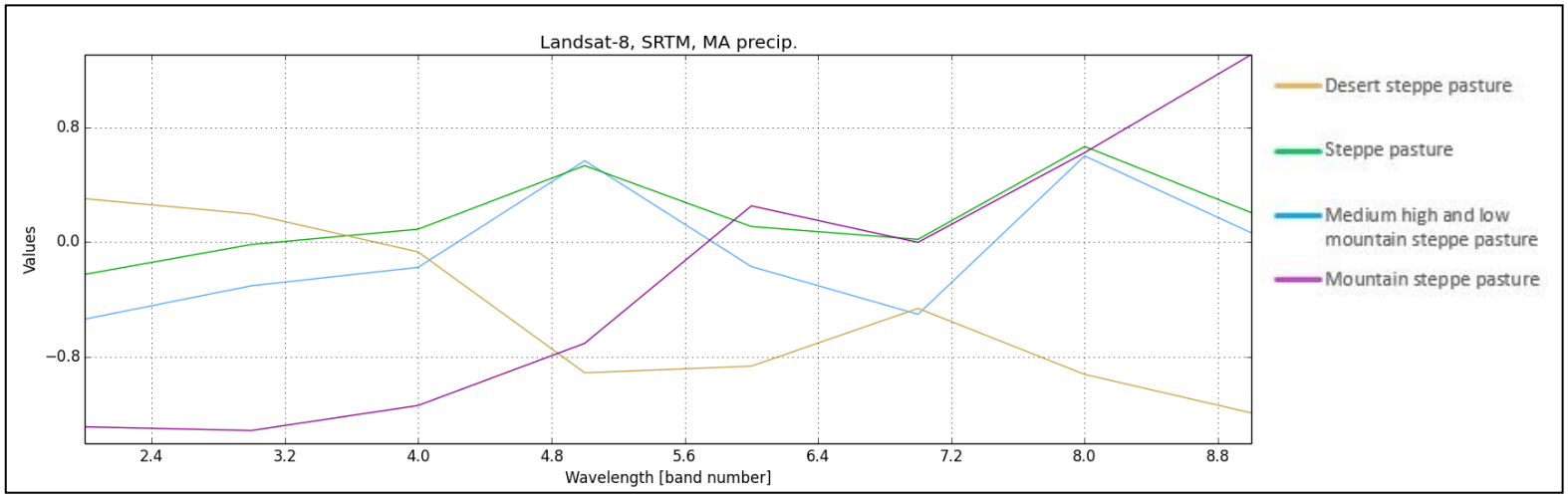

Figure A.6 - Spectral signatures for the steppe vegetation classes using Landsat-8 bands: OLI-2, OLI-3, OLI-4, OLI-5, OLI-6 and OLI-7, SRTM [band 8] and mean annual precipitation (MA precip.) [band 9] – Model 7

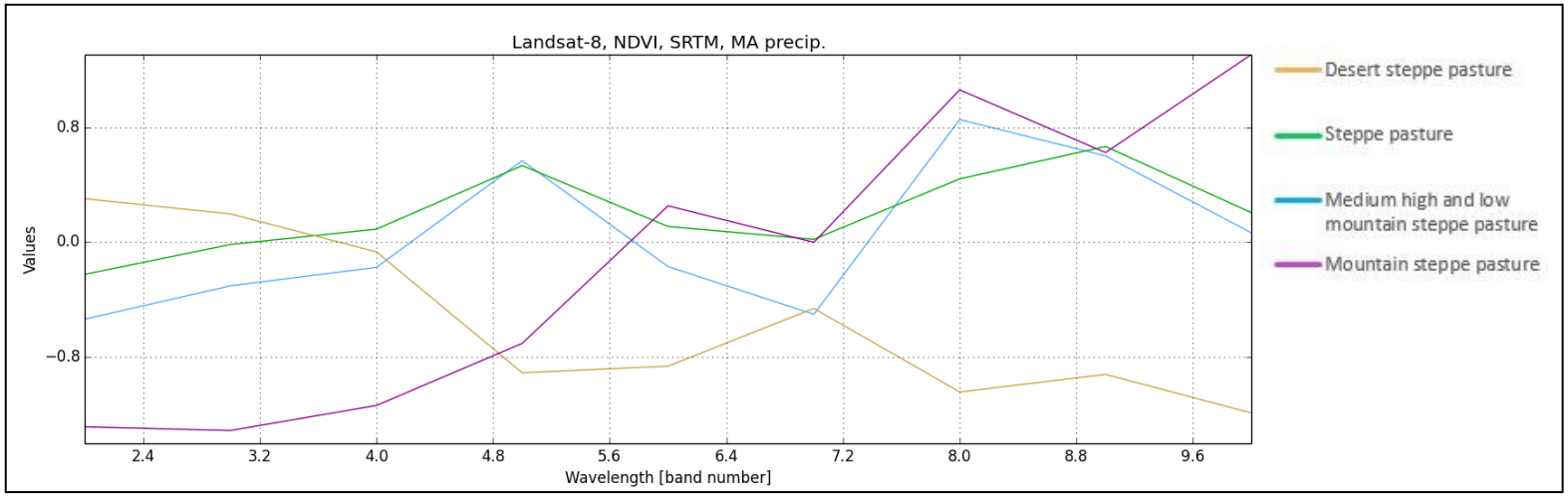

Figure A.7 - Spectral signatures for the steppe vegetation classes using Landsat-8 bands: OLI-2, OLI-3, OLI-4, OLI-5, OLI-6 and OLI-7, NDVI [band 8], SRTM [band 9] and mean annual precipitation (MA precip.) [band 10] – Model 8

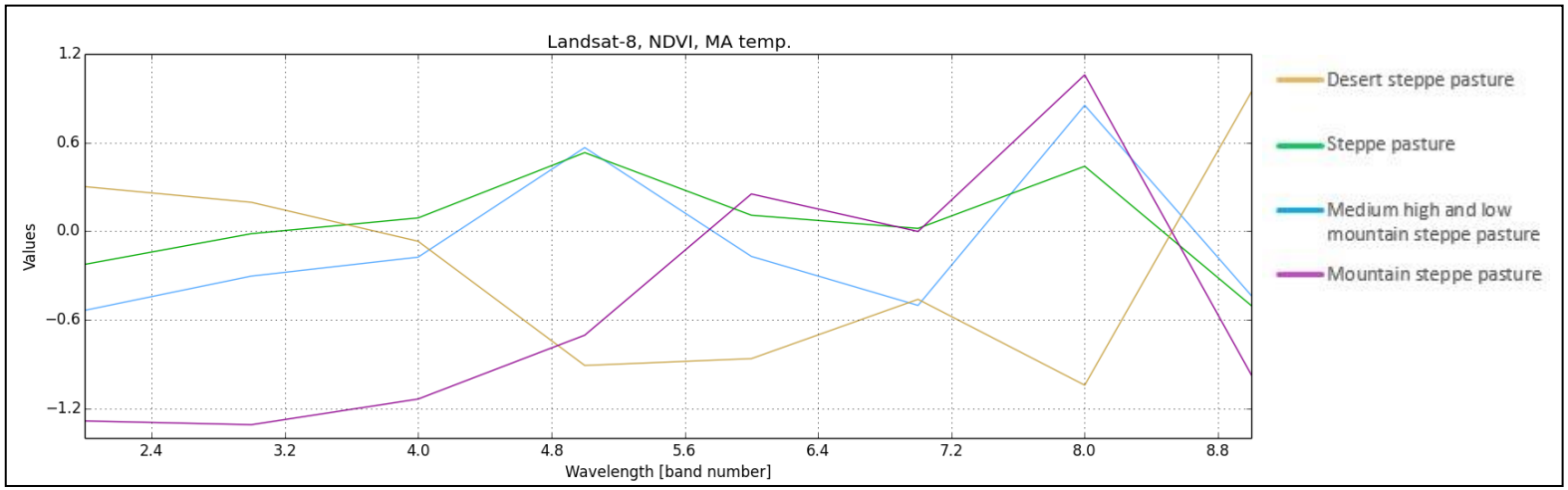

Figure A.8 - Spectral signatures for the steppe vegetation classes using Landsat-8 bands: OLI-2, OLI-3, OLI-4, OLI-5, OLI-6 and OLI-7, NDVI [band 8] and mean annual temperature (MA temp.) [band 9] – Model 10

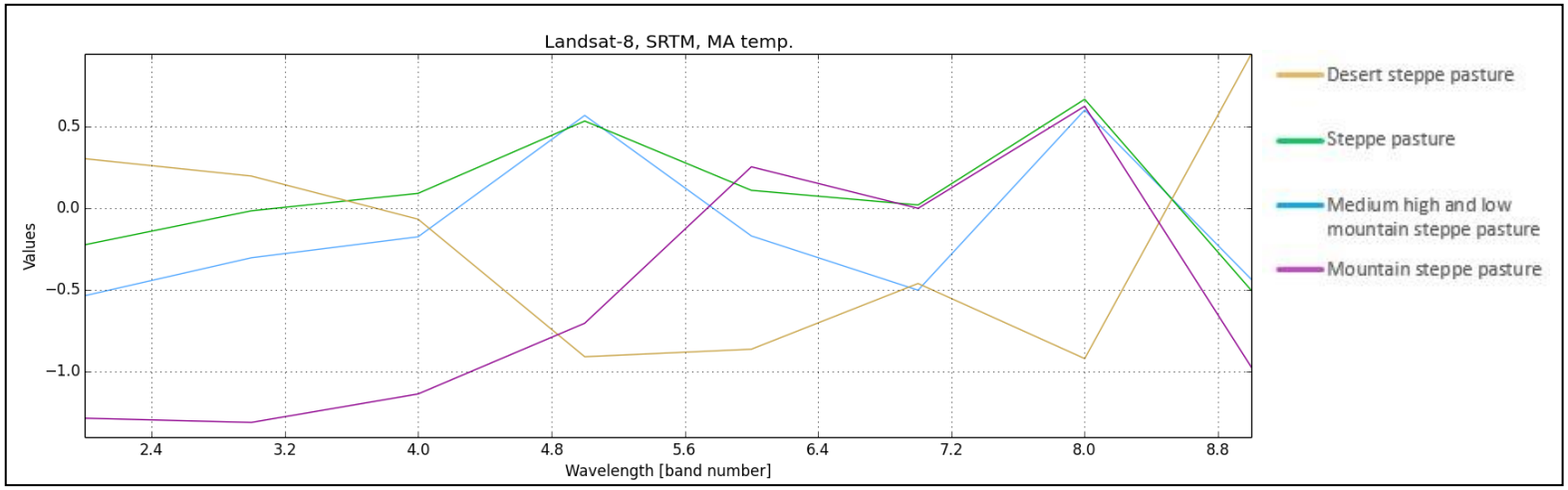

Figure A.9 - Spectral signatures for the steppe vegetation classes using Landsat-8 bands: OLI-2, OLI-3, OLI-4, OLI-5, OLI-6 and OLI-7, SRTM [band 8] and mean annual temperature (MA temp.) [band 9] – Model 11

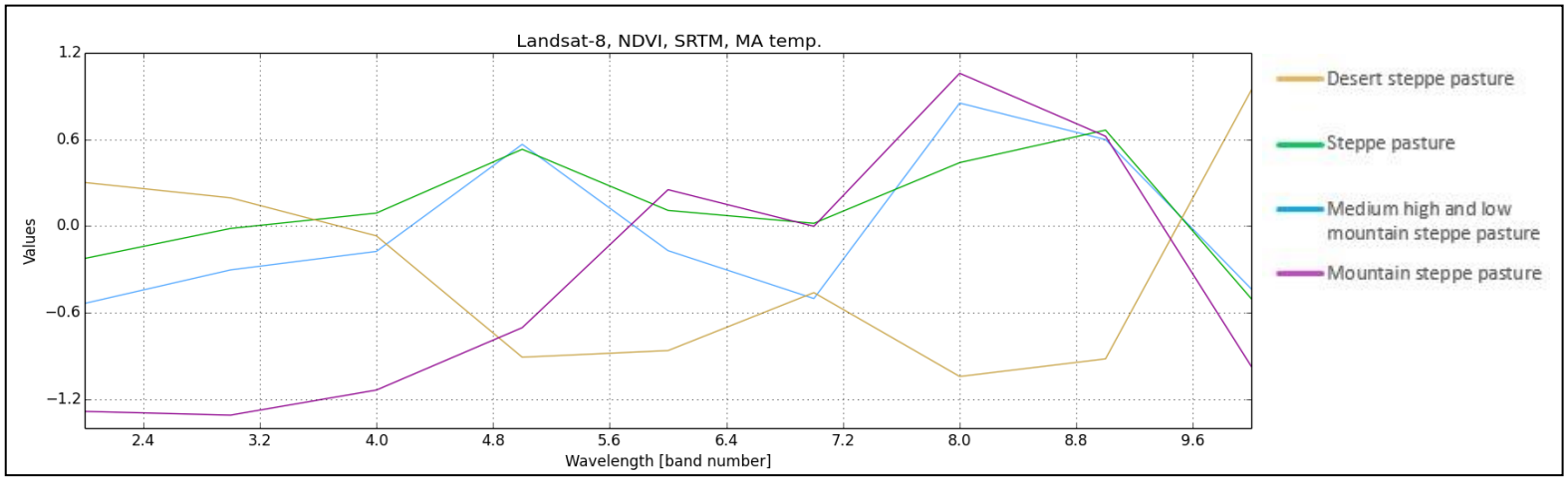

Figure A.10 - Spectral signatures for the steppe vegetation classes using Landsat-8 bands: OLI-2, OLI-3, OLI-4, OLI-5, OLI-6 and OLI-7, NDVI [band 8], SRTM [band 9] and mean annual temperature (MA temp.) [band 10] – Model 12

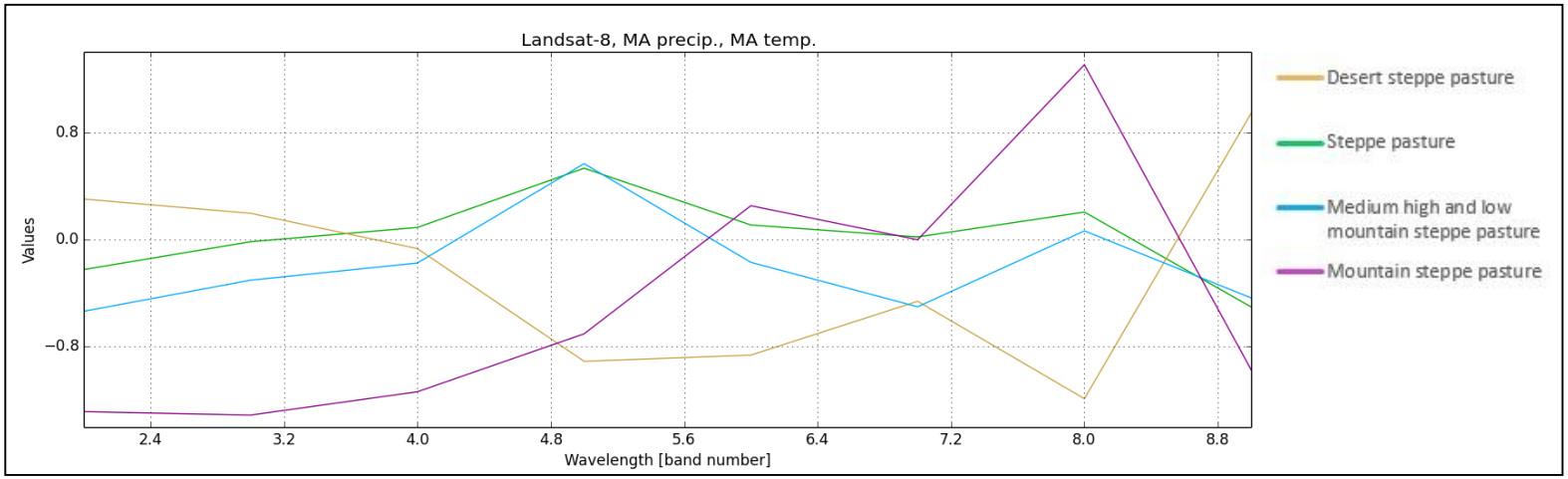

Figure A.11 - Spectral signatures for the steppe vegetation classes using Landsat-8 bands: OLI-2, OLI-3, OLI-4, OLI-5, OLI-6 and OLI-7, mean annual precipitation (MA precip.) [band 8] and mean annual temperature (MA temp.) [band 9] – Model 13

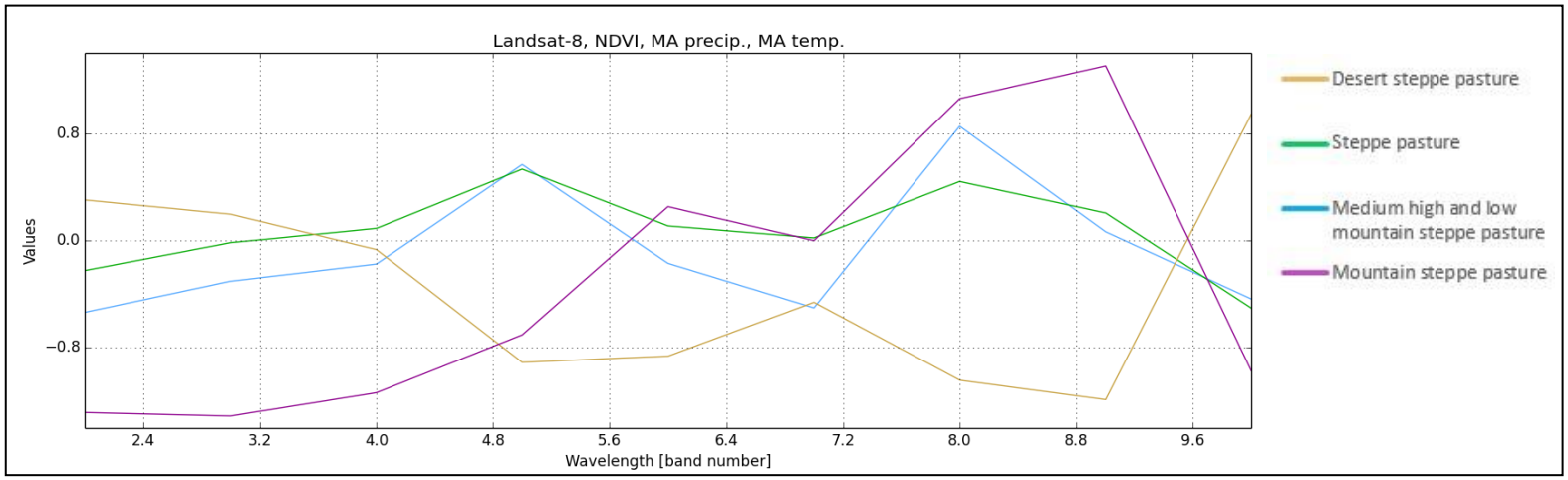

Figure A.12- Spectral signatures for the steppe vegetation classes using Landsat-8 bands: OLI-2, OLI-3, OLI-4, OLI-5, OLI-6 and OLI-7, NDVI [band 8], mean annual precipitation (MA precip.) [band 9] and mean annual temperature (MA temp.) [band 10] – Model 14

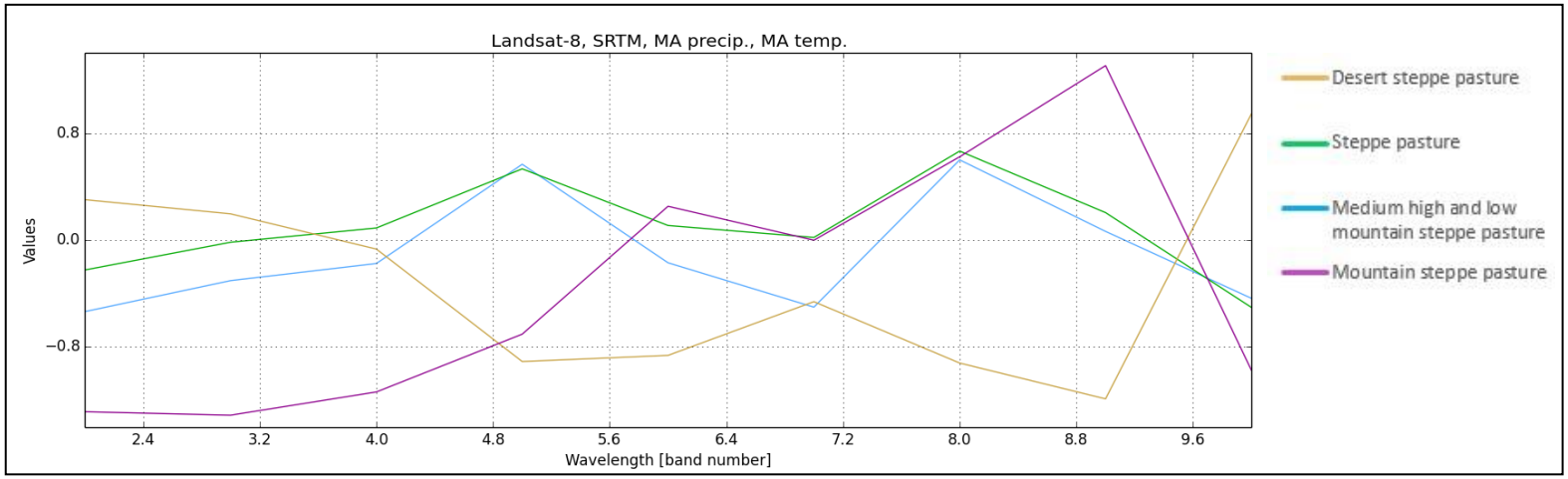

Figure A.13 - Spectral signatures for the steppe vegetation classes using Landsat-8 bands: OLI-2, OLI-3, OLI-4, OLI-5, OLI-6 and OLI-7, SRTM [band 8], mean annual precipitation (MA precip.) [band 9] and mean annual temperature (MA temp.) [band 10] – Model 15

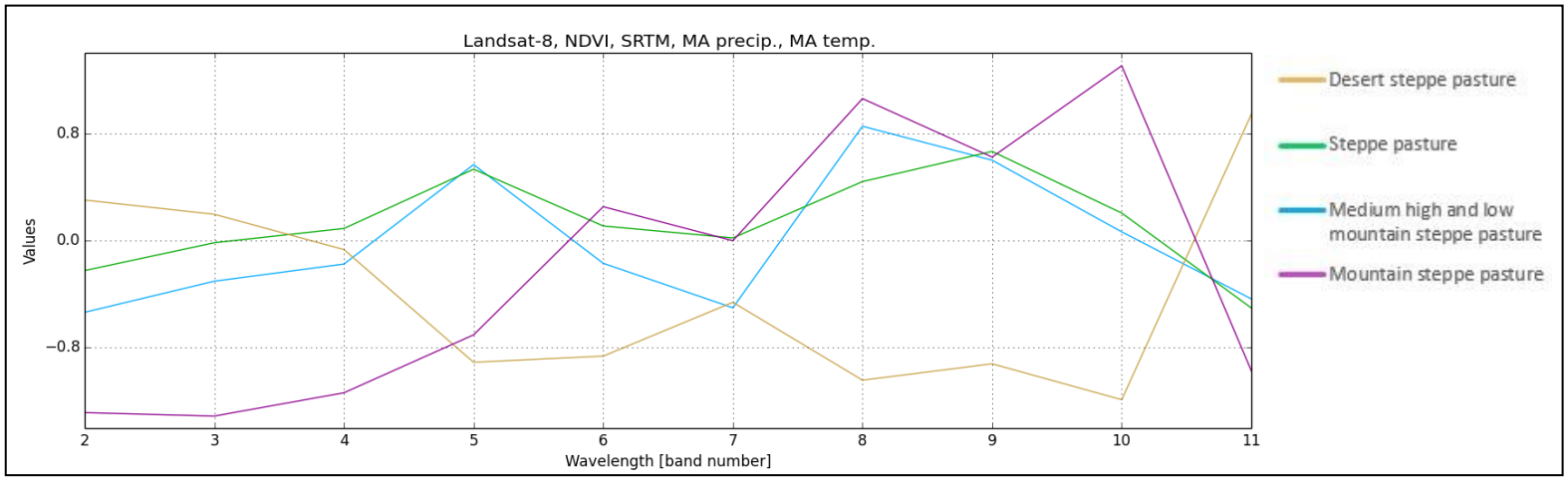

Figure A.14 - Spectral signatures for the steppe vegetation classes using Landsat-8 bands: OLI-2, OLI-3, OLI-4, OLI-5, OLI-6 and OLI-7, NDVI [band 8] SRTM [band 9], mean annual precipitation (MA precip.) [band 10] and mean annual temperature (MA temp.) [band 11] – Model 16

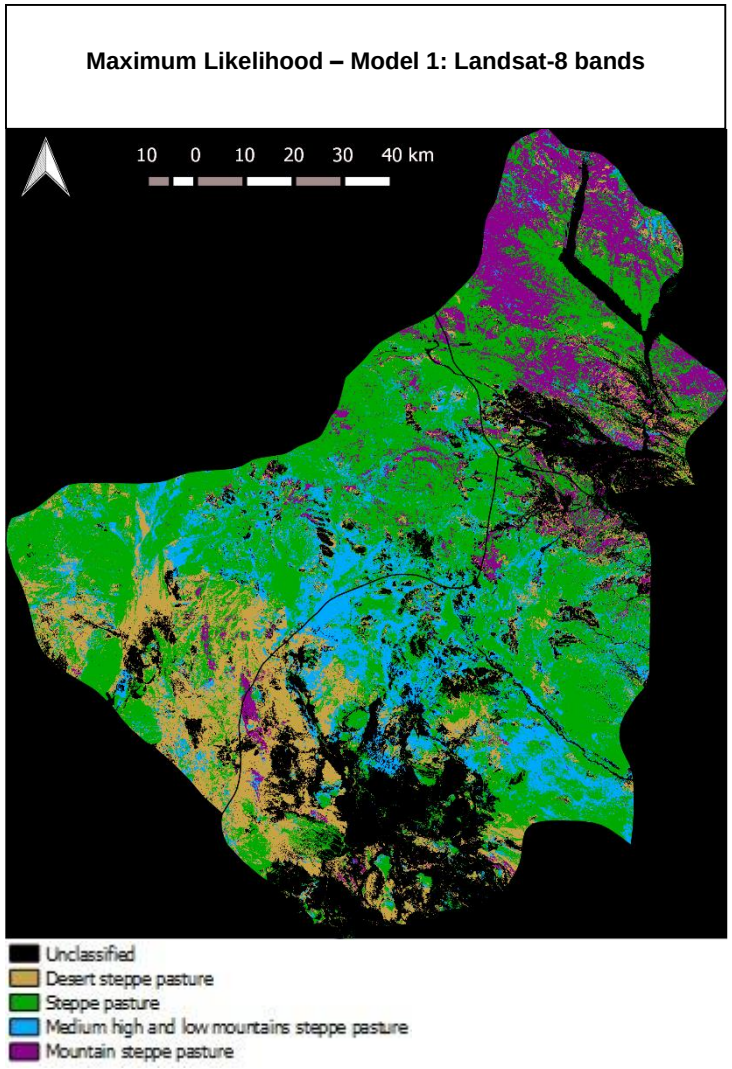

Figure A.15 - Steppe classification using maximum likelihood - Model 1: Landsat-8 bands

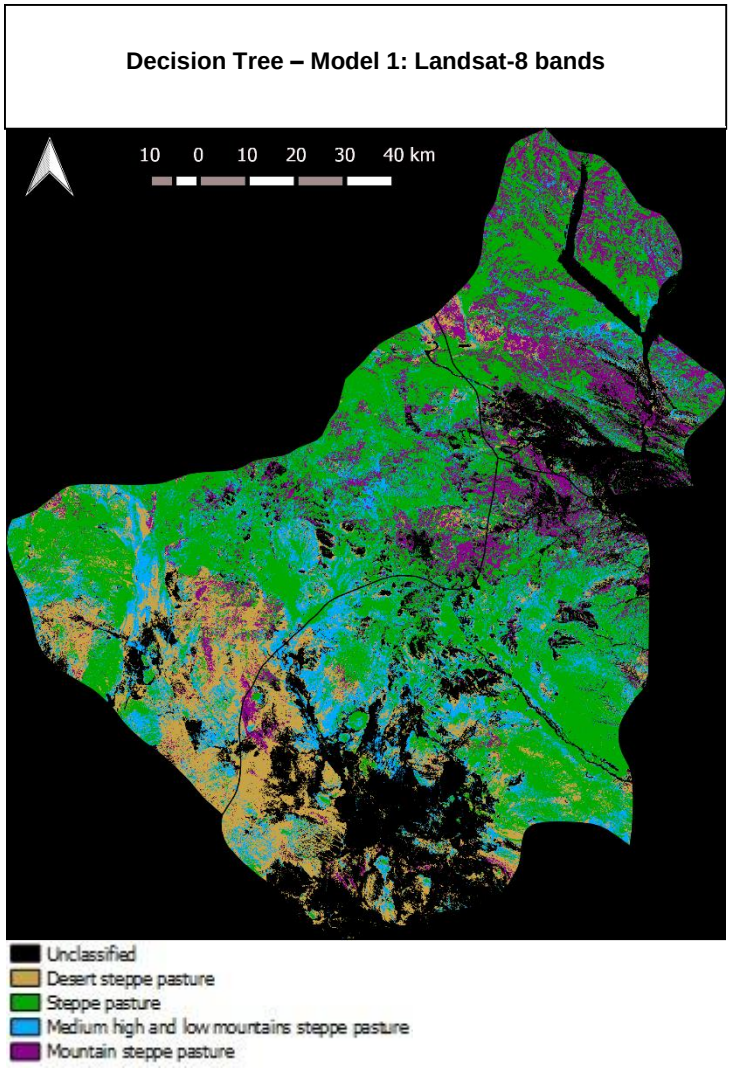

Figure A.16 - Steppe classification using decision tree - Model 1: Landsat-8 bands

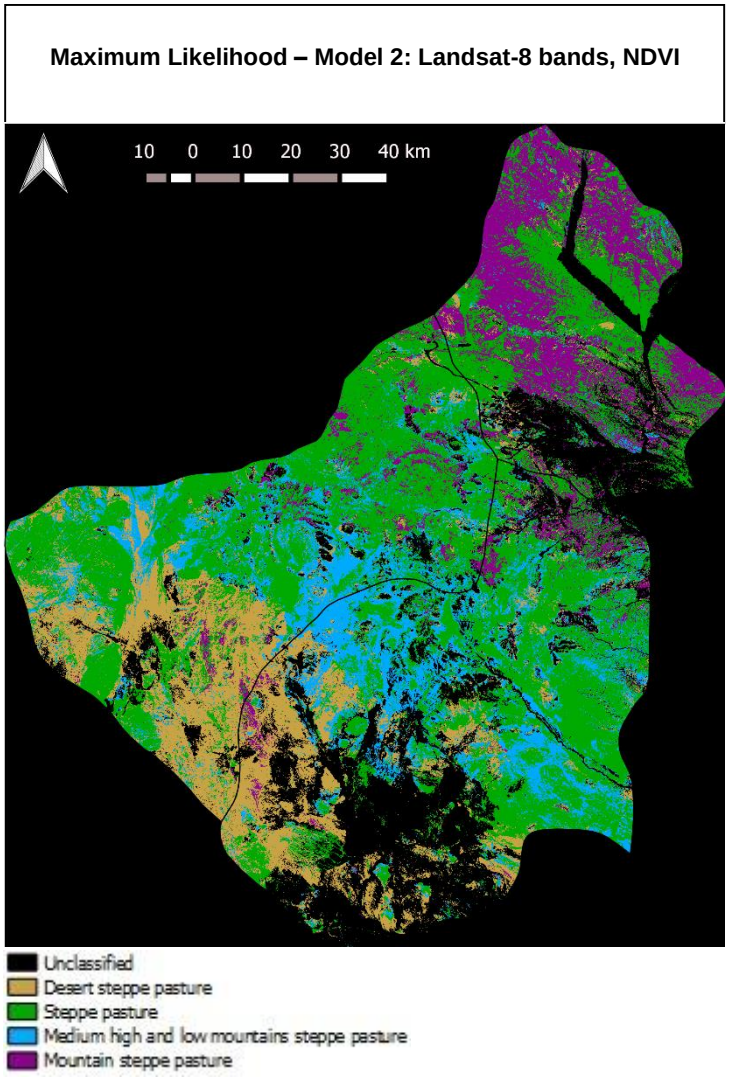

Figure A.17 - Steppe classification using maximum likelihood - Model 2: Landsat-8 bands and NDVI

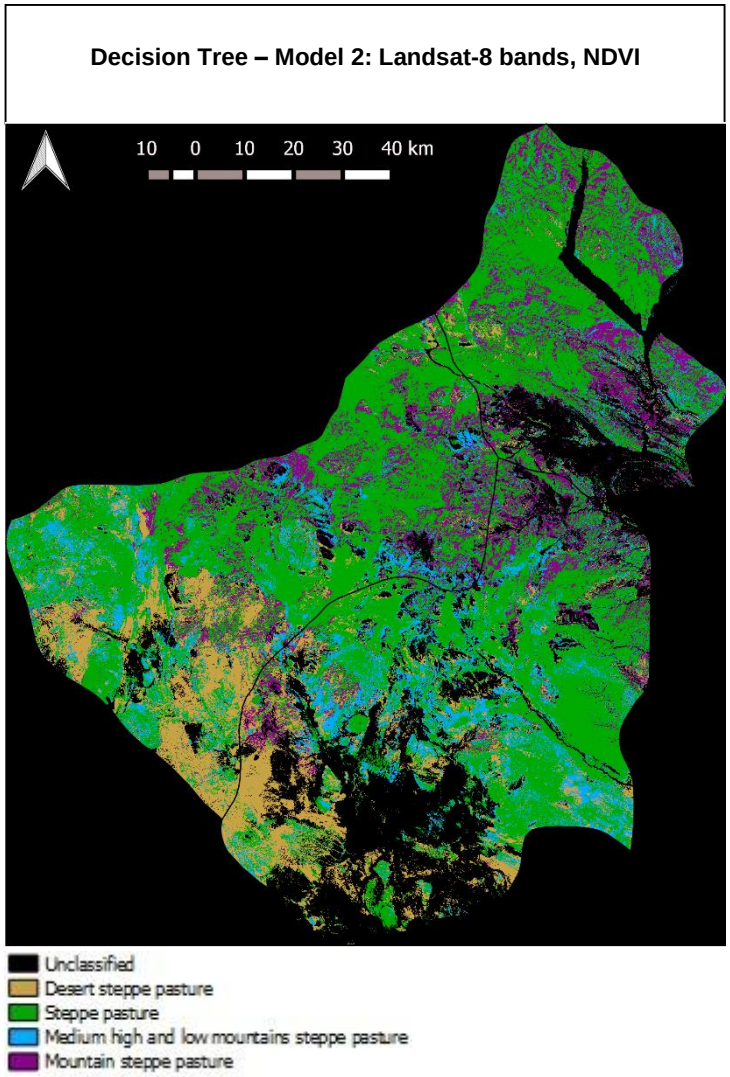

Figure A.18- Steppe classification using decision tree - Model 2: Landsat-8 bands and NDVI

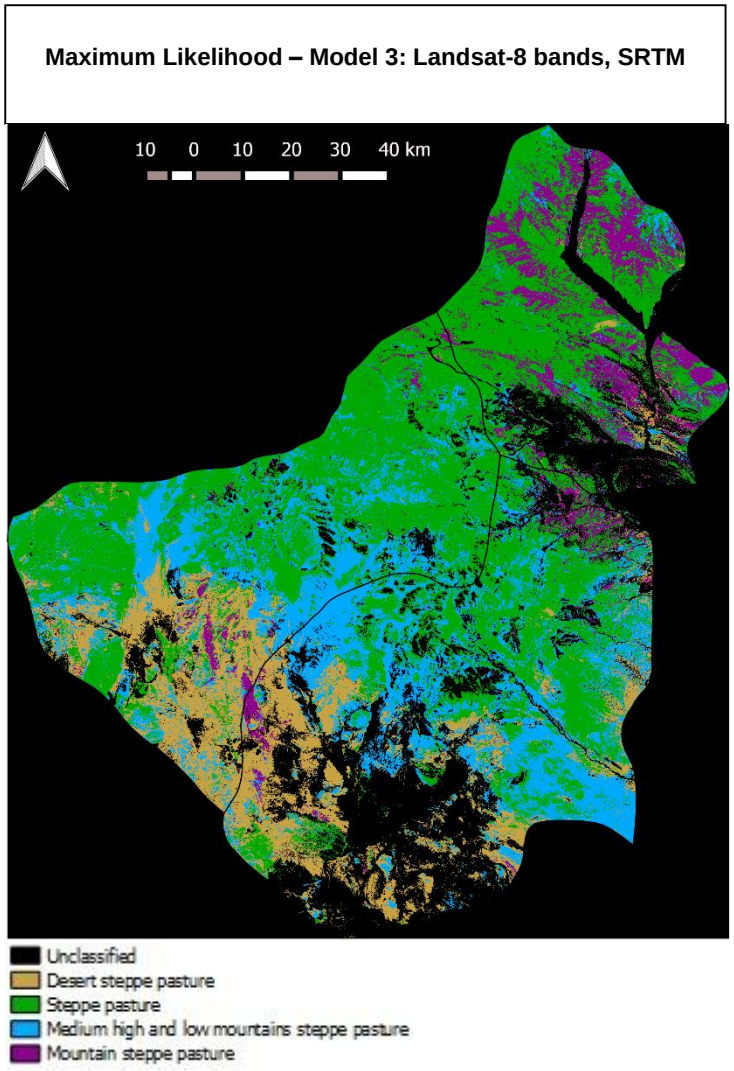

Figure A.19 - Steppe classification using maximum likelihood - Model 3: Landsat-8 bands and SRTM

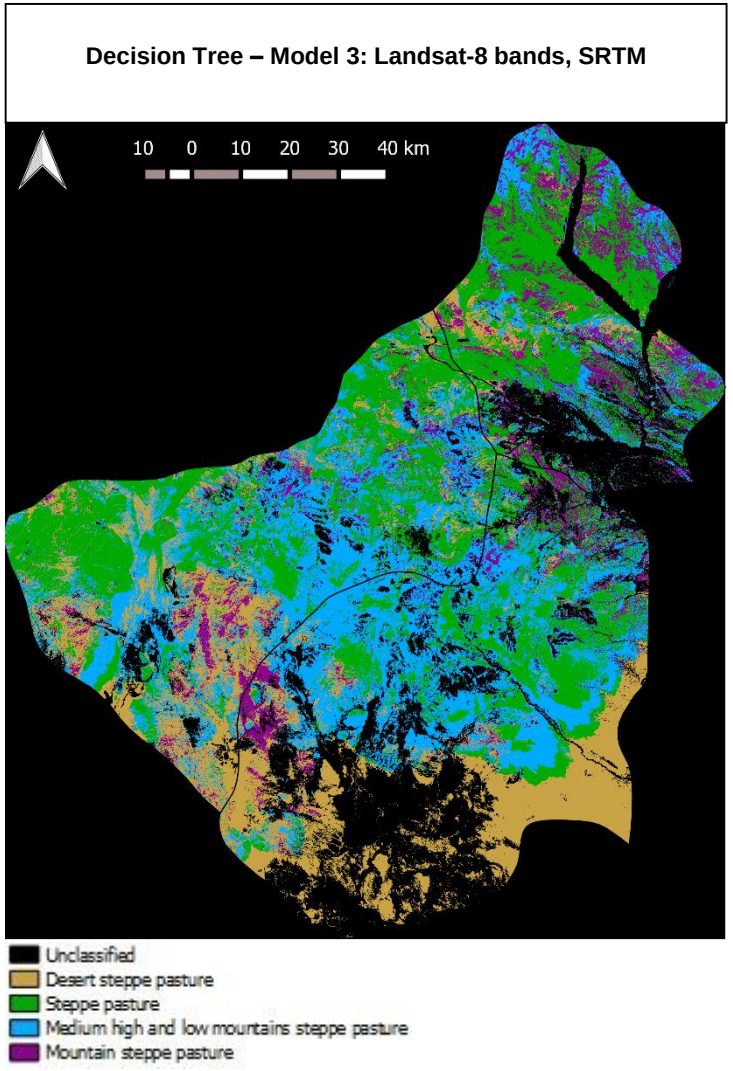

Figure A.20 - Steppe classification using decision tree - Model 3: Landsat-8 bands and SRTM

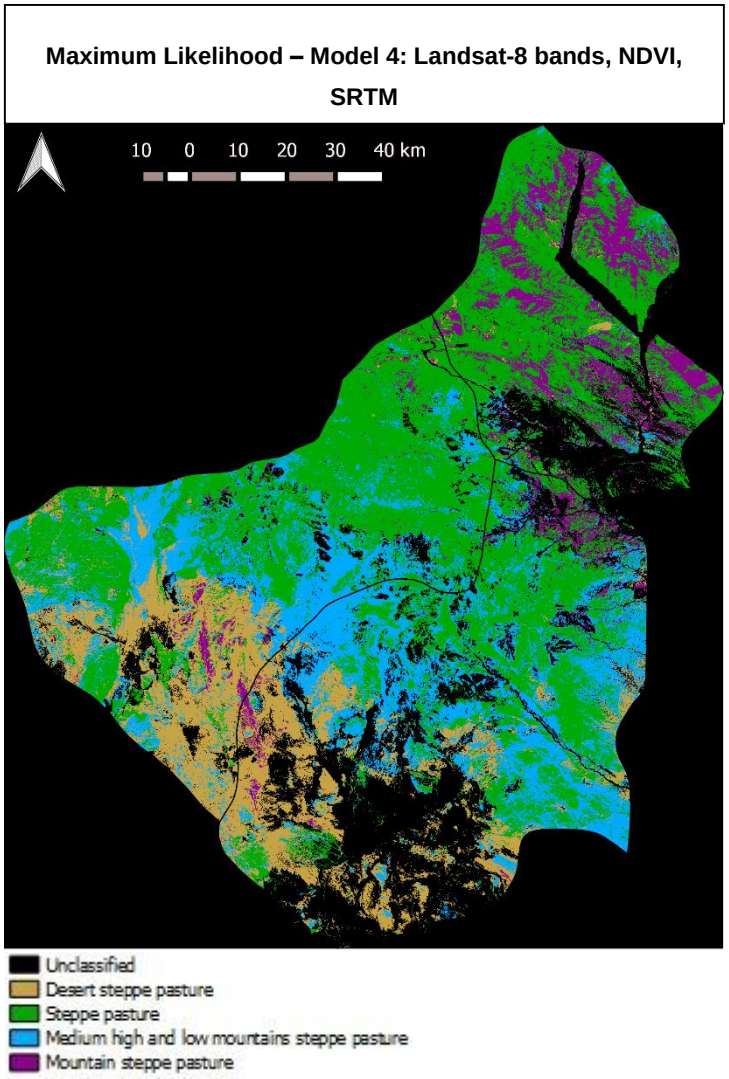

Figure A.21 - Steppe classification using maximum likelihood - Model 4: Landsat-8 bands, NDVI and SRTM

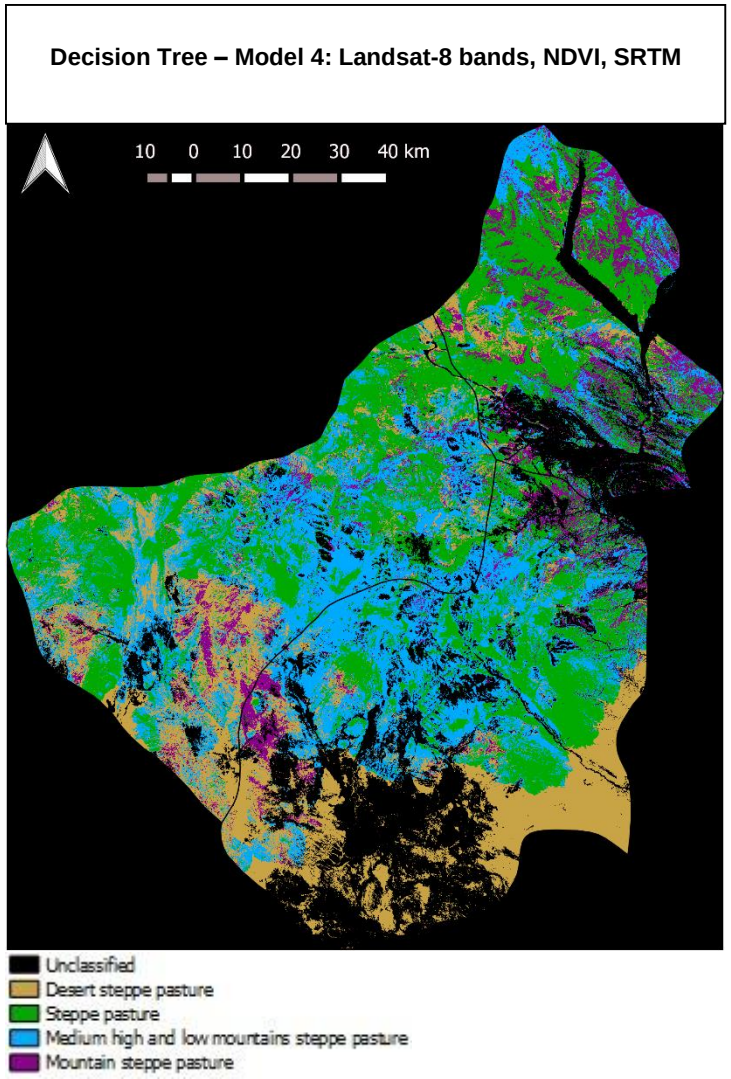

Figure A.22 - Steppe classification using decision tree - Model 4: Landsat-8 bands, NDVI and SRTM

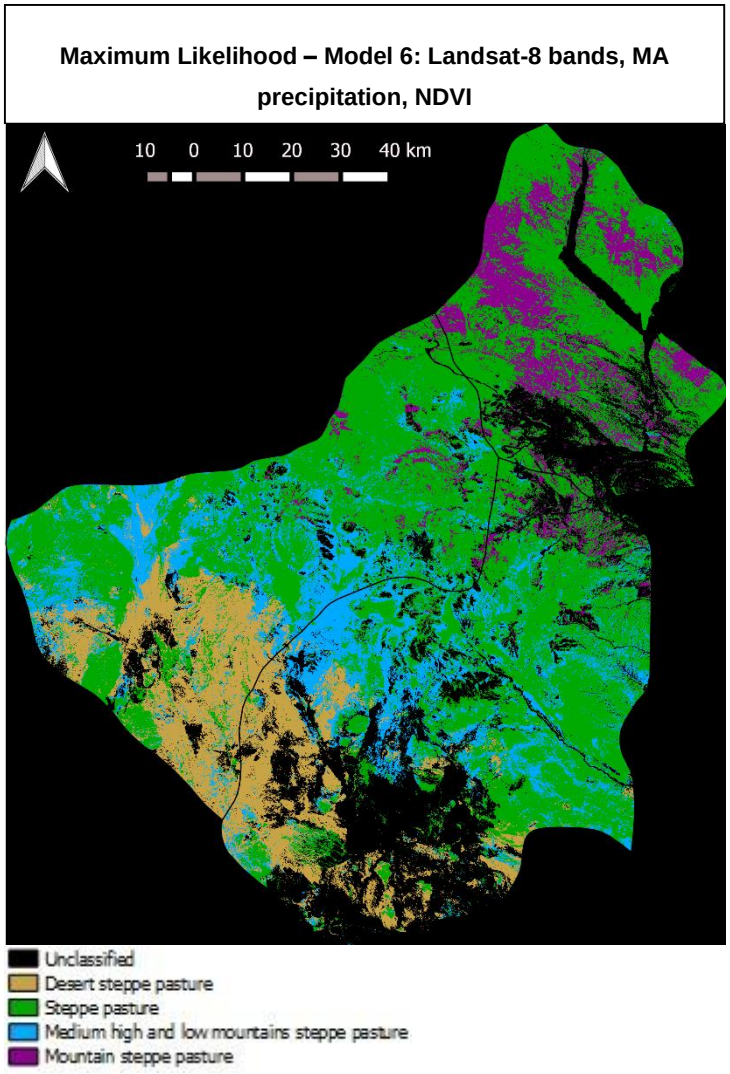

Figure A.23 - Steppe classification using maximum likelihood - Model 6: Landsat-8 bands, MA precipitation and NDVI

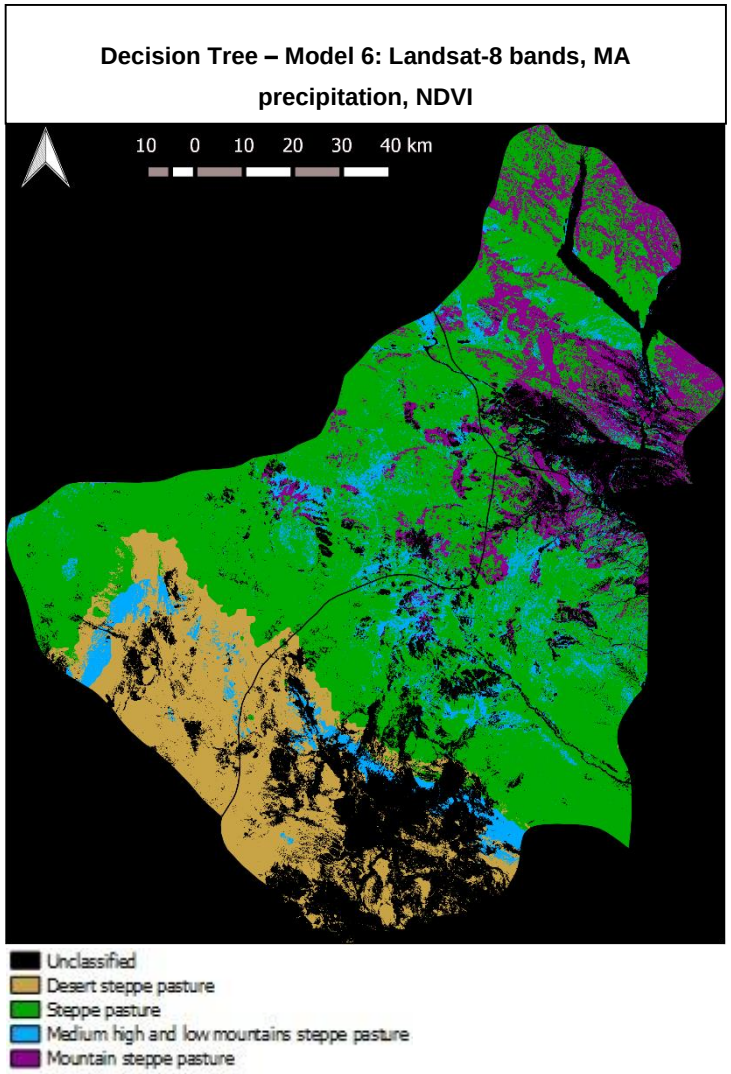

Figure A.24 - Steppe classification using decision tree - Model 6: Landsat-8 bands, MA precipitation and NDVI

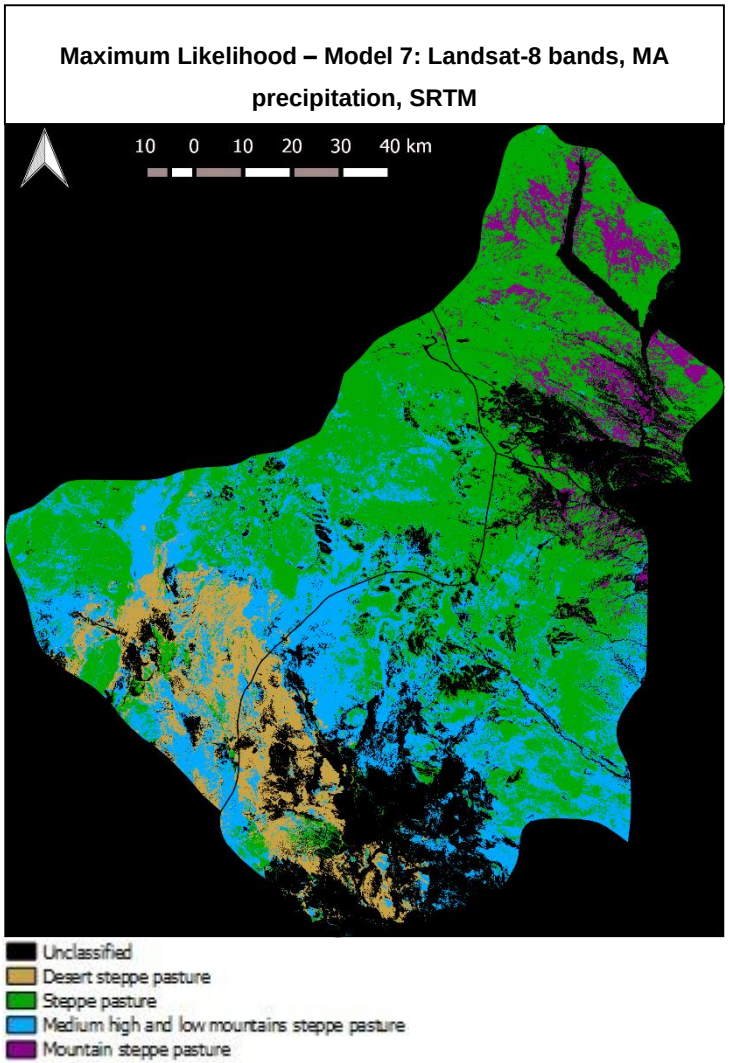

Figure A.25 - Steppe classification using maximum likelihood - Model 7 Landsat-8 bands, MA precipitation and SRTM

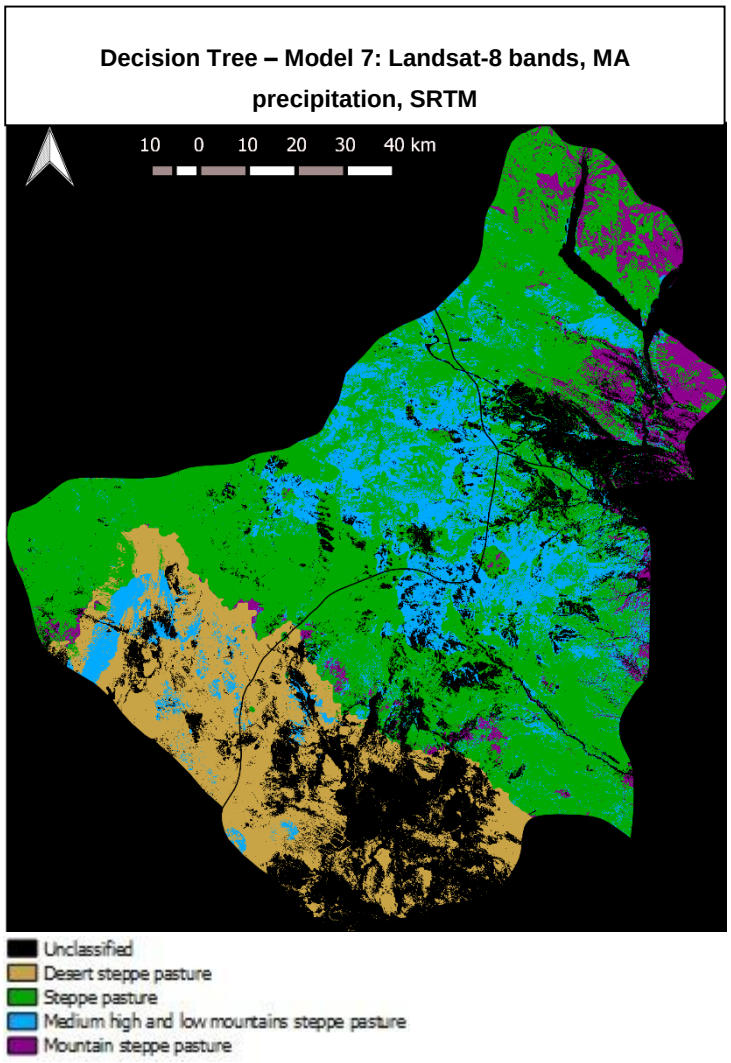

Figure A.26 - Steppe classification using decision tree - Model 7 Landsat-8 bands, MA precipitation and SRTM

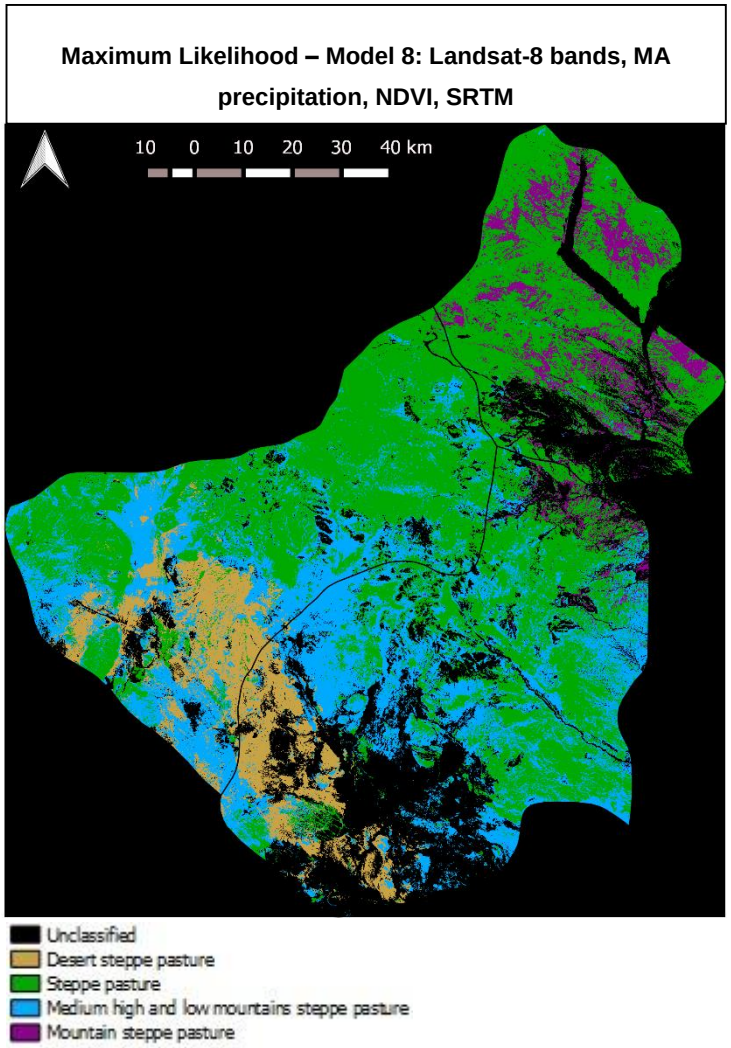

Figure A.27 - Steppe classification using maximum likelihood - Model 8: Landsat-8 bands, MA precipitation, NDVI and SRTM

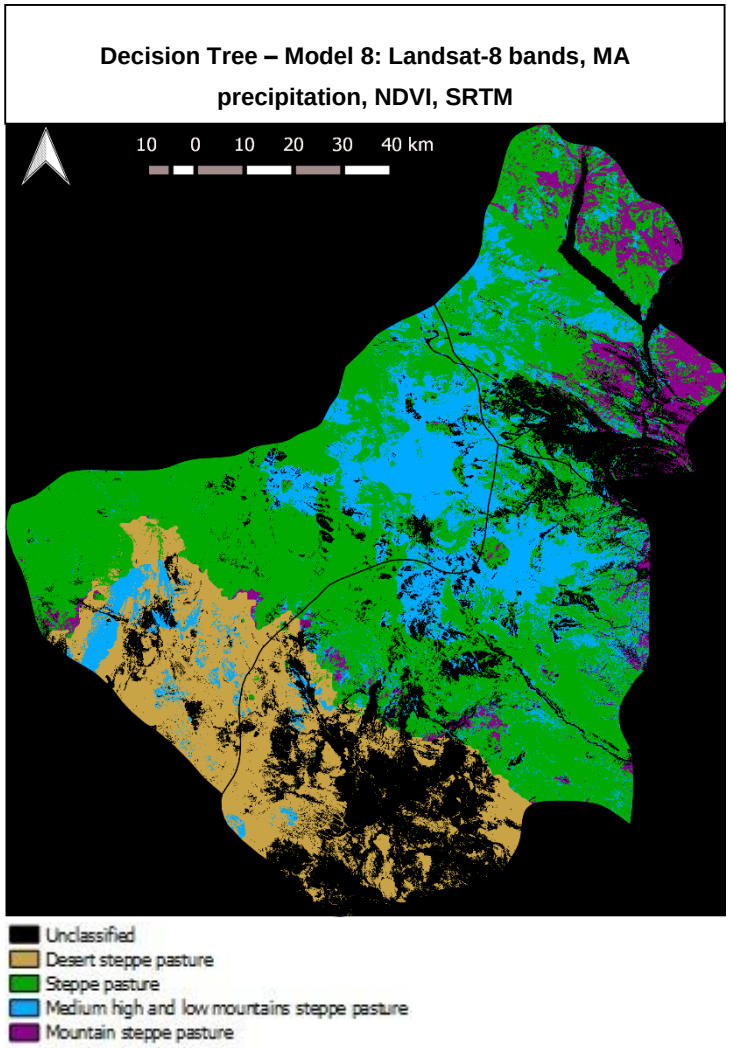

Figure A.28 - Steppe classification using decision tree - Model 8: Landsat-8 bands, MA precipitation, NDVI and SRTM

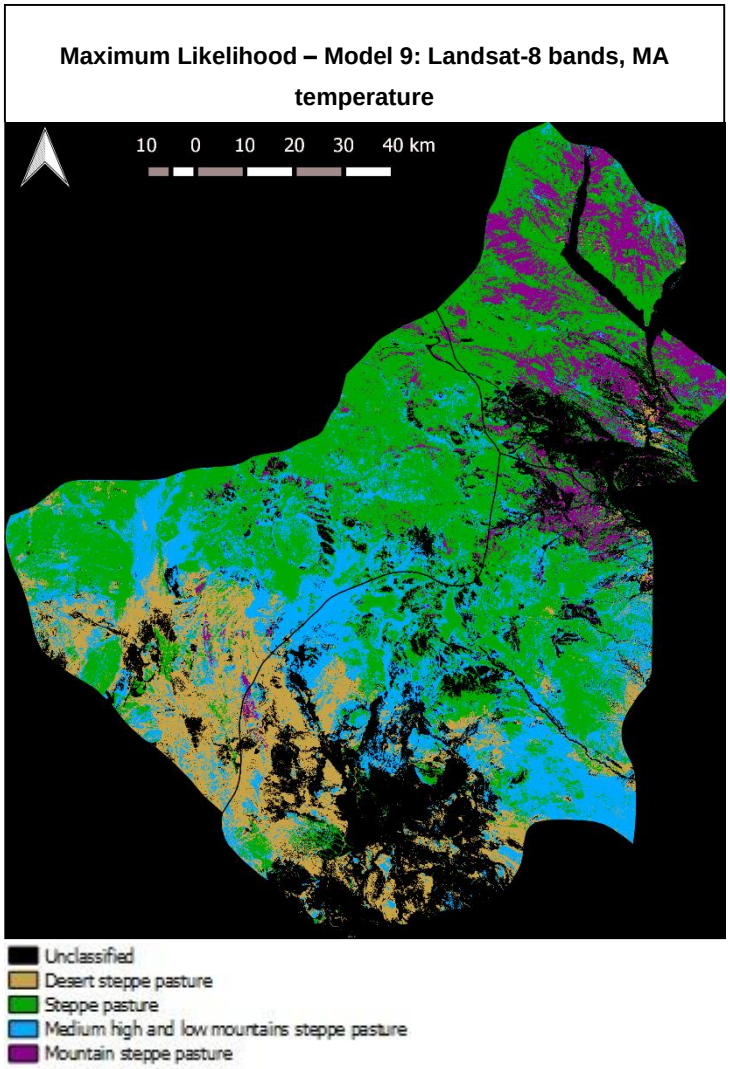

Figure A.29 - Steppe classification using maximum likelihood - Model 9: Landsat-8 bands, MA temperature

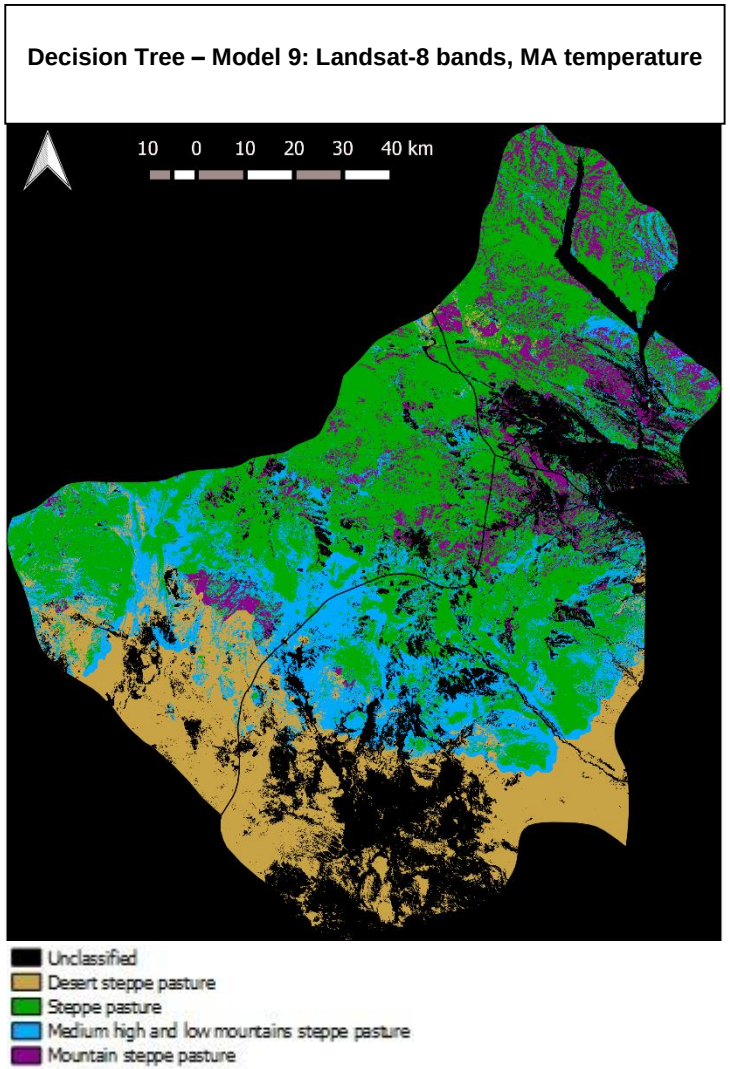

Figure A.30 - Steppe classification using decision tree - Model 9: Landsat-8 bands, MA temperature

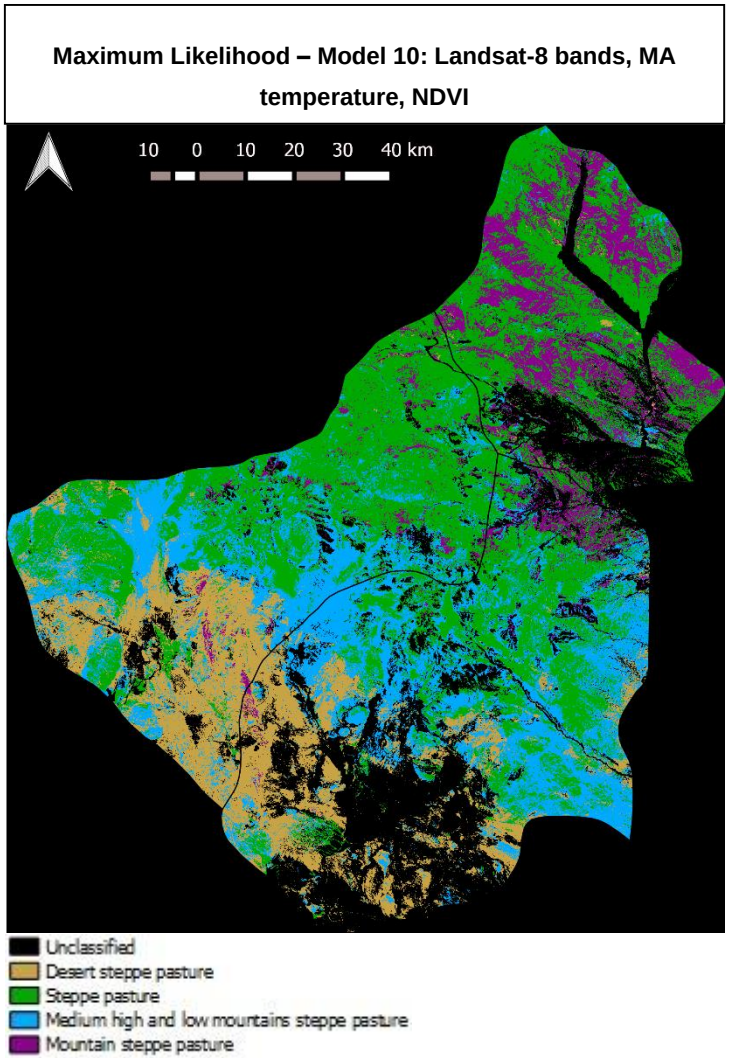

Figure A.31 - Steppe classification using maximum likelihood - Model 10: Landsat-8 bands, MA temperature and NDVI

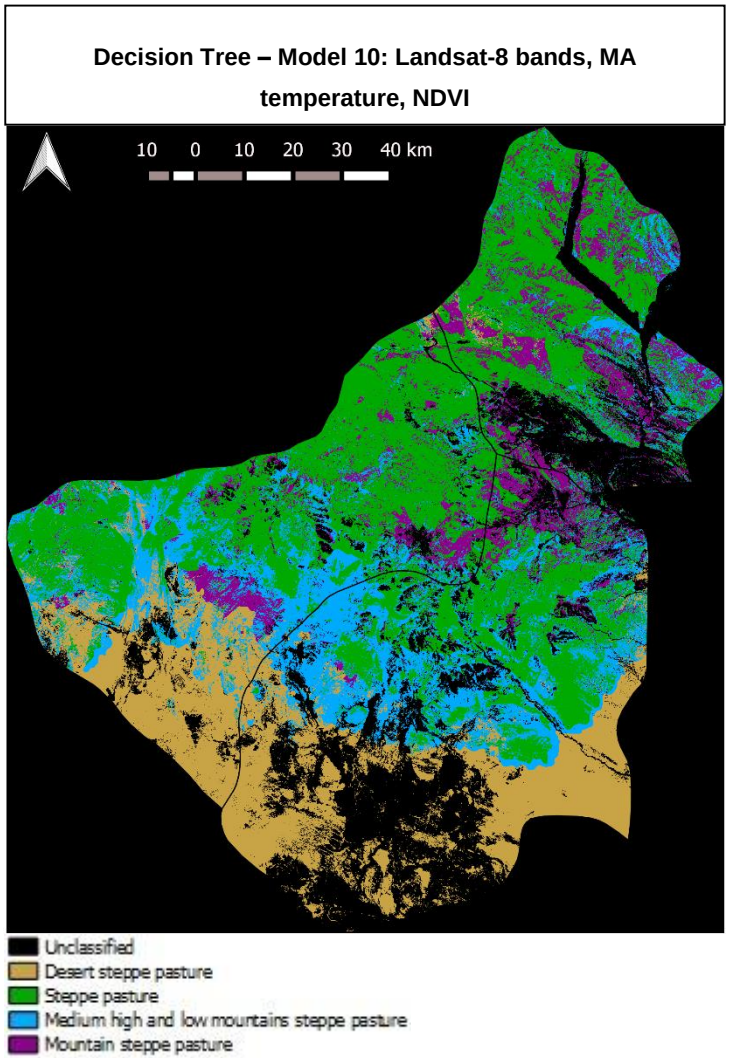

Figure A.32 - Steppe classification using decision tree - Model 10: Landsat-8 bands, MA temperature and NDVI

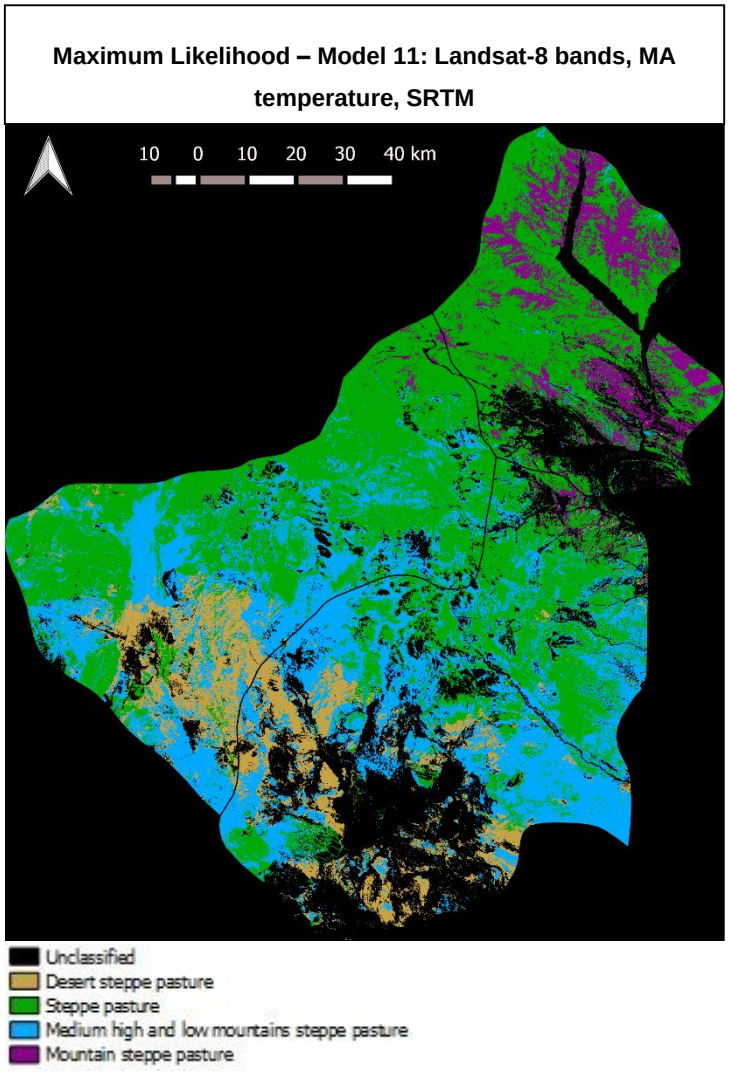

Figure A.33 - Steppe classification using maximum likelihood - Model 11: Landsat-8 bands, MA temperature and SRTM

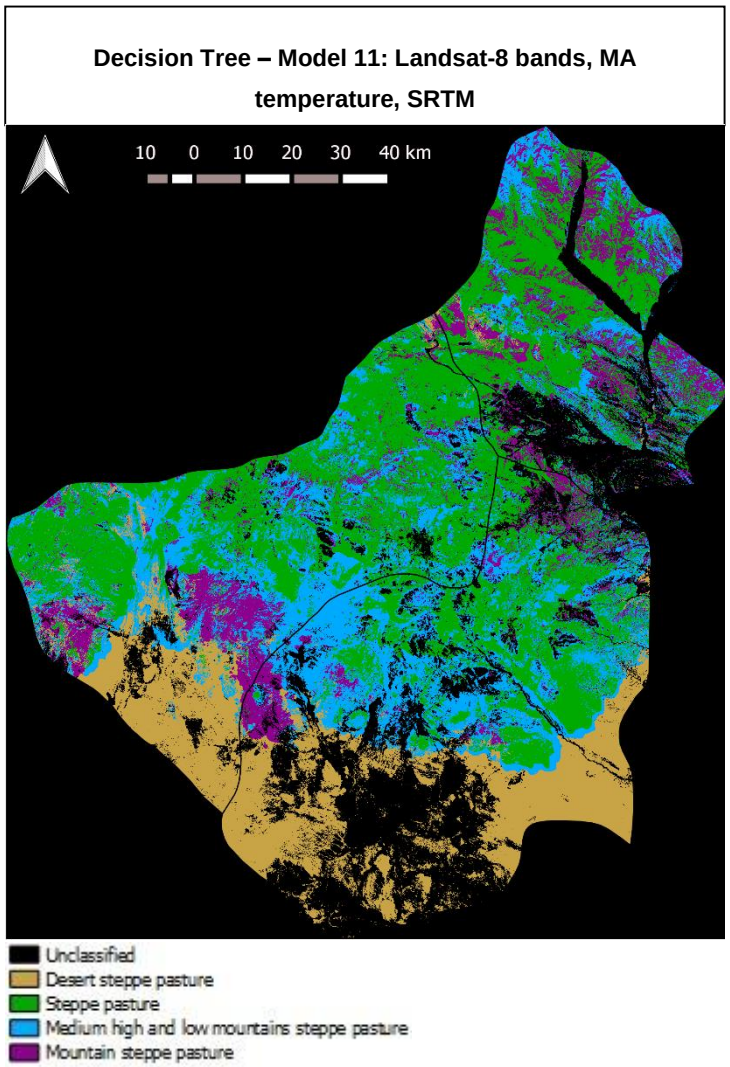

Figure A.34 - Steppe classification using decision tree - Model 11: Landsat-8 bands, MA temperature and SRTM

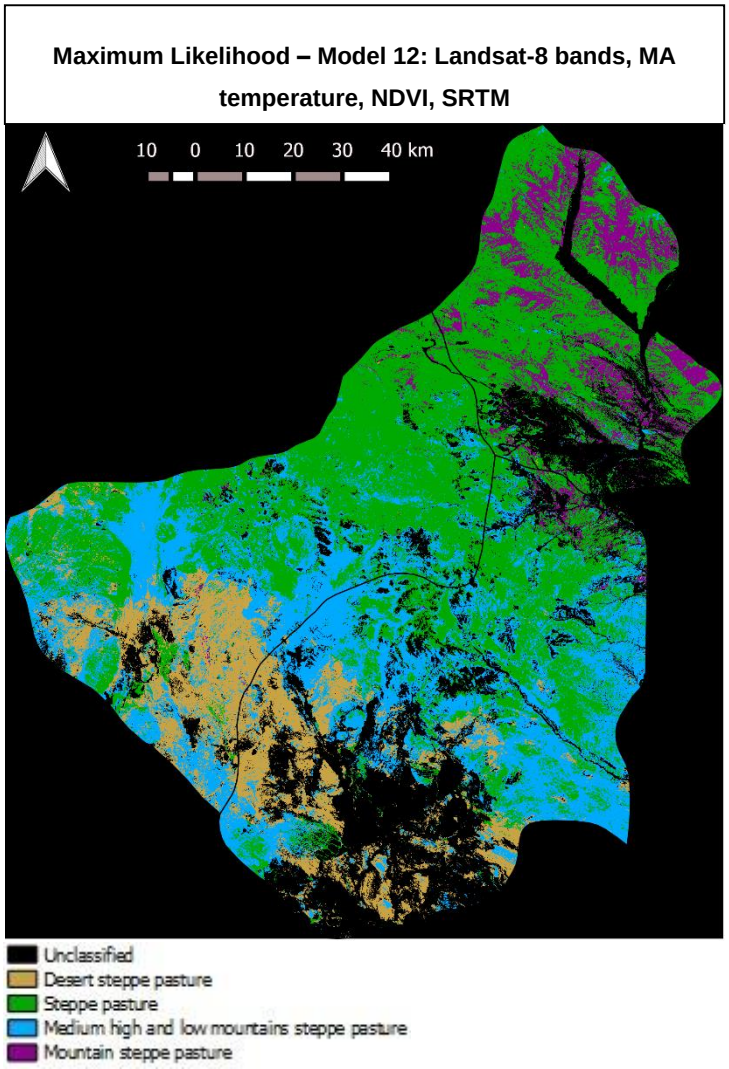

Figure A.35 - Steppe classification using maximum likelihood - Model 12: Landsat-8 bands, MA temperature, NDVI and SRTM

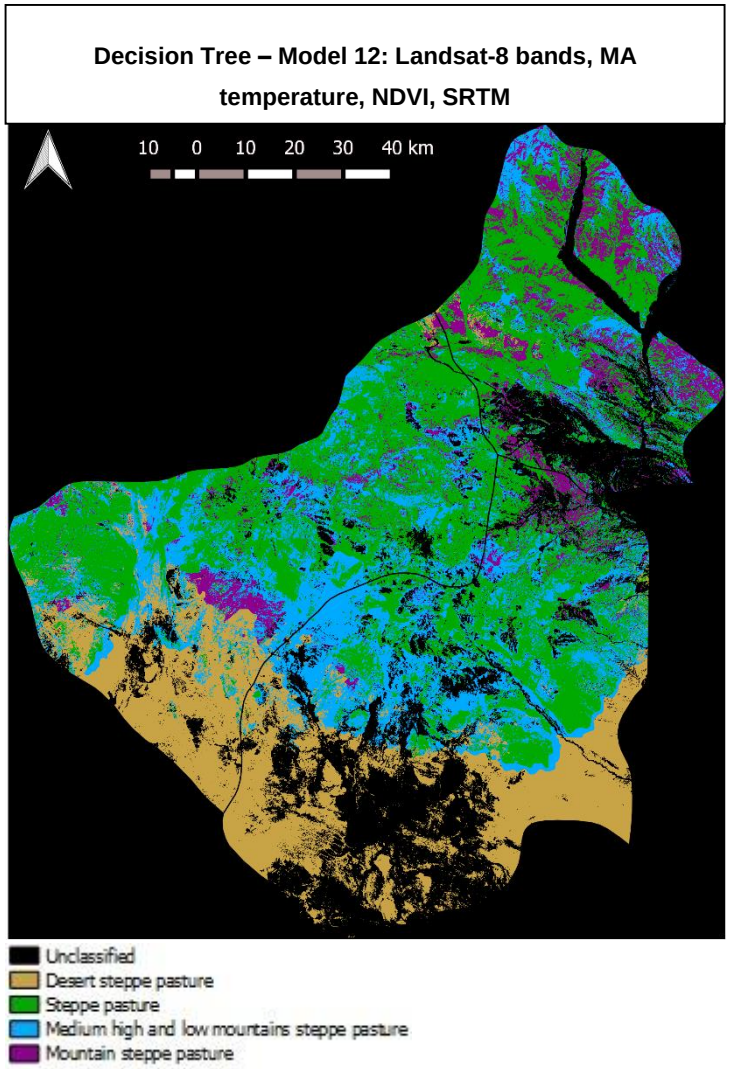

Figure A.36 - Steppe classification using decision tree - Model 12: Landsat-8 bands, MA temperature, NDVI and SRTM

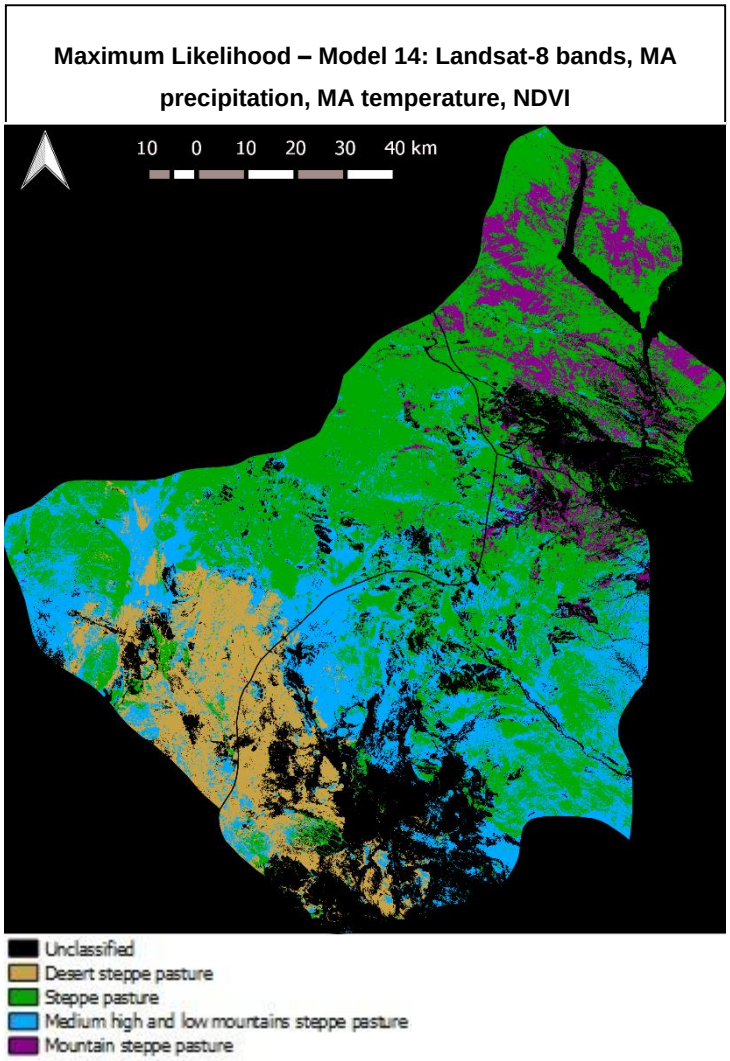

Figure A.37 - Steppe classification using maximum likelihood - Model 14: Landsat-8 bands, MA precipitation, MA temperature, NDVI

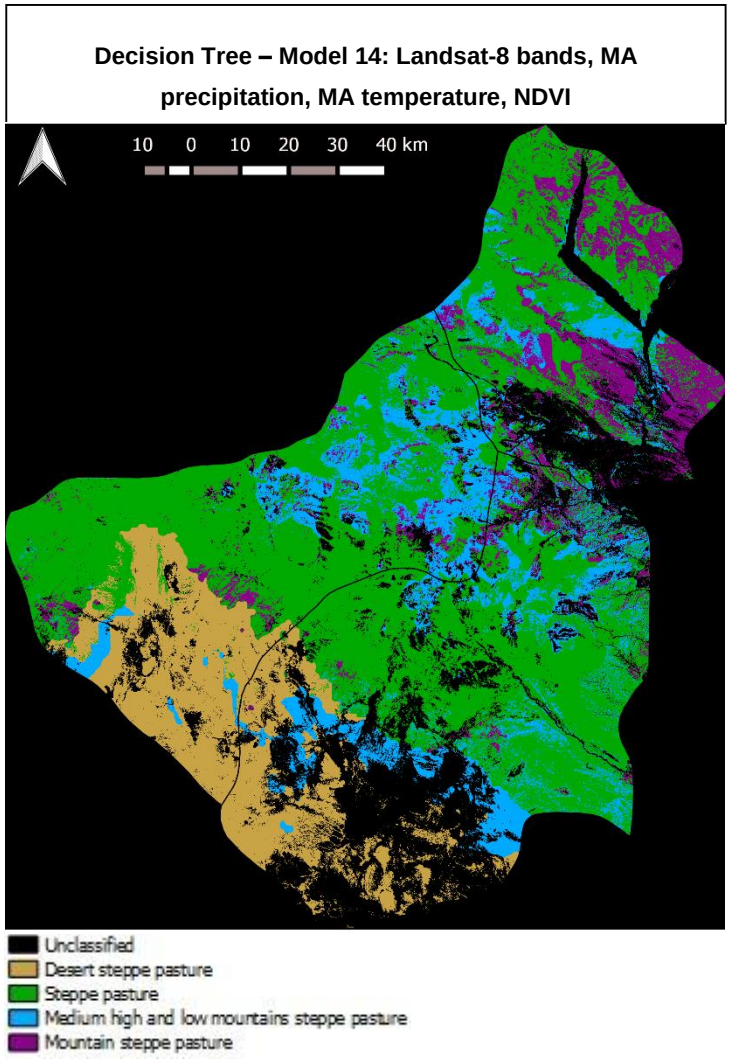

Figure A.38 - Steppe classification using decision tree - Model 14: Landsat-8 bands, MA precipitation, MA temperature, NDVI

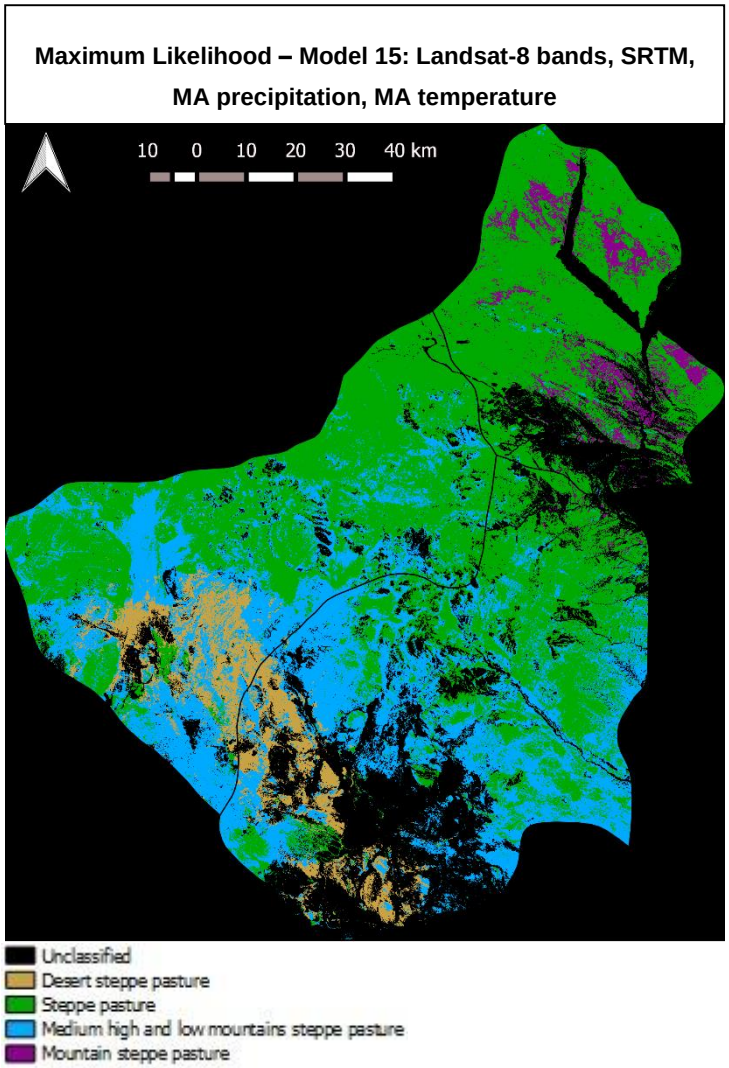

Figure A.39 - Steppe classification using maximum likelihood - Model 15: Landsat-8 bands, MA precipitation, MA temperature, SRTM

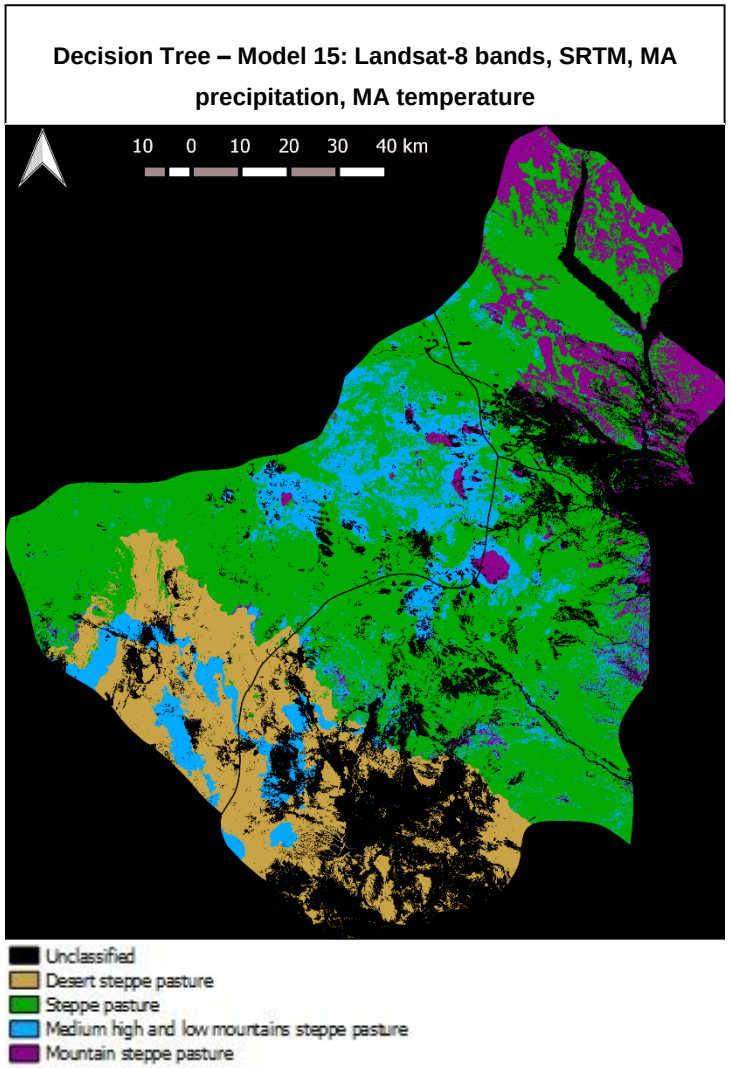

Figure A.40 - Steppe classification using decision tree - Model 15: Landsat-8 bands, MA precipitation, MA temperature, SRTM

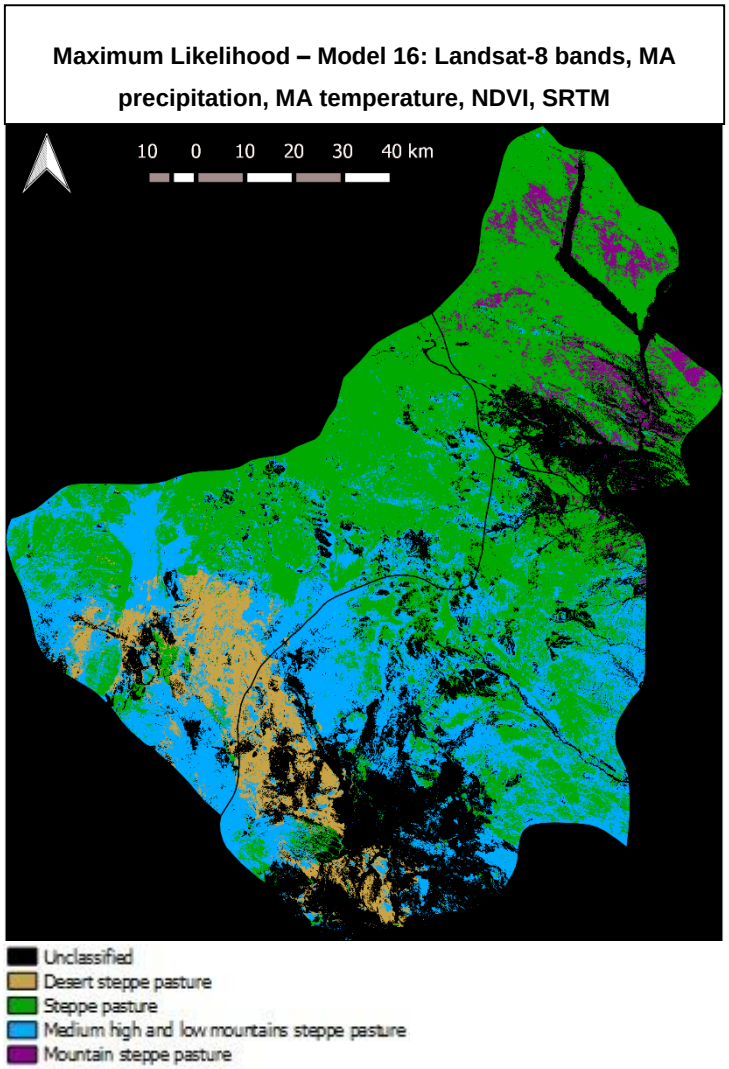

Figure A.41 - Steppe classification using maximum likelihood - Model 16: Landsat-8 bands, MA precipitation, MA temperature, NDVI, SRTM

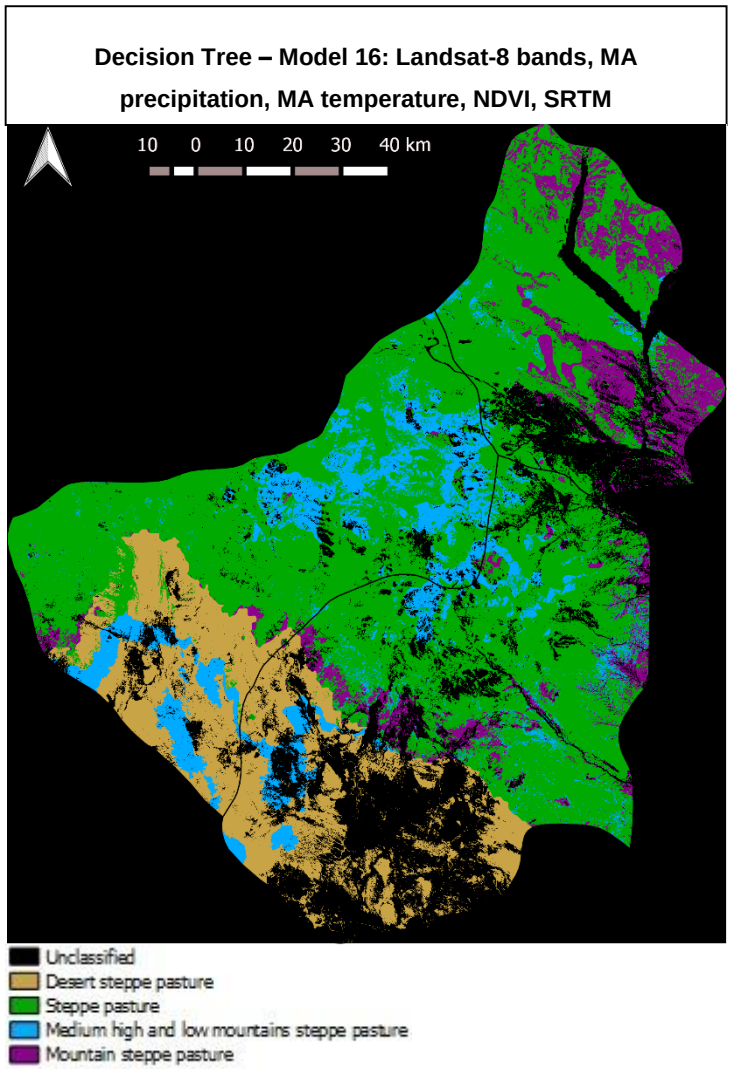

Figure A.42 - Steppe classification using decision tree - Model 16: Landsat-8 bands, MA precipitation, MA temperature, NDVI, SRTM

Table A.1 - Accuracy report of the Pasture Steppe using maximum likelihood and decision tree classifiers for Model 1, Model 2 and Model 3

Model 1: Landsat-8 bands	**Maximum likelihood**					**Decision tree**				
	F1-score [%]	**F1-score weighted average [%]**	**Precision [%]**	**Recall [%]**	**Overall accuracy [%]**	**F1-score [%]**	**F1-score weighted average [%]**	**Precision [%]**	**Recall [%]**	**Overall accuracy [%]**
Desert steppe pasture	31	**47**	26	37	**60**	73	**56**	75	71	**66**
Steppe pasture	71		78	65		76		81	72	
Medium high and low mountain steppe pasture	27		23	34		22		18	27	
Mountain steppe pasture	62		52	76		67		65	70	
Model 2: Landsat-8 bands, NDVI	**Maximum likelihood**					**Decision tree**				
	F1-score [%]	**F1-score weighted average [%]**	**Precision [%]**	**Recall [%]**	**Overall accuracy [%]**	**F1-score [%]**	**F1-score weighted average [%]**	**Precision [%]**	**Recall [%]**	**Overall accuracy [%]**
Desert steppe pasture	32	**42**	26	41	**55**	55	**45**	69	46	**65**
Steppe pasture	66		76	58		78		76	81	
Medium high and low mountain steppe pasture	19		14	27		1		1	1	
Mountain steppe pasture	58		48	74		64		65	64	
Model 3: Landsat-8 bands, SRTM	**Maximum likelihood**					**Decision tree**				
	F1-score [%]	**F1-score weighted average [%]**	**Precision [%]**	**Recall [%]**	**Overall accuracy [%]**	**F1-score [%]**	**F1-score weighted average [%]**	**Precision [%]**	**Recall [%]**	**Overall accuracy [%]**
Desert steppe pasture	32	**45**	26	40	**59**	66	**57**	73	60	**66**
Steppe pasture	72		84	64		79		85	73	
Medium high and low mountain steppe pasture	20		13	36		28		21	40	
Mountain steppe pasture	61		52	74		63		63	64	

Table A.2 - Accuracy report of the Pasture Steppe *using maximum likelihood and decision tree classifiers for Model 4, Model 6 and Model 7*

Model 4: Landsat-8 bands, NDVI, SRTM	**Maximum likelihood**					**Decision tree**				
	F1-score [%]	**F1-score weighted average [%]**	**Precision [%]**	**Recall [%]**	**Overall accuracy [%]**	**F1-score [%]**	**F1-score weighted average [%]**	**Precision [%]**	**Recall [%]**	**Overall accuracy [%]**
Desert steppe pasture	43	**45**	32	66	**55**	66	**57**	73	60	**66**
Steppe pasture	67		80	57		79		85	73	
Medium high and low mountain steppe pasture	21		19	23		28		21	40	
Mountain steppe pasture	58		50	69		63		63	64	
Model 6: Landsat-8 bands, MA precipitation, NDVI	**Maximum likelihood**					**Decision tree**				
	F1-score [%]	**F1-score weighted average [%]**	**Precision [%]**	**Recall [%]**	**Overall accuracy [%]**	**F1-score [%]**	**F1-score weighted average [%]**	**Precision [%]**	**Recall [%]**	**Overall accuracy [%]**
Desert steppe pasture	53	**49**	78	40	**75**	86	**58**	100	75	**69**
Steppe pasture	85		82	88		74		75	74	
Medium high and low mountain steppe pasture	6		5	8		21		21	22	
Mountain steppe pasture	65		60	72		73		70	76	
Model 7: Landsat-8 bands, MA precipitation, SRTM	**Maximum likelihood**					**Decision tree**				
	F1-score [%]	**F1-score weighted average [%]**	**Precision [%]**	**Recall [%]**	**Overall accuracy [%]**	**F1-score [%]**	**F1-score weighted average [%]**	**Precision [%]**	**Recall [%]**	**Overall accuracy [%]**
Desert steppe pasture	57	**56**	100	39	**79**	86	**61**	100	75	**67**
Steppe pasture	90		89	92		76		79	73	
Medium high and low mountain steppe pasture	19		12	41		36		28	50	
Mountain steppe pasture	68		63	74		50		53	47	

Table A.3 - Accuracy report of the Pasture Steppe *using maximum likelihood and decision tree classifiers for Model 8, Model 9 and Model 10*

Model 8: Landsat-8 bands, MA precipitation, NDVI, SRTM	**Maximum likelihood**					**Decision tree**				
	F1-score [%]	**F1-score weighted average [%]**	**Precision [%]**	**Recall [%]**	**Overall accuracy [%]**	**F1-score [%]**	**F1-score weighted average [%]**	**Precision [%]**	**Recall [%]**	**Overall accuracy [%]**
Desert steppe pasture	55	**53**	100	37	**75**	86	**60**	100	**75**	**65**
Steppe pasture	89		90	88		74		78	**70**	
Medium high and low mountain steppe pasture	11		7	31		35		27	**50**	
Mountain steppe pasture	67		63	71		50		53	**47**	
Model 9: Landsat-8 bands, MA temperature	**Maximum likelihood**					**Decision tree**				
	F1-score [%]	**F1-score weighted average [%]**	**Precision [%]**	**Recall [%]**	**Overall accuracy [%]**	**F1-score [%]**	**F1-score weighted average [%]**	**Precision [%]**	**Recall [%]**	**Overall accuracy [%]**
Desert steppe pasture	49	**53**	67	**38**	**76**	70	**57**	83	**61**	**70**
Steppe pasture	88		88	**88**		81		80	**83**	
Medium high and low mountain steppe pasture	16		12	**27**		22		19	**26**	
Mountain steppe pasture	64		54	**79**		69		77	**62**	
Model 10: Landsat-8 bands, MA temperature, NDVI	**Maximum likelihood**					**Decision tree**				
	F1-score [%]	**F1-score weighted average [%]**	**Precision [%]**	**Recall [%]**	**Overall accuracy [%]**	**F1-score [%]**	**F1-score weighted average [%]**	**Precision [%]**	**Recall [%]**	**Overall accuracy [%]**
Desert steppe pasture	35	**42**	30	42	**58**	70	**54**	83	**61**	**65**
Steppe pasture	73		87	63		79		83	**75**	
Medium high and low mountain steppe pasture	10		7	25		21		17	**26**	
Mountain steppe pasture	58		49	72		55		50	**62**	

Table A.4 - Accuracy report of the Pasture Steppe *using maximum likelihood and decision tree classifiers for Model 11, Model 12 and Model 14*

Model 11: Landsat-8 bands, MA temperature, SRTM	**Maximum likelihood**					**Decision tree**				
	F1-score [%]	**F1-score weighted average [%]**	**Precision [%]**	**Recall [%]**	**Overall accuracy [%]**	**F1-score [%]**	**F1-score weighted average [%]**	**Precision [%]**	**Recall [%]**	**Overall accuracy [%]**
Desert steppe pasture	51	**49**	78	38	**73**	56	**51**	100	41	**61**
Steppe pasture	85		86	84		75		79	71	
Medium high and low mountain steppe pasture	8		5	17		21		16	30	
Mountain steppe pasture	60		51	74		57		51	64	
Model 12: Landsat-8 bands, MA temperature, NDVI, SRTM	**Maximum likelihood**					**Decision tree**				
	F1-score [%]	**F1-score weighted average [%]**	**Precision [%]**	**Recall [%]**	**Overall accuracy [%]**	**F1-score [%]**	**F1-score weighted average [%]**	**Precision [%]**	**Recall [%]**	**Overall accuracy [%]**
Desert steppe pasture	56	**49**	81	42	**72**	70	**53**	83	61	**62**
Steppe pasture	85		89	82		73		78	68	
Medium high and low mountain steppe pasture	8		5	22		21		16	30	
Mountain steppe pasture	57		48	69		62		62	62	
Model 14: Landsat-8 bands, MA precipitation, MA temperature, NDVI	**Maximum likelihood**					**Decision tree**				
	F1-score [%]	**F1-score weighted average [%]**	**Precision [%]**	**Recall [%]**	**Overall accuracy [%]**	**F1-score [%]**	**F1-score weighted average [%]**	**Precision [%]**	**Recall [%]**	**Overall accuracy [%]**
Desert steppe pasture	58	**56**	97	41	**77**	86	**72**	100	75	**78**
Steppe pasture	89		91	87		84		79	89	
Medium high and low mountain steppe pasture	20		12	53		58		75	47	
Mountain steppe pasture	63		57	72		58		57	60	

Table A.5 - Accuracy report of the Pasture Steppe *using maximum likelihood and decision tree classifiers for Model 15 and Model 16*

Model 15: Landsat-8 bands, MA precipitation, MA temperature, SRTM	**Maximum likelihood**					**Decision tree**				
	F1-score [%]	**F1-score weighted average [%]**	**Precision [%]**	**Recall [%]**	**Overall accuracy [%]**	**F1-score [%]**	**F1-score weighted average [%]**	**Precision [%]**	**Recall [%]**	**Overall accuracy [%]**
Desert steppe pasture	57	**56**	100	39	**79**	86	**54**	100	75	**67**
Steppe pasture	90		89	92		79		73	85	
Medium high and low mountain steppe pasture	16		10	34		19		21	17	
Mountain steppe pasture	71		69	74		33		38	29	
Model 16: Landsat-8 bands, MA precipitation, MA temperature, NDVI, SRTM	**Maximum likelihood**					**Decision tree**				
	F1-score [%]	**F1-score weighted average [%]**	**Precision [%]**	**Recall [%]**	**Overall accuracy [%]**	**F1-score [%]**	**F1-score weighted average [%]**	**Precision [%]**	**Recall [%]**	**Overall accuracy [%]**
Desert steppe pasture	56	**56**	100	39	**78**	86	**57**	100	75	**70**
Steppe pasture	90		90	90		81		74	90	
Medium high and low mountain steppe pasture	19		12	51		25		50	17	
Mountain steppe pasture	66		66	67		30		31	29	